Dissertation

submitted to the

Combined Faculty of Natural Sciences and Mathematics

of the Ruperto Carola University Heidelberg, Germany

for the degree of

Doctor of Natural Sciences

Presented by

M.Sc. Johannes Paul Walther Heidbüchel

born in: Lübeck, Germany

Oral examination: May 27, 2019

Oncolytic measles viruses to support BiTE and CAR T cell re-direction immunotherapies of solid tumors

Referees: Prof. Dr. Ralf Bartenschlager
           Prof. Dr. Dirk Grimm

Abstract

Bispecific T cell engagers (BiTEs), artificial antibodies designed to cross-link T cells to tumor cells, and chimeric antigen receptors (CARs), expressed on the surface of modified T cells and transferring activating signals via intracellular domains, can re-direct T cells to tumor surface antigens for efficient treatment of hematological malignancies. In solid tumors, however, these novel immunotherapies face fundamental challenges: Physical exclusion of T cells and an immuno-suppressive microenvironment prevent efficacy while systemic administration is associated with severe toxicities. Oncolytic viruses have emerged as ideal agents for combination immunotherapies, as lytic replication in tumors does not only induce tumor debulking, but also immunogenic cancer cell death and local inflammation. We therefore hypothesized that oncolytic virotherapy, by eliminating physical barriers and reversing local immunosuppression, can promote anti-tumor T cell responses and thus provide a potent treatment option for solid tumors in combination with T cell re-direction. We furthermore hypothesized that tumor-targeted expression of a virus-encoded BiTE could achieve local BiTE activity without systemic side effects.

To test these hypotheses, we engineered oncolytic measles viruses (MV) encoding BiTEs targeting CD20 or carcinoembryonic antigen, respectively, as model antigens (MV-BiTE). Kinetics of viral replication and virus-mediated cytotoxicity showed minor differences compared to unmodified virus, and functional BiTEs could be obtained from the supernatant of virus-infected cells. A newly established syngeneic solid tumor model of B16-CD20-CD46 murine melanoma cells stably expressing human antigens CD20 and CD46 as BiTE target antigen and measles virus entry receptor, respectively, engrafted in immunocompetent C57BL/6 mice when implanted subcutaneously. In this model, treatment with MV-BiTE targeting CD20 significantly prolonged survival compared to control treatments with unmodified MV, MV encoding CEA-specific control BiTE, purified BiTE, or carrier fluid only, respectively. UV irradiation of MV-BiTE completely inhibited viral replication but did not abrogate efficacy in this model. Treatment efficacy was furthermore not impaired in mice previously immunized with MV. Increased T cell infiltration into tumors and an effector T cell phenotype characterized by high intratumoral CD8+ T cell levels and low relative abundance of regulatory T cells was observed upon MV-BiTE treatment. Targeted transcriptome analysis revealed upregulation of genes associated with T cell activation, proliferation, and differentiation, but also with inhibition and exhaustion, providing a rationale for combination with checkpoint inhibitors.

Combinations of MV, BiTE, and CAR T cell therapies were investigated in a pancreatic cancer model. Cytotoxic potential of each treatment alone towards human pancreatic adenocarcinoma cells was observed *in vitro*. However, no significant benefit of combinations was observed in a pilot experiment in immunodeficient mice, and T cell persistence was limited. For future *in vivo* monitoring of T cells by magnetic resonance imaging, labeling with iron oxide nanoparticles was established. In addition, we describe a mathematical model for *in silico* predictions of treatment outcome to optimize scheduling of combination therapies.

Taken together, this study shows for the first time efficacy of a BiTE-encoding oncolytic virus in an immunocompetent mouse model. This warrants further investigations towards future translation. We furthermore introduced a mathematical model of combination immunovirotherapy to further support the development of novel treatment options for cancer patients.

Zusammenfassung

Mithilfe von künstlichen bispezifischen Antikörpern (BiTEs) oder durch gentechnische Einführung chimärer Rezeptoren (CARs) lassen sich T-Zellen auf Tumor-Oberflächenantigene umlenken. Diese neuen Immuntherapien werden klinisch bereits zur Behandlung von hämatologischen Neoplasien eingesetzt. Der therapeutische Nutzen von BiTE- oder CAR-T-Zell-Therapien über diese Entitäten hinaus ist allerdings begrenzt, da die systemische Gabe mit schweren bis lebensbedrohlichen Nebenwirkungen verbunden sein kann und solide Tumoren über physikalische Barrieren und immunsuppressive Mechanismen verfügen, die das Eindringen sowie die anti-tumorale Aktivität von T-Zellen verhindern. Onkolytische Viren sind gekennzeichnet durch einen Tumorzell-spezifischen, lytischen Replikationszyklus, was einerseits zu einer direkten Reduktion der Tumorlast und andererseits zu einer lokalen Entzündungsreaktion führen kann, die eine anti-tumorale T-Zell-Antwort begünstigt. Daraus leiten wir die Hypothese ab, dass die Kombination von Virotherapie mit T-Zell-Umlenkung eine wirksame Behandlung von soliden Tumoren ermöglicht, was in dieser Arbeit experimentell untersucht wurde. Wir vermuteten weiterhin, dass die gezielte Expression von virus-kodierten BiTEs durch infizierte Tumorzellen eine starke, lokal begrenzte Umlenkung von T-Zellen bei geringerer Toxizität gegenüber systemischer Applikation bewirken kann.

Um diese Hypothesen zu testen, entwickelten wir Masern-Impfstamm-Viren (MV), die in ihrem Genom BiTEs kodieren, die entweder CD20 oder CEA, zwei Modell-Tumorantigene, erkennen und T-Zellen darauf umlenken können (MV-BiTE). Diese Viruskonstrukte zeigten im Vergleich zu unmodifizierten Impfviren nur geringe Unterschiede im Hinblick auf Replikationsgeschwindigkeit und lytische Aktivität, und funktionelle BiTEs konnten aus dem Überstand virusinfizierter Zellen isoliert werden. Eine neue Tumorzelllinie auf Basis der Maus-Melanom-Zelllinie B16, die zusätzlich die humanen Antigene CD20 als BiTE-Zielantigen und CD46 als Masernvirus-Rezeptor auf der Zelloberfläche exprimiert, formte subkutane Tumoren in syngenen immunkompetenten C57BL/6-Mäusen. In diesem Modell verlängerte die Tumorbehandlung mit CD20-spezifischen MV-BiTE das Überleben von Mäusen signifikant im Vergleich zu unmodifizierten MV, zu Kontrollviren, die den CEA-spezifischen BiTE kodieren, zu aufgereinigten BiTEs, und zur Injektion von Pufferlösung ohne Viren. Bestrahlung von MV-BiTE mit UV-Licht inhibierte effektiv die Replikationsfähigkeit der Viren, führte aber nicht zur Unwirksamkeit der Behandlung. Außerdem war die Behandlung auch in zuvor mit Masernviren immunisierten Tieren wirksam. Im Vergleich zu Kontrollbehandlungen wiesen die mit MV-BiTE behandelten Tumoren eine erhöhte Infiltration von T-Zellen sowie ein von zytotoxischen Effektorzellen geprägtes T-Zell-Profil mit wenigen regulatorischen T-Zellen auf. Die Transkriptomanalyse von Tumorproben zeigte eine verstärkte Expression von Genen, die mit der Aktivierung, Proliferation und Differenzierung, aber auch der Inhibition und Erschöpfung von T-Zellen assoziiert sind. Dies bietet eine Rationale für zukünftige Kombination von MV-BiTE mit Immuncheckpoint-Inhibitoren.

Kombinationen von CAR-T-Zell-, BiTE- und MV-Therapien wurden in einem Pankreastumor-Modell untersucht. Alle untersuchten Kombinationen zeigten zytotoxisches Potential gegenüber menschlichen Pankreas-Adenokarzinom-Zellen *in vitro*. In einem Pilotexperiment in immundefizienten Mäusen wurde jedoch keine erhöhte Wirksamkeit der Therapiekombinationen nachgewiesen und die Persistenz von transferierten humanen T-Zellen war limitiert. Um zukünftig transferierte T-Zellen in Mäusen über einen längeren Zeitraum hinweg mittels nichtinvasiver Magnetresonanztomographie visualisieren zu können, wurde ein Protokoll zur T-Zell-Markierung mit

Eisenoxid-Nanopartikeln etabliert. Außerdem wurde im Rahmen dieser Arbeit ein mathematisches Modell zur Simulation kombinierter Viro- und T-Zell-Immuntherapien erstellt, um die Behandlungsplanung durch *in silico*-Experimente zu optimieren.

Zusammengefasst liegt hiermit erstmals eine Studie vor, die die Wirksamkeit von BiTE-kodierenden onkolytischen Viren in einem immunkompetenten Modell nachweist. Diese Ergebnisse machen weitere translationale Forschung nötig, um das Konzept auf seine klinische Anwendbarkeit hin zu prüfen. Auch das entwickelte mathematische Modell kombinierter Immunovirotherapien kann zu einer Entwicklung neuer Behandlungsoptionen für Krebspatienten beitragen.

Contents

Abbreviations

ABAM	antibiotic-antimycotic
ACK	ammonium-chloride-potassium
AML	acute myeloid leukemia
APCs	antigen-presenting cells
ATU	additional transcription unit
B-ALL	B cell acute lymbhoblastic leukemia
BCA	bicinchoninic acid
BCG	Bacillus Calmette-Guérin
BiTE	bispecific T cell engager
BSA	bovine serum albumin
CAR	chimeric antigen receptor
CD	cluster of differentiation
cDNA	complementary DNA
CDR	complementary-determining region
CEA	carcinoembryonic antigen
ciu	cell infectious units
CLIO	dextran coated cross-linked iron oxide
CTLA-4	cytotoxic T lymphocyte-associated protein 4
cUV	complete UV inactivation
DAPI	4',6-diamino-2-phenylindole
dATP	deoxyadenosine triphosphate
DCs	dendritic cells
dCTP	deoxycytosine triphosphate
dGTP	deoxyguanosine triphosphate
DKFZ	German Cancer Research Center
DMEM	Dulbecco's Modified Eagle's Medium
DMSO	dimethyl sulfoxide
DNA	deoxyribonucleic acid
dNTP	deoxynucleotide triphosphate
DPBS	Dulbecco's Phosphate-Buffered Saline
dT	deoxythymidine
dTTP	deoxythymidine triphosphate
e. g.	exempli gratia
E:T ratio	effector-to-target cell ratio
EB	elution buffer
EDTA	ethylenediaminetetraacetic acid
eGFP	enhanced green fluorescent protein
ELISA	enzyme-linked immunosorbent assay
EMA	European Medicines Agency
EMBL-EBI	The European Bioinformatics Institute
Esp	spontaneous effector cell release
F	fusion
FBS	fetal bovine serum
Fc	fragment crystallizable region
FDA	Food and Drug Administration
FGF	fibroblast growth factor

Fig.	figure
FITC	fluorescein isothiocyanate
FMO	fluorescence minus one
G	glycin
GM-CSF	granulocyte-macrophage colony-stimulating factor
H	hemagglutinin
H1-PV	parvovirus H1
HA	influenza hemagglutinin peptide tag
hCD3	human CD3 (applies for other proteins, e.g. CD46)
HEPES	4-(2-hydroxyethyl)-1-piperazineethanesulfonic acid
His	hexa-histidine tag
HP	heparin and protamine
HPAC	human pancreatic adenocarcinoma
HPC	heparin, protamine, and CLIO-FITC
HPF	heparin, protamine, and ferumoxytol
HSV	herpes simplex virus
i. e.	id est
IACUC	Institutional Animal Care and Use Committee
IL-12	interleukin 12
IMGT	the international ImMunoGeneTics information system
L	large
LDH	lactate dehydrogenase
M	matrix
MACS	magnetic-activated cell sorting
mCD3	murine CD3
MHC	major histocompatibility complex
MOI	multiplicity of infection
MRD	minimal residual disease
MRI	magnetic resonance imaging
mRNA	messenger RNA
MV	oncolytic measles vaccine virus
MV-BiTE	BiTE-encoding MV
MV-CEA	MV encoding soluble carcinoembryonic antigen
MV-NIS	MV encoding sodium iodide symporter
N	nucleocapsid
nCI	normalized cell index
Ni-NTA	nickel nitrilotriacetic acid
NK	natural killer
NSG	NOD.Cg-$Prkdc^{scid}$ $Il2rg^{tm1Wjl}$/SzJ
nt	nucleotide
NTC	non tissue culture-treated
ORF	open reading frame
P	phosphoprotein
PBMCs	peripheral blood mononuclear cells
PD-1	programmed cell death protein 1
PD-L1	programmed death-ligand 1
PE	phycoerythrin
PEI	polyethylenimine

PSCA	prostate stem cell antigen
PSCA2/3	PSCA-specific CAR of second and third generation, respectively
RNA	ribonucleic acid
RNP	ribonucleoprotein complex
RPMI	Roswell Park Memorial Institute
RT-qPCR	reverse transcriptase quantitative polymerase chain reaction
S	serine
scFv	single chain variable fragment
SLAM	signaling lymphocytic activation protein
TCM	T cell medium
TCR	T cell receptor
Tmax	maximal target cell lysis
T_{reg}	regulatory T cell
Tsp	spontaneous target cell release
T-VEC	talimogene laherparepvec
U. S.	United States of America
UT	untransduced T cells
UV	ultraviolet
vBiTEs	virus-derived BiTEs
VH	variable heavy chain
VL	variable light chain
WB	washing buffer
XTT	2,3-Bis-(2-methoxy-4-nitro-5-sulfophenyl)-2H-tetrazolium-5-carboxanilide

List of Figures

1 Introduction

1.1 Motivation

Despite significant scientific and clinical advances in the last century, cancer diseases remain the second leading cause of death worldwide, with an estimated total of 9.6 million deaths in 2018 attributable to cancer according to the World Health Organization. While relative cancer mortality is expected to decrease at least in the European Union, the total number of cancer deaths is not declining, partly due to population ageing[1]. Thus, in addition to better prevention and diagnostic procedures, improved treatment options are desperately needed.

1.2 Immunotherapy: A brief historical perspective

Therapies that are in clinical use since decades, including chemotherapy and radiotherapy, often only reduce tumor burden while failing to prove truly curative potential[2]. Immunotherapeutic approaches, i.e. therapies manipulating the patient's own immune system to achieve detection and elimination of cancerous structures, are now widely appreciated as a promising way to achieve long-term tumor control. However, immunotherapy has long been regarded as an impossible or at least impractical idea. First promising practical evidence has been brought about by William Coley testing the application of heat-inactivated bacterial suspensions against cancer[3], which has been met with reluctance by the medical community, as was Paul Ehrlich's theoretical concept of tumor immunosurveillance[4]. In particular, a lacking understanding of the underlying biology together with experimental setbacks had prevented large-scale clinical application for a long time.

While a potential role of lymphocytes, in particular T cells, had been discussed in the context of tumor control, a study in athymic nude mice showing no evidence of increased tumor incidence compared to phenotypically normal heterozygotic mice challenged this hypothesis[5]. It was not until several decades later that in a novel mouse model, which in contrast to athymic nude mice completely lacked functional T cells, earlier tumor onset was observed, proving the importance of T cells in tumor immunosurveillance[6]. This exemplifies the challenges the field has faced due to insufficient theoretical and experimental knowledge, which had to be overcome by scientific investigation. Following early clinical studies in the 1970s[7], the BCG vaccine was introduced for treatment of superficial bladder cancer as the first anti-cancer immunotherapeutic and continues to be standard-of-care for this disease entity (reviewed in[8]). The efficacy of chemotherapeutic, radiotherapeutic, and even more recently developed targeted approaches aiming at tumor cell-specific aberrations has later in part been attributed to immunological consequences[9,10], warranting further investigation of these mechanisms of action and revealing a potential of combining different treatment options for improved efficacy[11]. Importantly, by thorough basic research in a variety of scientific fields and many clinical trials, it is now well established that a complex interplay of tumor and immune cells[12] defines the dynamics of tumor development and that manipulation of this interplay has the potential to ameliorate disease and even induce long-term cures.

In a landmark paper published in 2013, Chen and Mellman comprehensively reviewed the available scientific literature and established the concept of the "Cancer-Immunity Cycle", describing the

essential steps required for a successful anti-tumor T cell response[13]: Initial cancer cell death induces the release of tumor antigens, which are taken up by antigen-presenting cells (APCs) such as dendritic cells (DCs). APCs then travel to the lymph node, where antigen presentation results in priming and activation of cytotoxic T cells. Subsequently, activated cytotoxic T cells traffic via the vasculature to tumors, where they extravasate and infiltrate into the tumor. Cancer cells expressing the target antigen of primed T cells are then recognized via the T cell receptor (TCR) complex, inducing T cell activation and tumor cell killing. This simplified model already illustrates the complexity of processes underlying anti-tumor immunity and thus the vulnerability to deficiencies at any of the described steps. However, it also provides a theoretical framework for rational immunotherapeutic intervention with a multitude of potential targets.

1.3 The rise of T cell-based therapies

In the 1980s, the first study showed the anti-tumor potential of adoptively transferred autologous tumor-infiltrating T lymphocytes in melanoma patients[14]. Efficacy was improved by increasing persistence of transferred T cells via nonmyeloablative pre-conditioning[15], leading to complete durable regressions in patients with metastatic melanoma. These results verified earlier observations from animal experiments[16-18], showing that immune cells of a cancer patient had the potential to eliminate the tumor under certain conditions, but were inhibited in situ (reviewed in[19]).

While adoptive cell transfer makes use of activating and expanding T cells to high numbers ex vivo, investigating an alternative principle of blocking T cell inhibitory signals within the patient has led to the development of checkpoint inhibition antibodies (reviewed in[20-22]). These bind to co-inhibitory receptors on T cells, e.g. programmed cell death protein 1 (PD-1), which is upregulated upon antigen encounter[23], or corresponding ligands such as programmed death-ligand 1 (PD-L1)[24], which is often overexpressed on the surface of tumor cells[25]. This enables sustained or renewed anti-tumor activity of T cells and has thereby induced durable complete remissions in entities previously considered mainly incurable such as metastatic melanoma, leading to market approval by the U.S. Food and Drug Administration (FDA) of seven individual products since 2011[26] and the denomination as "Breakthrough of the Year" in 2013 by the journal Science [27]. This has made major impact on clinical use of immunotherapy, and immune checkpoint inhibitors are investigated in numerous clinical trials as mono- or combination therapy for diverse tumor entities*.

Both adoptive T cell transfer and checkpoint inhibition approaches require the presence of T cells with receptor specificity for haplotype-restricted antigenic epitopes presented on class I major histocompatibility complex molecules (MHC I) of tumor cells. This represents a major limitation of such approaches relying on original T cell specificity. As spontaneous recognition of malignantly transformed cells by the immune system is suboptimal in case of tumor development, in situ therapeutic vaccination approaches are under extensive investigation. However, so far prediction and validation of appropriate targets is laborious and time-consuming. In addition, therapeutic vaccination against defined targets in advanced disease is hampered due to local immunosuppression and antigenic escape[28]. A number of approaches are being developed to address these limitations, including targeting of the patient-specific "mutanome", i.e. more than

---

*313 studies found on clinicaltrials.gov as of March 28, 2019

one predicted epitope[29,30]. However, even in the case of relevant TCR specificity, anti-tumor activity can be absent, e.g. due to MHC loss on tumor cells[31].

1.4 Manipulating specificity: The concept of T cell re-direction

Regarding these limitations of relying on TCR specificity for cancer treatment, using polyclonal T cells can provide an advantage by targeting a broad range of potentially tumor-associated antigens. To overcome inefficient tumor cell recognition, approaches to re-direct polyclonal T cells to tumor surface antigens via single chain variable fragments (scFvs) have been developed, the most advanced being bispecific T cell engagers (BiTEs) and chimeric antigen receptors (CARs) (reviewed in[32]).

BiTEs are artificial bispecific antibodies composed of two scFvs targeting a tumor surface antigen and the T cell receptor-associated molecule CD3ε, respectively (Fig. 1, reviewed in[33-36]). The scFvs are connected by a flexible, non-immunogenic peptide linker, allowing for cross-linking of T cells and target tumor cells. This subsequently induces T cell activation and the formation of a regular immunological synapse, irrespective of MHC expression[37], haplotype, TCR specificity, and co-stimulation[38]. However, BiTE-mediated activation is not observed in naïve T cells[39]. Both CD8+ and CD4+ T cells have been shown to induce apoptosis in tumor cells upon BiTE-mediated crosslinking by release of cytotoxic granules containing perforin and granzyme B, indistinguishable from normal T cell receptor-mediated activation[40], but maximal lysis is reached faster by CD8+ compared to CD4+ T cells[41]. Interestingly, patient-derived regulatory T cells (T_{reg}) were able to trigger BiTE-mediated tumor cell lysis *in vitro*[42]. Two- to three-fold expansion of total T cell numbers in peripheral blood was observed upon BiTE treatment[43] and individual BiTE-engaged T cells are capable of serial killing of multiple tumor cells[44], indicating potential even at low effector-to-target cell (E:T) ratios.

Chimeric antigen receptors also contain an scFv targeting a tumor surface antigen, but are directly expressed by genetically modified T cells and linked via hinge and transmembrane domains to intracellular CD3ζ signaling and additional co-stimulatory domains providing T cell activation upon antigen binding (Fig. 2, reviewed in[45-47]). As with BiTEs, CAR engagement has been shown to induce T cell proliferation and serial lysis of tumor cells by both CD4+ and CD8+ T cells, with CD4+ T cells killing more slowly but persisting longer[48]. However, atypical synapses are formed between CAR T cells and target tumor cells, resulting in rapid detachment and faster serial killing capacity[49]. *in vivo* proliferation of over 1,000-fold has been observed for CAR T cells[50,51], while proliferation and persistence strongly depend on the subtype of the CAR-expressing T cell. In contrast to BiTE therapy relying on activation of resting, antigen-experienced T cells, it has been shown that for CAR-mediated re-direction, less differentiated cells with higher self-renewal capacity proliferate more strongly, persist longer, and thus show improved total anti-tumor activity[52,53].

In addition to scFv specificity, the activation potential of a given CAR is influenced by the length of the hinge region which determines effectivity of cross-linking[54,55] and the choice of co-stimulatory domains. First-generation CARs contained a CD3ζ-derived signaling molecule only[56]. Introduction of a CD28 co-stimulatory domain drastically increased CAR T cell activity of second-generation CARs[57,58], which have now advanced to the clinics. A multitude of novel
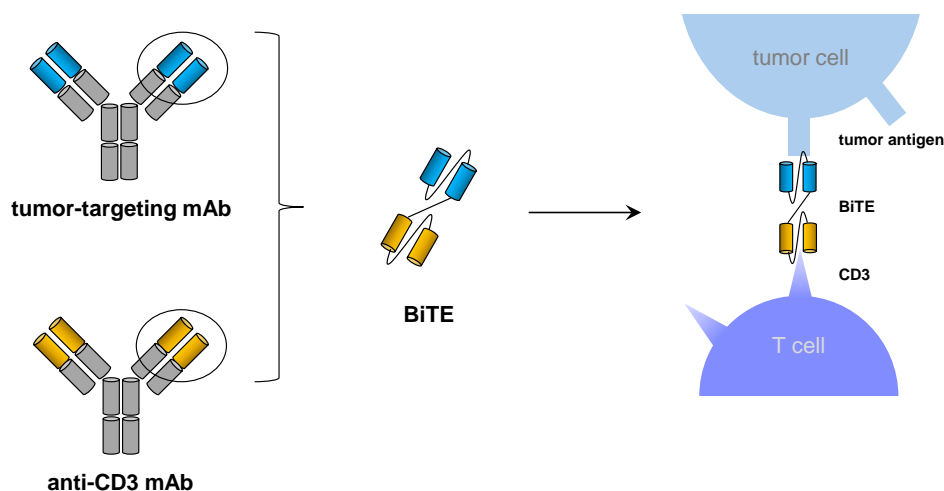
Figure 1: The bispecific T cell engager (BiTE) principle. Single chain variable fragments derived from two monoclonal antibodies directed against a tumor surface antigen (blue) and the epsilon chain of the T cell receptor-associated molecule CD3 (CD3ε) are connected by a flexible peptide linker to form a BiTE. By cross-linking a T cell to a target antigen-expressing tumor cell, the T cell is activated, inducing tumor cell lysis.

compositions, e.g. including additional co-stimulatory domains (third-generation CARs), is currently under investigation for improved safety, efficacy and persistence of CAR T cells[59,60].

1.5 Clinical applications of T cell re-direction therapies

Both BiTE and CAR therapies have been approved for treatment of certain hematological malignancies. The clinically most advanced agent of the BiTE class is blinatumomab (Blincyto®), a CD19-targeting BiTE that has first been approved by the FDA for treatment of Philadelphia chromosome-negative relapsed or refractory precursor B cell acute lymphoblastic leukemia (B-ALL) in 2014[61], followed by approval also in Philadelphia chromosome-positive B-ALL in 2017[62] and patients in B-ALL remission with minimal residual disease (MRD) in 2018[63]. In a phase 3 study, blinatumomab therapy was superior to standard-of-care chemotherapy. Complete remissions were reported in 34% of BiTE-treated patients, but short response durations have been reported with median overall survival of 7.7 months[64]. Due to small molecular size, blinatumomab shows beneficial tissue penetration but limited serum half-life of around 2 h[65], requiring continuous application via infusion pumps in up to five cycles of four weeks[66], which is inconvenient for patients. Furthermore, severe and sometimes fatal toxicities associated with systemic application have been reported including infections, neurologic events, neutropenia, anemia, and cytokine release syndrome.

Two products containing CAR-expressing T cells, tisagenlecleucel (Kymriah®) and axicabtagene ciloleucel (Yescarta®), both also targeting CD19, have recently been FDA-approved for treatment of B-ALL patients up to 25 years of age in second or later relapse[67] and adult large B cell lymphoma patients without response to or in relapse following at least two previous lines of
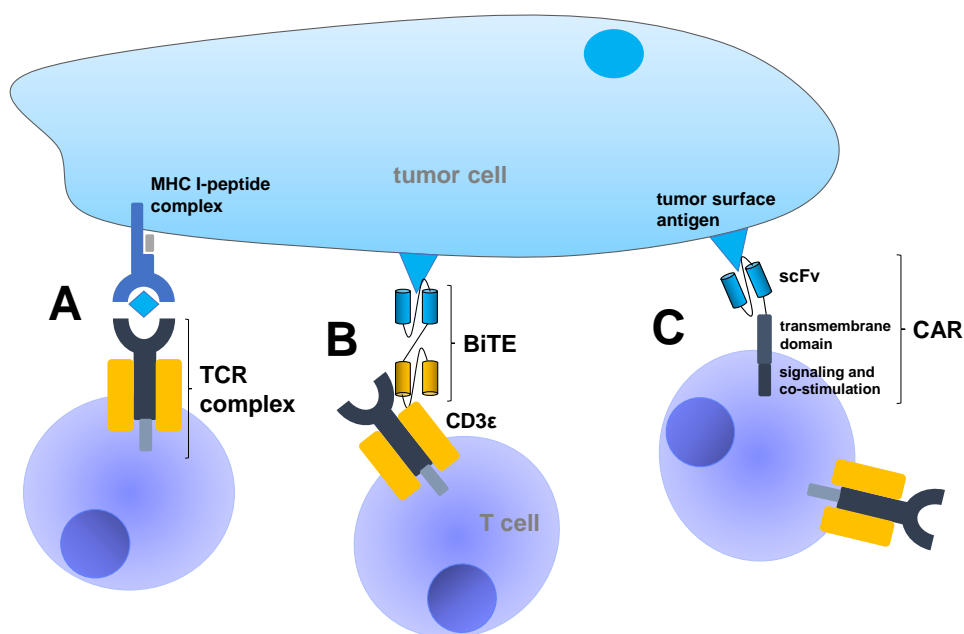
Figure 2: T cell re-direction. A. Target cell lysis by cytotoxic T cells requires T cell receptor (TCR)-specific recognition of the respective target peptide presented by major histocompatibility complex I (MHC I) on the target cell surface as well as additional co-stimulatory signals (not shown). T cell activation and release of cytotoxic granules follows intra-cellular signaling downstream of the TCR complex. B. Bispecific T cell engagers (BiTEs) circumvent the requirement of MHC presentation by directly cross-linking a tumor surface antigen with CD3ε on non-naïve T cells, inducing the formation of a classical immunological synapse irrespective of TCR specificity or co-stimulation. C. T cells genetically modified to express a chimeric antigen receptor (CAR) bind to tumor surface antigens via a single chain antibody displayed on the extracellular part of the CAR. CAR T cell efficacy in terms of target cell lysis is determined by various parameters, including the affinity of the single chain to its antigen, the structure of the hinge and transmembrane region, and, importantly, the composition of intracellular signaling and co-stimulatory domains.

treatment[68], respectively. In general, systemic targeting of CD19-expressing cells induces B cell aplasia. In addition, similar to blinatumomab, severe neurologic toxicities and frequent occurrence of cytokine release syndrome including fatal cases have been observed, requiring close monitoring and management of side effects by appropriate countermeasures such as immunosuppressive regimens[69]. In addition, relapses are frequently observed, sometimes associated with proliferation of tumor cell clones that have lost CD19 expression[70]. While both BiTE and CAR products have been approved for treatment of hematological malignancies, this is not the case for solid tumors. Due to the potentially severe systemic side effects, the therapeutic window of these therapies is narrow. Physical barriers to T cell infiltration into solid tumors, such as high interstitial pressure, dense stroma, and disorganized vasculature, as well as an immunosuppressive microenvironment have so far prevented efficacious application. This requires novel approaches and combination therapies to increase efficacy[32].

1.6 Oncolytic viruses: novel immunotherapeutics

In the past decades, oncolytic virotherapy has emerged as a novel form of immunotherapy after being widely regarded as an impractical, ineffective and even dangerous idea for over a century (reviewed in[71]), much like the field of immunotherapy in general. Oncolytic viruses can be found among different virus families[72] and share the characteristic of lytic replication in malignantly transformed tissue without affecting healthy cells (reviewed in[73]). First anecdotal observations of tumor remissions upon infection with influenza were made in the early 20th century[74], at a time when viruses had not even been discovered as infectious agents. Tissue culturing methods allowing the propagation of viruses advanced the field of virology in the middle of the century[75], simultaneously stimulating studies with oncolytic viruses in animal experiments and humans that sometimes did not meet scientific standards of modern medical research[76]. Cancer patients were treated with infectious body fluids in the hope to induce tumor remissions[77], and even tumor cell lines were intentionally implanted into cancer patients and healthy volunteers to test oncolytic activity of viruses *in vivo*[78,79].

Fortunately, the field has since advanced to rational scientific evaluation of non-pathogenic viruses that are of foreign host specificity or attenuated by either passaging on non-human cell lines or genetic modification. These strategies are exemplified by rodent parvovirus H1 (H1-PV), oncolytic measles virus vaccine strains, and thymidine kinase-deficient herpes simplex virus (HSV), respectively. The latter example represents the first application of genetic engineering for oncolytic viruses, showing enhanced tumor specificity and decreased neurovirulence in the treatment of glioma in nude mice[80] and sparking renewed interest in the field in 1991. Genetic engineering is now regularly applied in the development of novel oncolytics to increase specificity and efficacy.

While anti-tumor efficacy of oncolytic virotherapy was initially believed to rely solely on direct tumor cell lysis with the immune system being an impediment to successful treatment, it is now appreciated that virus-mediated induction of anti-tumor immune responses represents a major mechanism of action (reviewed in[81-83]), in addition to stromal and vascular targeting[84]. Immunogenic lysis of infected cells results in the release of tumor antigens, pathogen- and danger-associated molecular patterns, chemokines, and cytokines and can thus induce local inflammation and reversion of immunosuppression within the tumor microenvironment, which has been referred to as "turning an immunologically cold tumor hot"[85].

This naturally encourages combinations of oncolytic viruses with immunotherapeutic approaches. Indeed, talimogene laherparepvec (T-VEC, Imlygic®), the first and so far only oncolytic therapeutic that has been approved by the FDA and the European Medicines Agency (EMA), is a type I HSV genetically engineered not only for attenuation, but also to achieve increased tumor immune recognition. The viral genome was modified by disruption of *γ-34.5*, a gene involved in suppressing antiviral responses, by translocating *US11*, a gene preventing host cell protein synthesis shutoff, for expression under an early rather than a late promoter, by deleting *ICP47*, a gene interfering with antigen processing, and by inserting a transgene encoding granulocyte macrophage colony-stimulating factor to induce APC activation and maturation for enhanced anti-tumor T cell priming[86]. T-VEC was approved in 2015 for treatment of advanced melanoma based on a phase III study showing both local and abscopal efficacy upon intralesional administration[87]. No virus was detected in regressing non-injected lesions and abscopal efficacy was attributed to virus-mediated induction of an anti-tumor T cell response[88]. This demonstrates the potential of oncolytic virotherapy to evoke systemic, polyclonal T cell responses directed against solid tumors and thus warrants investigations of combining oncolytic virotherapy and T cell-based therapies. It has been shown in earlier animal experiments that local treatment with oncolytic Newcastle disease virus, an avian paramyxovirus, can induce systemic sensitivity to immune checkpoint inhibition[89]. A similar effect has later also been observed in triple-negative breast cancer patients after injection of an oncolytic Maraba virus[90]. Consequently, clinical evaluation of T-VEC in combination with immune checkpoint inhibitors has been initiated[91,92].

1.7 Measles vaccine viruses as oncolytic agents

A promising platform for oncolytic virotherapy has been developed based on live attenuated measles virus vaccine strains (MV, reviewed in[93-96]). The measles virus is a member of the genus *Morbillivirus* in the family *Paramyxoviridae* with a non-segmented, single-stranded, negative sense RNA genome containing 15,894 nucleotides (nt) and six genes encoding six structural and two additional regulatory proteins[97-99] (Fig. 3). Untranscribed RNA of 107 and 109 nt in the 3' leader and 5' trailer sequences, respectively, contain regulatory elements for encapsulation, transcription, and replication[100,101]. Nucleocapsid (N) proteins, each binding six nucleotides of the genome and thus requiring the genome to be divisible by six for assembly of functional particles[102,103], form a helical structure[104] that together with the large (L) protein and the phosphoprotein (P) is referred to as ribonucleoprotein complex (RNP). The L protein is the RNA-dependent RNA polymerase of the measles virus and requires P protein-mediated interaction with measles RNA for both transcription and replication of the genome[105-107]. Binding of a fully assembled RNP complex by matrix (M) proteins attaching to the inner layer of the host cell membrane inhibits transcription and induces budding of virus particles[108]. Hemagglutinin (H) and fusion (F) transmembrane glycoproteins are inserted into the host cell membrane as tetramers and trimers, respectively. H proteins, which are present both on the surface of infected cells and on free virus particles, attach to cell entry receptors, inducing fusion with the target cell via conformational changes in the F protein[109]. By this, measles virus-infected cells can form large multinucleated syncytia with uninfected neighboring cells[110]. Furthermore, measles virus can exploit cell-to-cell contacts for spreading[111]. C and V accessory proteins are alternatively expressed from the *P* open reading frame (ORF) by usage of an alternative reading frame and by mRNA editing, respectively, and are involved in measles virulence by interfering with the host cell-intrinsic antiviral interferon response[112,113]. Stop signals at the 5' end of the ORFs are followed by three-nucleotide intergenic

A

B
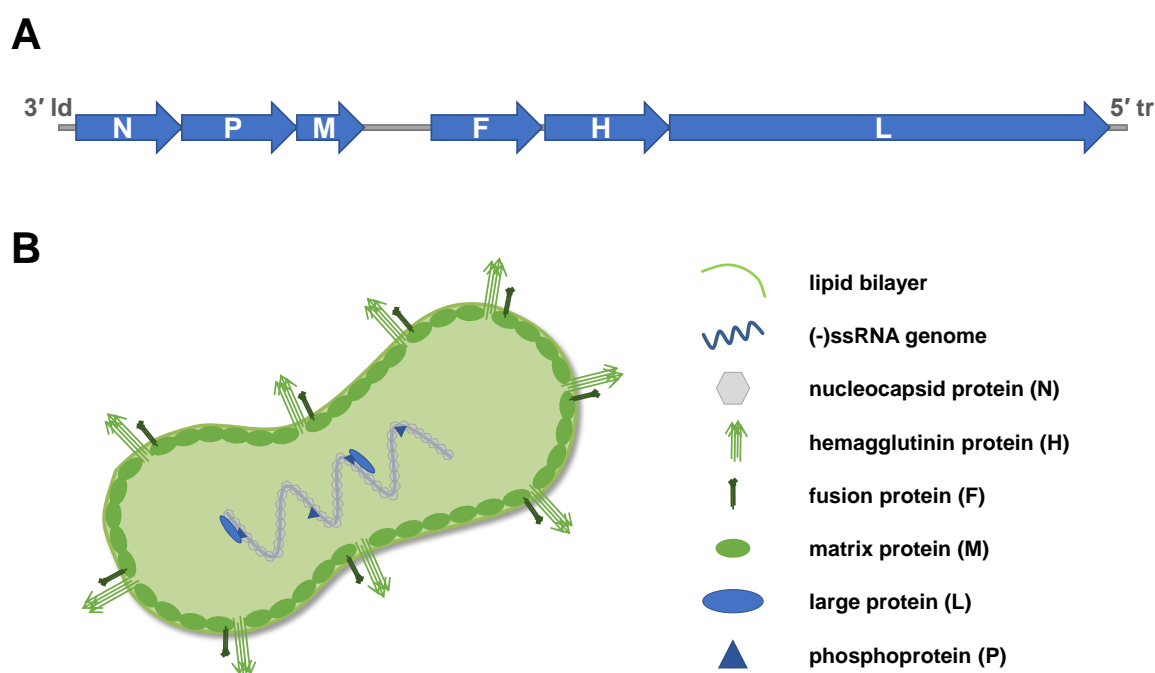
Figure 3: Measles virus genome (A) and structure (B). A. The negative sense RNA genome of the measles virus contains six genes arranged as indicated, encoding six structural proteins. Two additional regulatory proteins, C and V (not shown), are encoded in the P region. The viral genome also contains non-coding RNA between transcription units as well as in the 3' leader (3' ld) and 5' trailer (5' tr) sequences, which includes regulatory elements. B. The genome is encapsulated by the N protein, which binds to proteins P and L, forming the ribonucleoprotein complex (RNP) required for genome replication and transcription into positive sense mRNA. The M protein connects the RNP to the viral transmembrane glycoproteins H and F, facilitating budding of viral progeny from the host cell. H and F are present in the lipid bilayer as tetramers and trimers, respectively, and mediate host cell entry via binding to cellular receptors and induction of membrane fusion.

regions, at which the viral polymerase can fall off the genome with a particular probability, leading to an expression gradient of the encoded genes in the direction of gene expression, i.e. from 3' to 5'[114].

In the 1970s, cases of tumor regression upon contraction of measles virus infection were reported[115], indicating oncolytic potential. However, human-pathogenic wild-type measles virus is the causative agent of measles, a disease which is clinically characterized by flu-like symptoms, fever, skin rash, Koplik's spots and respiratory tract symptoms[116] due to infection of epithelial cells using nectin-4 as entry receptor[111,117,118]. Signaling lymphocytic activation molecule (SLAM, CD150) represents an additional entry receptor for wild-type measles virus, enabling infection of dendritic cells, T and B cells, and monocytes[119]. This can result in immunosuppression and subsequent complications by secondary infections such as pneumonia[120]. In rare cases of persistent infection, the central nervous system can be affected, leading to fatal subacute sclerosing panencephalitis[121,122]. Live attenuated vaccines for immunization against this potentially fatal virus have been in use since the 1960s[123-125] and have an excellent safety record, with no observed reversion to infectious wild-type virus[126]. For attenuation, wild-type viruses were serially passaged on non-human

cells[97]. Due to this, the viruses acquired mutations including a single point mutation in the H gene causing adaptation to the usage of CD46 as preferred cell entry receptor[127-130]. CD46 is a complement-regulatory protein present on all nucleated human cells[131] that is frequently upregulated on tumor cells as an immune escape mechanism, which provides a natural oncotropism to measles vaccine viruses[93]. In addition, mutations in the virulence factors C and V decrease the ability of attenuated measles vaccine viruses to interfere with the antiviral defense mechanisms of the host cell[132,133], requiring defective interferon signaling as often observed in malignantly transformed cells for propagation.

Tumor specificity can be further enhanced by genetic engineering using an established reverse genetics system[134-137]. Natural virus tropism can be abrogated by mutations in the H gene and MV can be re-targeted to cell surface structures by transgenic expression of e.g. receptor ligands or scFvs on the C-terminal extracellular domain of the H protein (reviewed in[93]). In addition, introduction of microRNA target sites into the genome has been shown to limit viral replication to tissues not expressing the corresponding microRNA[138-140].

Moreover, therapeutic or diagnostic transgenes can be introduced into the genome, which has led to the development of a number of pre-clinically and clinically tested oncolytic measles virus constructs. Most advanced are vectors of the Edmonston lineage encoding sodium iodide symporter for radiotherapeutic and imaging purposes (MV-NIS) and carcinoembryonic antigen for *in vivo* viral gene expression analyses (MV-CEA), respectively. For these viruses, clinical studies have confirmed safe delivery by diverse routes of administration and cases of anti-tumor efficacy have been observed (reviewed in[141]). A notable case of complete remission of multiple myeloma upon injection of a single dose of MV-NIS has been described[142]. Further pre-clinical development has yielded promising results for MV constructs armed with immunomodulatory transgenes targeting diverse tumor immune escape mechanisms, including GM-CSF to promote APC activation and maturation and thus T cell priming[143], Helicobacter pylori neutrophil-activating protein to promote inflammation and anti-tumor T cell responses[144], or tumor-associated antigens for therapeutic vaccination[145]. Recent work in our lab showed delayed tumor growth and prolonged survival in immunocompetent C57BL/6 mice bearing subcutaneous B16 murine melanoma tumors treated with MV encoding checkpoint inhibitors[146] and complete tumor remissions in 90% of animals treated with an IL-12-encoding MV in an MC38 murine colon carcinoma model. Efficacy was dependent on CD8+ T cells, as evidenced by depletion experiments[147].

Oncolytic measles viruses are attenuated and have a natural oncotropism. Routine vaccination and clinical trials in cancer patients have demonstrated safety. Moreover, MV replication is strictly cytosolic without any risk of insertional mutagenesis. MVs are strongly immunogenic and MV-induced syncytia formation facilitates spread as a bystander effect and induces immunogenic cell death. Furthermore, there is strong pre-clinical evidence for efficacy in combination with additional immunotherapeutics. The established reverse genetics system and large transgene capacity add to the beneficial properties of MV as an oncolytic agent. Oncolytic measles virotherapy thus provides a safe, versatile and efficacious platform for combination immunotherapies.

1.8 Aim of the study

T cell re-direction by both bispecific T cell engagers (BiTEs) and chimeric antigen receptors (CARs) has shown promising results in the treatment of hematological malignancies. However,
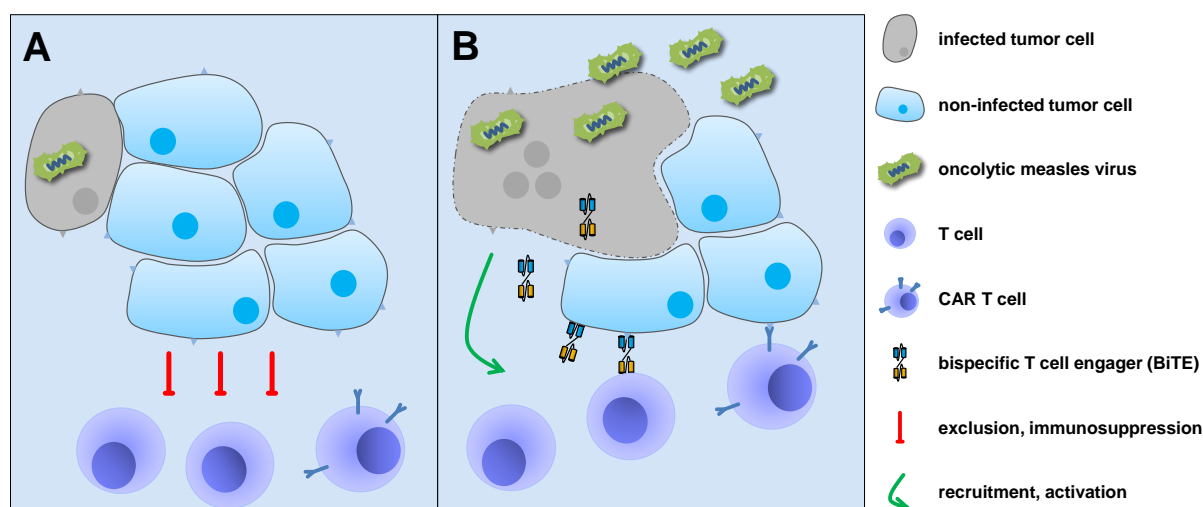
Figure 4: Proposed mechanism of action of combined oncolytic measles virus and T cell re-direction immunotherapy. Suppression of anti-tumor T cell responses and toxicities associated with systemic application of BiTEs and CAR T cells so far prevented approval of such therapies in solid tumors. We propose the following mechanism of action for successful oncolytic measles virus (MV) and T cell re-direction combination therapy. A. Malignant transformation and suppressed anti-viral immunity promote the infection of tumor cells by MV. B. In the course of viral replication and spread throughout the tumor, infected cells fuse with neighboring tumor cells, forming large syncytia (grey). Virus-induced immunogenic cell death results in local inflammation and the recruitment of immune cells, creating a favorable environment for anti-tumor (CAR) T cell activity. In addition, MV-encoded BiTEs are expressed locally by infected cells, recruiting T cells to lyse tumor cells without systemic toxicities.

limited efficacy due to physical exclusion and immunosuppression of T cells and severe toxicities associated with systemic treatment prevent successful application in solid tumors.

Oncolytic virotherapy provides ideal properties for combination treatment: Tumor-specific cell lysis causes debulking and can facilitate T cell infiltration. Furthermore, virus-mediated immunogenic tumor cell death and local inflammation have the potential to reverse immunosuppression and provide antigen-agnostic in situ vaccination[148]. In addition, locally restricted expression of systemically toxic transgenes can enhance anti-tumor efficacy while preventing side effects. Oncolytic measles vaccine strain viruses (MV) can be safely administered and cause tumor remissions in cancer patients. T cell-mediated efficacy and potential for combination immunotherapy has been demonstrated in pre-clinical studies.

We therefore hypothesized that oncolytic measles virotherapy can support T cell re-direction therapies of solid tumors by tumor debulking and reversion of immunosuppression (Fig. 4). Furthermore, we hypothesized that tumor-targeted BiTE expression by genetically modified MV can achieve local recruitment of resting T cells and enhance anti-tumor immune responses.

To test these hypotheses, we first generated BiTE-encoding MV to analyze efficacy *in vitro* and *in vivo* in the context of an intact immune system. Specific aims of this project included:

- Generation of a syngeneic murine tumor model susceptible to MV entry and BiTE binding

via expression of human antigens

- *in vitro* evaluation of MV-BiTE vectors regarding replicative and cytotoxic potential

- Assessing functionality of MV-encoded BiTEs *in vitro* in terms of target cell binding and mediating specific tumor cell lysis by T cells

- Efficacy analysis of MV-BiTE using in the context of an intact immune system *in vivo*

- Dissecting the mechanism of action of MV-BiTE by immunological analyses ex vivo

Re-direction by CARs rather than BiTEs allows the use of a more defined antigen-specific effector cell population in terms of cell number and activation state. Establishing a CAR model to be used for analyses of MV-mediated effects on infiltration, anti-tumor activity, and persistence of T cells was the aim of the second part of this study. For longitudinal monitoring of T cell distribution *in vivo* via non-invasive magnetic resonance imaging, a protocol for labeling of T cells with iron oxide nanoparticles was to be evaluated.

The complexity of the immune system in the context of malignant disease in combination with oncolytic viruses requires careful choice of potential treatment regimens. Mathematical modeling can provide support in this respect by identification of crucial determinants of treatment success and by predicting outcomes of experimental treatment schedules *in silico*. To achieve this, we collaborated with mathematicians to conceive a model describing the dynamic interplay between tumor and immune compartments in the context of oncolytic virotherapy in combination with T cell re-direction strategies.

My overarching aim and personal motivation for my doctoral studies was to advance the development of safe and effective immunotherapies for cancer treatment, based on the promising combination of oncolytic viruses and T cell re-direction.

2 Materials and Methods

2.1 Materials

2.1.1 Cell lines

Cell line	Description	Obtained from
293GP	HEK 293T cells stably expressing gag and pol proteins, used for production of retroviral vectors by transient transfection	D. Abate-Daga, Tampa, FL, USA
B16	murine melanoma cell line	D. Nettelbeck, Heidelberg
B16-CD20	B16 cells stably expressing human CD20	C. Großardt, Heidelberg
B16-CD20-CD46	B16-CD20 lentivirally transduced for stable expression of human CD46	
B16-CD46	B16 cells lentivirally transduced for stable expression of human CD46	
Granta-519	human mantle cell lymphoma cell line expressing human CD20	DSMZ
HEK 293T	human embryonal kidney cells transformed with simian virus 40 large T antigen, used for production of lentiviral vectors by transient transfection	ATCC
HPAC	human pancreatic adenocarcinoma cell line	D. Abate-Daga, Tampa, FL, USA
PC05	primary pancreatic tumor cell culture	N. Kang and C. R. Ball, Heidelberg
Vero	African green monkey kidney epithelial cell line for production of recombinant measles viruses	ATCC

2.1.2 Cell culture media

Component	Obtained from
Advanced DMEM/F-12 medium	Thermo Fisher Scientific
Dulbecco's Modified Eagle's Medium (DMEM), high glucose, GlutaMAX Supplement, pyruvate	Thermo Fisher Scientific
Fetal bovine serum (FBS)	Biosera and PAN-Biotech
Human serum from human male AB plasma, USA origin, sterile filtered	Sigma-Aldrich
Opti-MEM I Reduced Serum Medium, GlutaMAX Supplement	Thermo Fisher Scientific
OptiPRO SFM	Thermo Fisher Scientific
Roswell Park Memorial Institute 1640 medium (RPMI), GlutaMAX Supplement	Thermo Fisher Scientific
X-VIVO 15, serum-free, L-glutamine, without gentamicin or phenol red	Biozym/ Lonza

2.1.3 Oligonucleotides

Name	Sequence 5' to 3'
mCD3 Fw	GTGCAACCAGGCAAATCTCT
His-tag BiTE Rev	GTGGTGATGATGGTGGTGAG
T-bet Fw	TAAGCAAGGACGGCGAATGTT
T-bet Rev	TGCCTTCTGCCTTTCCACAC
L13A Fw	GGCTGCCGAAGATGGCGGAG
L13A Rev	GCCTTCACAGCGTACGACCACC
FoxP3 Fw	GGCCCTTCTCCAGGACAGA
FoxP3 Rev	GCTGATCATGGCTGGGTTGT

2.1.4 Buffers and chemicals

Component	Manufacturer
1-Step Ultra TMB-ELISA Substrate Solution	Thermo Fisher Scientific
4',6-diamidino-2-phenylindole (DAPI)	Sigma-Aldrich
Accutase solution	Sigma-Aldrich
ACK Lysing Buffer	Lonza
Antibiotic Antimycotic Solution (ABAM) (100x)	Sigma-Aldrich
Aqua ad Injectabilia (RNase-free H_2O)	B. Braun
B27 supplement	Thermo Fisher Scientific
Bovine serum albumin (BSA)	Sigma-Aldrich
D-Glucose (Dextrose)	Thermo Fisher Scientific
Dimethyl sulfoxide (DMSO), sterile filtered	Sigma-Aldrich
Dulbecco's Phosphate Buffered Saline (DPBS), no calcium, no magnesium	Thermo Fisher Scientific
ELISA Stop Solution	Takara Bio
Fibroblast growth factor 10 (FGF10)	R&D Systems
Fibroblast growth factor basic (FGF2)	R&D Systems
Ficoll® Paque PLUS	GE Healthcare
FuGENE® HD Transfection Reagent	Promega
Heparin sodium salt	Sigma-Aldrich
HEPES solution (1M)	Sigma-Aldrich
Imidazole	Carl Roth
Isopropyl alcohol (2-propanol 99,8%)	Carl Roth
Kanamycin solution 10 mg/mL in 0.9% NaCl, suitable for cell culture	Sigma-Aldrich
L-Glutamine (200 mM)	Thermo Fisher Scientific
Lipofectamine 2000	Thermo Fisher Scientific
MS4A1 Human Recombinant Protein (CD20 full length)	Abnova
Nodal	R&D Systems
Penicilin-Streptomycin (Pen/Strep) (5,000 U/mL)	Thermo Fisher Scientific
Polybrene (Hexadimethrene bromide)	Sigma-Aldrich
Polyethyleneimine, branched, average Mw 25.000 by LS	Sigma-Aldrich
Protamine sulfate	Sigma-Aldrich
Recombinant human IL-2	BioLegend
RetroNectin Recombinant Human Fibronectin Fragment	Clontech/Takara Bio
Sodium Chloride	Carl Roth
Trypan Blue solution, 0.4%, sterile filtered, suitable for cell culture	Sigma-Aldrich
Trypsin-EDTA (0.05%), phenol red	Thermo Fisher Scientific
Tween20	Biotium

2.1.5 Antibodies

Name	Description	Manufacturer
anti-HA-biotin	rat IgG1κ, clone 3F10, 1:500 for ELISA	Sigma-Aldrich
anti-HA-PE	mouse IgG1κ, clone GG8-1F3.3.1, 1:5 for flow cytometry	Miltenyi Biotec
anti-His-FITC	mouse IgG1κ, clone 13/45/31-2, 1:5 for flow cytometry	Dianova
anti-human CD20-PE	mouse IgG2bκ, clone 2H7, 1:5 for flow cytometry	BD Biosciences
anti-human CD3	clone OKT3, 0.5 µg/mL for stimulation of human T cells	Abcam
anti-human CD46-PE	mouse IgG1κ, clone TRA-2-10, 1:20 for flow cytometry	BioLegend
anti-mCD25-PE-Cy7	rat IgG1κ, clone PC61, 1:100 for flow cytometry	BD
anti-mCD3-PerCP-Cy5.5	rat IgG2bκ, clone 17A2, 1:100 for flow cytometry	BD
anti-mCD4-APC-Cy7	rat IgG2bκ, clone GK1.5, 1:100 for flow cytometry	BD
anti-mCD69-PE	Armenian hamster IgG, clone H1.2F3, 1:80 for flow cytometry	BioLegend
anti-mCD8a-APC	rat IgG2aκ, clone 53-6.7, 1:100 for flow cytometry	BD
anti-mCTLA4-FITC	Armenian hamster IgG, clone 1B8	Thermo Fisher Scientific
Armenian hamster IgG-PE	isotype control, clone HTK888	BioLegend
Kiovig	human IgG and IgA, 1:60 for blocking in flow cytometry	Baxalta
mouse IgG1κ-FITC	isotype control, clone X40	BD
mouse IgG1κ-PE	isotype control, clone MOPC-21	BD
Protein L Biotin	1:300 for flow cytometry	Genscript
Purified Rat Anti-Mouse CD16/CD32 (Mouse BD Fc Block)	rat IgG2bκ, clone 2.4G2, 1:100 for blocking in flow cytometry	BD
rat IgG2aκ-APC	isotype control, clone R35-95	BD
rat IgG2bκ-APC-Cy7	isotype control, clone A95-1	BD
rat IgG2bκ-PerCP-Cy5.5	isotype control, clone A95-1	BD
Streptavidin-HRP	1:500 for ELISA	Dianova
Streptavidin-PE	1:100 for flow cytometry	BioLegend

2.1.6 Plasmids

Name	Description
pcDI-dsRed	mammalian expression vector encoding Discosoma sp. red fluorescent protein
pCG-L	mammalian expression vector encoding the measles virus large protein
pCG-N	mammalian expression vector encoding the measles virus nucleocapsid protein
pCG-P	mammalian expression vector encoding the measles virus phosphoprotein
pcpNSe-H-ATU	vector encoding Edmonston B vaccine lineage measles virus cDNA antigenome containing an additional transcription unit downstream of the *H* open reading frame (ORF) for virus rescue via RNA polymerase II
pcpNSe-H-hCD3xCD20	vector encoding Edmonston B vaccine lineage measles virus cDNA antigenome with hCDxCD20 BiTE downstream of the *H* ORF for virus rescue via RNA polymerase II
pcpNSe-H-hCD3xCEA	vector encoding Edmonston B vaccine lineage measles virus cDNA antigenome with hCDxCEA BiTE downstream of the *H* ORF for virus rescue via RNA polymerase II
pcpNSe-H-mCD3xCD20	vector encoding Edmonston B vaccine lineage measles virus cDNA antigenome with mCDxCD20 BiTE downstream of the *H* ORF for virus rescue via RNA polymerase II
pcpNSe-H-mCD3xCEA	vector encoding Edmonston B vaccine lineage measles virus cDNA antigenome with mCDxCEA BiTE downstream of the *H* ORF for virus rescue via RNA polymerase II
pcpNSe-ld-eGFP-mCD3xCD20	vector encoding Edmonston B vaccine lineage measles virus cDNA antigenome with enhanced green fluorescent protein in the leader position and mCDxCD20 BiTE downstream of the *H* ORF for virus rescue via RNA polymerase II
pLTR-RD114A	mammalian expression vector encoding RD114 envelope glycoprotein; RRID: Addgene 17576
pMDLg/pRRE, pRSV-rev, pMD2.VSV-G	vectors for production of non-replication competent lentiviruses
pMSGV1-Ha1-4.117scFv-28-BBZ	retroviral vector encoding a third-generation chimeric antigen receptor targeting human prostate stem cell antigen (PSCA3)
pMSGV1-Ha1-4.117scFv-28Z	retroviral vector encoding a second-generation chimeric antigen receptor targeting human prostate stem cell antigen (PSCA2)
pRRL.pptCMV-hCD46BC1.PRE	transfer vector encoding human CD46 for lentivirus production

2.1.7 Recombinant measles viruses

Virus name	Description
MV	unmodified measles virus of the Edmonston B vaccine lineage
MV-H-hCD3xCD20	measles virus of the Edmonston B vaccine lineage encoding an hCD3xCD20 BiTE downstream of the *H* ORF
MV-H-hCD3xCEA	measles virus of the Edmonston B vaccine lineage encoding an hCD3xCEA BiTE downstream of the *H* ORF
MV-H-mCD3xCD20	measles virus of the Edmonston B vaccine lineage encoding an mCD3xCD20 BiTE downstream of the *H* ORF
MV-H-mCD3xCEA	measles virus of the Edmonston B vaccine lineage encoding an mCD3xCEA BiTE downstream of the *H* ORF
MV-IgG	measles virus of the Edmonston B lineage encoding human immunoglobulin G4 downstream of the *H* ORF
MV-ld-eGFP-H-mCD3xCD20	measles virus of the Edmonston B vaccine lineage harboring an eGFP-encoding transgene in the leader position and an mCD3xCD20 BiTE-encoding sequence downstream of the *H* ORF
MV-Nivo	measles virus of the Edmonston B vaccine lineage encoding Nivolumab downstream of the *H* ORF
MV-Pembro	measles virus of the Edmonston B vaccine lineage encoding Pembrolizumab downstream of the *H* ORF

2.1.8 Kits and consumables

Product	Manufacturer
Amicon Ultra-15, PLGC Ultracel-PL Membran, 10 kDa	Merck
BCA Protein Assay Kit, Calbiochem-Novabiochem	Novagen
Cell lifter	Corning
Cell strainer 100 µm	Falcon
Colorimetric Cell Viability kit III	PromoCell
CytoTox 96 Non-Radioactive Cytotoxicity Assay kit	Promega
Maxima H Minus First Strand cDNA Synthesis Kit and oligo(dT)18 primers	Thermo Fisher Scientific
Needles (26G)	B. Braun
Nunc MaxiSorp plates	Thermo Fisher Scientific
Pan T cell Isolation Kit II, mouse	Miltenyi Biotec
Pestle for microcentrifuge tube	schuett-biotec
Power SYBR Green PCR Master Mix	Thermo Fisher Scientific
QIAshredder homogenizer columns	Qiagen
RNAlater RNA Stabilizing Reagent	Qiagen
RNeasy Protect Mini Kit	Qiagen
Syringes (1 mL)	B. Braun

2.2 Methods

2.2.1 MV-BiTE analysis *in vitro*

Generation of oncolytic measles virus (MV) genomes of the Edmonston B vaccine lineage encoding bispecific T cell engagers (BiTEs) and of lentiviral vectors encoding human CD46 for stable expression in transduced target cells was performed prior to the start of my doctoral studies and will be described here in brief. Detailed descriptions of the applied molecular cloning methods can be found elsewhere[149-151]. General methods describing the cloning, rescue, and propagation of recombinant oncolytic measles viruses and *in vitro* testing of virus constructs as well as of encoded immunomodulators have been published as a video protocol accompanied by a written manuscript[134].

General cell culture

Cell culture was performed in class II biological safety cabinets. Cells were propagated in humidified incubators at 37°C and 5% CO2. Adherent cells were grown in tissue-culture treated T75 or T175 cell culture flasks with filter caps. Murine melanoma B16 cells and derivatives and human pancreatic adenocarcinoma (HPAC) cells were cultured in Roswell Park Memorial Institute medium 1640 (RPMI) supplemented with 10% fetal bovine serum (FBS). HEK 293T cells, Vero cells, and 239GP cells were grown in Dulbecco's Modified Eagle's Medium (DMEM) supplemented

with 10% FBS. PC05 cells were cultured in DMEM Advanced F12+ medium supplemented with 1% glutamine, 2% B27 supplement, 5 mM HEPES, 12 µg/mL heparin, 6 mg/mL glucose, 10 ng/mL FGF2, 20 ng/mL FGF10, and 20 ng/mL Nodal, and accutase was used to detach cells. In general, cells were detached every two to three days by addition of 0.05% Trypsin-EDTA solution after washing wells with Dulbecco's Phosphate Buffered Saline (DPBS) and sub-cultured 1:2 – 1:20, according to cell density, in fresh medium. Cells were frozen for long-term storage after expansion at 1×10^6 cells/ mL in 1 mL cell type-specific medium supplemented with 20% FBS and 10% DMSO in screw-cap tubes. After resuspending in freezing medium, cells were directly placed in a Freezing Container (Thermo Fisher Scientific) containing isopropyl alcohol and transferred to -80°C. The next day, vials were transferred to liquid nitrogen in a designated storage tank. Frozen cells were thawed at 37°C for 1 min, immediately transferred to a 15 mL tube containing 9 mL cell type-specific medium, pelleted at 300 x g for 5 min, resuspended in 10 mL medium, and transferred to a T75 cell culture flask for propagation.

Generation of murine melanoma cell lines stably expressing human CD46

For stable expression of human CD46 in murine cell lines to allow for measles vaccine virus entry, I had generated replication-deficient lentiviruses encoding human CD46 isoform BC1 (hCD46BC1) during my master's thesis project prior to the start of my PhD studies as described previously[149]. Briefly, 1×10^7 HEK 293T cells had been incubated overnight on 15 cm dishes in 10 mL DMEM, 10% FBS before transient transfection. Transfection mix was prepared by adding 2.5 mL DMEM containing 126 µL 18 mM polyethylenimine (PEI) to 2.5 mL DMEM containing DNA plasmids (12.5 µg pMDLg/pRRE, 6.25 µg pRSV-rev, 9 µg pMD2.VSV-G, and 28 µg of transfer vector pRRL.pptCMV-hCD46BC1.PRE, into which I had introduced the hCD46BC1-encoding sequence from complementary DNA (cDNA)), mixing, and incubating at room temperature for 30 min. Medium on cells was replaced by fresh 10 mL DMEM, 10% FBS, transfection mix was added, and cells were incubated at 37°C, 5% CO2 overnight. The next day, medium was replaced with 12 mL fresh DMEM, 10% FBS, and incubation was continued for 24 h. Supernatant containing lentivirus particles was harvested and 12 mL fresh medium were added to the dish. The supernatant was kept at 4°C and stored until pooling with a second harvest after incubation of cells for another 24 h. For purification of lentiviruses, pooled supernatants were centrifuged for 5 min at 1,000 x g and 4°C prior to passing through 0.22 µm filters. Filtrates were then centrifuged for 2 h at 70,000 x g and pelleted lentiviruses were resuspended in 50 µL DPBS.

Murine melanoma cells B16 and B16-CD20, respectively, at 70% confluence were inoculated with purified lentivirus suspension diluted 1:100 in a total volume of 800 µL RPMI, 10% FBS, containing 8 µg/mL Polybrene. After incubation at 37°C, 5% CO2 overnight, cells were washed with PBS and detached from the plate by incubation with 250 µL Trypsin-EDTA solution for 5 min at room temperature. Cells were pelleted by centrifugation for 5 min at 300 x g, resuspended in 2 mL RPMI with 10% FBS and transferred to a T25 cell culture flask for expansion at 37°C, 5% CO2. After 13 days, CD46 expression was analyzed by flow cytometry using anti-CD46-PE antibody and CD46-positive cells were sorted into individual wells of a 96-well round-bottom plate by fluorescence-associated cell sorting using a BD FACSAria II flow cytometer. After outgrowth of clonal colonies, these were analyzed for CD46-expression on an LSR II flow cytometer and subjected to MV susceptibility testing. For this, 3×10^5 cells were inoculated with 3×10^5 and 3×10^4 cell infectious units (ciu), respectively, of MV encoding enhanced green fluorescent protein in the leader position and mCD3xCD20 BiTE downstream of the H gene (MV-ldeGFP-H-mCD3xCD20)

in 1 mL Opti-MEM. After 48 h of incubation at 37°C, 5% CO2, cells were analyzed for syncytia formation and eGFP expression using ZEISS AxioVert 200 fluorescence microscope and AxioVision software.

BiTE Design

Sequences of single chain variable fragments (scFvs) targeting human CD3 (antibody clone OKT3) and murine CD3 (antibody clone 145-2C11) were obtained from publicly available databases (EMBL-EBI European Nucleotide Archive: A22261, A22259; IMGT: AF000356, AF000357). Sequences were codon-optimized for expression in mice and synthesized by GeneArt Strings and Eurofins Genomics, respectively. scFvs against human CD20 and carcinoembryonic antigen (CEA) based on antibody clones B9E9 and MFE-23, respectively, were derived from anti-genomes of measles virus constructs re-targeted to these antigens by scFV fusion to hemagglutinin[143,152] by polymerase chain reaction (PCR). Variable heavy (VH) and light (VL) chains are connected by peptide linkers containing thrice the amino acid sequence of four glycin (G) and one serine (S) residues (G4S)3 to enable conformation analogous to the complementary-determining region (CDR) of the original antibodies[153,154]. A shorter version of the linker (G4S) was introduced between the two scFvs encoded in tandem by one BiTE sequence.

Generation of oncolytic measles viruses from anti-genomic DNA

Measles virus particles were rescued by co-transfection of Vero cells with recombinant DNA encoding the viral anti-genome (pcp-NSe) and plasmids encoding the N, P, and L proteins using the established reverse genetics system[135-137]. One day before transfection, $2x10^5$ Vero cells were seeded in a volume of 2 mL DMEM, 10% FBS, per well on a six well plate and incubated at 37°C and 5% CO2 overnight to achieve approximately 70 % confluence. The next day, in a total volume of 200 µL DMEM, 5 µg of the respective anti-genomic DNA, 500 ng each of pCG-N and pCG-L, and 100 ng each of pCG-P and pcDI-dsRed as a reporter of transfection efficiency were mixed. 18.6 µL of FugeneHD were added and the tube was mixed immediately by flicking, followed by 25 min incubation at room temperature (RT). Medium on Vero cells was replaced by 1.8 mL DMEM, 2% FBS, 50 µg/mL kanamycin. The transfection mix was added dropwise to the well and distributed by swirling. Cells were incubated at 37°C, 5% CO2 overnight before medium was replaced with 2 mL DMEM, 2% FBS, 50 µg/mL kanamycin. Incubation was continued and cells were observed daily by microscopy to detect syncytia formation. When syncytia were visible, cells were scraped into 1 mL Opti-MEM using a cell lifter to harvest viruses, followed by brief vortexing of the suspension prior to further virus propagation.

Propagation of oncolytic measles viruses

$6x10^6$ Vero cells were seeded in 12 mL DMEM, 10% FBS, on 10 cm dishes and incubated overnight to reach 80-90% confluency. Medium was replaced with 3 mL Opti-MEM and suspension obtained from MV rescue was added. Cells were incubated for at least 3 h at 37°C before 6 mL DMEM, 10% FBS were added and cells were transferred to 32°C, 5% CO2 for further incubation. After 48 to 72 h, when syncytia had spread throughout the whole cell monolayer, cells were scraped into 1 mL Opti-MEM. The suspension was snap-frozen in liquid nitrogen, thawed at 37°C, vortexed

three times for 10 s at half-maximal speed, and centrifuged at 5,000 x g for 5 min to remove cell debris. 100 µL of the resulting cell-free supernatant were used for titer determination and the rest was stored at -80°C.

For further propagation of viruses, $4x10^6$ Vero cells per dish were seeded in 12 mL DMEM, 10% FBS, on 15 cm dishes and incubated overnight. Vero cells were inoculated with virus at a multiplicity of infection (MOI) of 0.03, i.e. 0.03 cell infectious units (ciu) per Vero cell (or $3x10^4$ ciu per 10^6 cells), in a final volume of 8 mL Opti-MEM per plate. After at least 2 h of incubation at 32°C, 5% CO2, 8 mL DMEM with 10% FBS were added to each plate and incubation was continued until syncytia had spread across the entire cell layer approximately 60 h post inoculation. To harvest virus, media was removed and cells were scraped from the plate bottom. Scraped cells infected with the same virus constructs were pooled in 50 mL tubes, subjected to a freeze-thaw cycle, vortexed briefly, and centrifuged at 2,500 x g for 5 min. Supernatants were transferred to screw-cap tubes in 500 µL aliquots and stored at -80°C.

Viral titer determination by Vero titration assay

For evaluation of viral titers, 90 µL DMEM, 10% FBS were transferred to each well of a 96-well plate. Into each well of the first row, 10 µL of one virus aliquot were added after brief vortexing to homogenize the suspension, yielding eight technical replicates. Using a multi-channel pipet, wells were mixed by pipetting up and down for at least 10 times and 10 µL of each well were transferred to the next row. This was repeated for the whole plate to prepare serial ten-fold dilutions of the virus suspension. 10 µL from each well of the last row were discarded to obtain equal volumes. $1.5x10^4$ Vero cells in 100 µL DMEM, 10% FBS, were added to each well and plates were incubated for 48 h at 37°C, 5% CO2. By light microscopy, the row with highest dilution of virus showing formation of syncytia was identified. Syncytia were counted in each well of that row, and the average number of syncytia per well was assessed. Viral titers were calculated by multiplication of the identified average number of syncytia with the dilution factor of the respective row (10^2 for the first row, containing 10^{-2} mL virus per well), yielding values of cell infectious units per mL virus suspension. For each virus, average titers of three independent aliquots were determined and used to calculate amounts of viral suspension used for further experimentation.

Viral replication kinetics

For assessing viral replication kinetics by one-step growth curve experiments, $1x10^5$ Vero, Granta-519, or murine melanoma cells per well were seeded in 1 mL of cell type-specific medium on 12-well plates in duplicates for each of the six time points of interest (12, 24, 36, 48, 72, 96 h post inoculation) and incubated at 37°C, 5% CO2. After 24 h, medium on cells was replaced with 300 µL Opti-MEM containing the respective virus at an MOI of 1 and cells were incubated for 12 h before medium was replaced by 1 mL of cell type-specific medium per well. At indicated time points, cells were scraped directly into the medium, snap-frozen in liquid nitrogen and stored at -80°C until samples from all time points were collected. Samples were thawed, vortexed, and centrifuged at 2,500 x g for 5 min simultaneously and titers were determined for each sample in quadruplicates on Vero cells by titration assay.

Virus-mediated cyototoxicity

To assess cytotoxic potential of oncolytic measles viruses, cell viability following virus inoculation was determined by 2,3-Bis-(2-methoxy-4-nitro-5-sulfophenyl)-2H-tetrazolium-5-carboxanilide (XTT) assay. For this, $1x10^5$ Vero or murine melanoma cells per well were seeded in 1 mL of cell type-specific medium on 12-well plates in triplicates for each time point and incubated at 37°C, 5% CO2 for 24 h. Medium was then replaced with 300 µL Opti-MEM only (mock) or Opti-MEM containing the respective virus at an MOI of 1. Cells were incubated for 12 h before medium was replaced by 1 mL of cell type-specific medium per well. At 12, 24, 36, 48, 72, and 96 h post inoculation, metabolic activity of cells was assessed using Colorimetric Cell Viability kit III according to the manufacturer's instructions. Briefly, medium was removed and 300 µL of freshly prepared substrate solution were added to each well and incubated until the reagent in the mock control wells had turned deep red. Supernatant was collected from each well and stored at -20°C until samples from all time points had been obtained. After thawing, 100 µL of each sample were transferred to a 96-well plate and absorbance at 450 nm was measured using Infinite M200 microplate reader and i-control software v1.6.19.2 (Tecan). Background absorbance at a reference wavelength of 630 nm was subtracted for each sample. Mean percentages were calculated for each sample relative to average mock values obtained for the respective time point.

Production, isolation and purification of MV-encoded BiTEs

For production of BiTEs from virus-infected cells (virus-derived BiTEs, vBiTEs), Vero cells were grown to 70% confluency in T175 flasks in 12 mL DMEM, 10% FBS at 37°C, 5% CO2. Medium was removed and cells were washed twice with PBS to remove residual FBS. 12 mL serum-free medium OptiPRO SFM containing BiTE-encoding MV at MOI of 0.03 was added to the cells. After 12 h of incubation, medium was replaced with 12 mL fresh OptiPRO SFM. Approximately 40 h post virus inoculation, when syncytia had formed but not yet spread entirely across the flask, cells were transferred to 32°C, 5% CO2 for additional 24 h of incubation to enhance BiTE secretion while preventing bursting of infected cells. Supernatants were then carefully collected and transferred to 50 mL tubes. Cell debris was removed by centrifugation for 5 min at 2,500 x g and cell-free supernatant was sterile-filtered by passing through a 0.22 µm filter with a syringe.

Affinity exchange chromatography was performed with QIAquick Ni-NTA Spin Columns to isolate vBiTEs via the hexa-histidine tag. Centrifugation of columns was 2 min with open lids at 800 x g for equilibration, washing, and elution steps and 5 min at 200 x g with closed lids following loading with supernatant. All steps were performed at 4°C and all solutions were kept on ice. Columns were equilibrated with 600 µL washing buffer 1 (WB1: DPBS, 200 mM sodium chloride, 10 mM imidazole, pH 8.0) each, followed by loading with 600 µL filtered supernatant. Several columns, six to eight in most cases, were used in parallel, depending on total volume of the collected supernatant. Each column was loaded up to twelve times with fresh supernatant, with a washing step with 600 µL WB1 after every third loading. After the last loading, columns were washed three times with WB1 and once with WB2 (DPBS, 200 mM sodium chloride, 20 mM imidazole, pH 8.0) before bound protein was eluted from the column matrix using elution buffer 5 (EB5: DPBS, 200 mM NaCl, 500 mM imidazole, pH 7.0). For desalting and to increase concentration of vBiTE, eluates from the same production were pooled, diluted with DPBS to a final volume of 15 mL, and transferred to Amicon Ultra-15 Centrifugal Filter Units with Ultracel-10 membranes. Tubes were centrifuged for 10 min at 4,000 x g, flow-through was discarded and the suspension

remaining above the membrane, containing concentrated vBiTE, was diluted to 15 mL with DPBS again. This was repeated twice to remove residual ions from the elution buffer. By final centrifugation for 30 min at 4,000 x g and 4°C, vBiTE suspension volumes were reduced to approximately 200 µL. vBiTE was stored at -80°C in 10 µL aliquots for further use.

Protein quantification

Bicinchoninic acid (BCA) assay was performed using BCA Protein Assay Kit according to the manufacturer's instructions to determine protein concentration of vBiTE solutions. Briefly, a two-fold dilution series of bovine serum albumin (BSA) in DPBS, starting at 2 mg/mL, was prepared. The vBiTE samples of interest and duplicates of each BSA concentration and DPBS alone were transferred to a 96-well plate and incubated with freshly prepared working solution containing BCA and cupric sulfate for 30 min at 37°C. Absorption at 562 nm was then measured using Infinite M200 microplate reader. A standard curve was calculated for the BSA dilution series and vBiTE concentration was determined accordingly by fitting the measured absorbance value to the standard curve.

Enzyme-linked immunosorbent assay (ELISA)

For detection of BiTE present in the supernatant of cells after inoculation with MV-BiTE, ELISA was performed on Nunc MaxiSorp 96-well plates coated with 100 ng recombinant human CD20 full length protein in 100 µL DPBS per well at 4°C overnight. Wells were washed twice with DPBS and blocked with 200 µL DPBS containing 5% FBS per well for 2 h at room temperature. Wells were washed thrice with PBS before 100 µL of cell-free supernatant or medium only were added per well and incubated for 2 h at room temperature, followed by three washing steps with DPBS, 0.05% Tween20. 100 µL anti-HA-biotin, diluted 1:500 in DPBS containing 5% FBS, were added to each well and incubated for 1 h at room temperature. Then, plates were washed five times with DPBS, 0.05% Tween20 and 100 µL streptavidin-coupled horseradish peroxidase diluted 1:500 in DPBS, 5% FBS were added to each well. After incubation for 15 min at room temperature, plates were washed seven times with DPBS, 0.05% Tween20 and 100 µL 1-Step Ultra TMB-ELISA Substrate Solution were applied to each well. Reaction was stopped after 30 min by adding 100 µL Stop Solution to each well and absorbance was measured at 450 nm using Infinite M200 microplate reader. Background absorbance at 570 nm was subtracted.

Isolation of human immune cells from peripheral blood

To isolate human peripheral blood mononuclear cells (PBMCs), blood was drawn from healthy donors into a syringe containing 123 µL 0.5 M ethylenediaminetetraacetic acid (EDTA) per 10 mL blood to prevent coagulation. Blood was diluted 1:1 with PBS, 2 mM EDTA and carefully layered on top of 15 mL Ficoll-Paque PLUS in a 50 mL tube. After centrifugation for 30 min at 400 x g and 20°C and without brakes, the PBMC-containing interphase between Ficoll and serum layers was transferred to a fresh 50 mL tube using a Pasteur pipet. DPBS was added to a final volume of 50 mL and cells were pelleted at 300 x g for 10 min. Washing was repeated twice before cells were resuspended in 1 to 10 mL DPBS for counting using a hemacytometer after dilution of 10 µL cell suspension in 90 µL of Trypan blue.

Isolation of murine splenocytes and enrichment of T cells by negative magnetic selection

For isolation of murine splenocytes, mice were killed by cervical dislocation. Spleens were explanted, transferred to 2 mL microcentrifuge tubes containing DPBS, and kept on ice. Spleens were passed through 100 µm cell strainers into individual 50 mL tubes containing a total volume of 10 mL DPBS. Cells were pelleted by centrifugation for 10 min at 300 x g and resuspended in 1 mL ACK lysing buffer to remove residual erythrocytes. After 10 min incubation at room temperature, 9 mL DPBS were added and cells were pelleted again. If red cells were still visible in the pellet, ACK lysis was repeated for 5 min at room temperature. Cells were resuspended in 10 mL DPBS and counted.

Separation of CD3+ T cells by negative selection was performed using Pan T cell Isolation Kit II, mouse according to the manufacturer's instructions. Briefly, separation buffer (DPBS, 0.5% BSA, 2 mM EDTA) was prepared and splenocytes were resuspended at 10^7 cells per 40 µL buffer. Per 40 µL buffer, 10 µL Biotin-Antibody Cocktail were added, mixed, and incubated for 5 min at 4°C. Subsequently, 30 µL buffer and 20 µL Anti-Biotin MicroBeads were added per 10^7 cells, respectively. After mixing, cells were incubated for 10 min at 4°C. LS columns were equilibrated with 3 mL buffer on a MACS Separator (Miltenyi Biotec) before cell suspension was added. Flow-throughs of loading with cell suspension and of subsequent washing with 3 mL buffer were collected, containing unlabeled T cells. Purified T cells were counted using a hemacytometer.

Flow cytometry-based BiTE binding assay

Binding of BiTEs to target tumor and immune cells by flow cytometry was assessed using phycoerythrin (PE)- and fluorescein isothiocyanate (FITC)-conjugated antibodies targeting BiTE-associated HA- and His-tags, respectively. For this, 10^6 cells were incubated with 1 µL Purified Rat Anti-Mouse CD16/CD32 for mouse cells and 0.83 µL Kiovig for human cells, respectively, to block unspecific binding to immunoglobulins, in 50 µL DPBS, 1% FBS, for 5 min at room temperature. Indicated amounts of MV-BiTE or vBiTE, typically 3 µL, were added and cells were incubated for 30 min on ice. Cells were washed by adding 1 mL DPBS, 1% FBS, and centrifugation at 300 x g and 4°C for 5 min. Cells were resuspended in a total volume of 50 µL DPBS containing 1% FBS and either anti-HA-PE or anti-His-FITC antibody was added at respective dilutions indicated in 2.1.5. After incubation for 30 min on ice, cells were washed as before and resuspended in 500 µL DPBS contai.ning 0.2 µg/mL 4',6-diamino-2-phenylindole (DAPI) for. staining of dead cells. Cells were directly washed again, resuspended in 300 µL DPBS, 1% FBS and transferred to flow tubes prior to analysis on an LSR II flow cytometer using BD FACSDiva software. For analysis of CD20 expression, cells were incubated for 30 min on ice once with anti-CD20-PE antibody instead of subsequent staining with BiTE and tag-specific antibody. For all flow cytometry analyses, appropriate single stain controls were applied for compensation and isotype controls were analyzed to control for unspecific binding by antibodies. Flow cytometry data were analyzed using BD FACSDiva v8.0.1 (BD Biosciences) and FlowJo VX v10.0.7r2 (TreeStar, Inc.) software.

Lactate dehydrogenase (LDH) release assay

To analyze BiTE-mediated cytotoxicity in co-cultures of target tumor and immune effector cells, LDH release assay was performed using Promega CytoTox 96 Non-Radioactive Cytotoxicity Assay

kit according to the manufacturer's instructions. In brief, 40 µL PBMC medium (RPMI, 10% FBS, 10 mM HEPES, 1% ABAM) containing 5,000 target cells (T) were added to a round-bottom 96-well plate. 40 µL PBMC medium containing 125,000 effector cells (E) were added for an E:T-ratio of 50:1. 20 µL PBMC medium containing vBiTE suspension were added to achieve indicated final concentrations. Each sample and control was prepared in triplicates. Controls containing medium only, target cells only (Tsp), and effector cells only (Esp) were included. For target cells only and medium only, additional controls were included for assessing maximum target cell (Tmax) lysis by addition of detergent and the appropriate volume control, respectively. Plates were incubated at 37°C for 24 h in case of human PBMCs as immune effector cells and for 48 h for murine T cells. 10 µL of 10x lysis solution were added to each well containing maximum target cell lysis and volume controls, respectively, and incubation was continued for 45 min.

Successful cell lysis was verified by light microscopy. Plates were then centrifuged for 4 min at 250 x g and 50 µL of cell-free supernatants were transferred carefully to a clean flat-bottom 96-well plate. To each well, 50 µL of freshly prepared substrate solution were added and plates were incubated for approximately 30 min at room temperature, until maximum lysis controls had turned deep red. Reaction was stopped by addition of 50 µL stop solution to each well. Air bubbles were removed by centrifugation for 1 min at 4,000 x g and absorbance was measured at 490 nm using Infinite M200 microplate reader. Background correction for Tmax samples was performed by subtracting average value of volume controls. For all other samples and controls, the average absorbance of medium controls was subtracted. Average values were calculated for background-corrected Tmax, Tsp, and Esp values, and % specific lysis was calculated for each sample using the following equation: $\% \ specific \ lysis = \frac{sample \ value - T_{sp} - E_{sp}}{T_{max} - T_{sp}} x 100$.

Ultraviolet C (UV) inactivation of MV-BiTE

UV irradiation of MV-BiTE was performed using UV Stratalinker 2400 (Stratagene). For complete inhibition of viral replication, $2x10^7$ ciu MV-BiTE diluted in 2 mL Opti-MEM in a 2 mL microcentrifuge tube were irradiated at a dose of 1.5 J/cm2 (cUV). For partial inhibition, the same dose was applied to a 1.5 microcentrifuge tube containing 500 µL undiluted virus suspension.

2.2.2 MV-BiTE *in vivo*

Animal experimentation

All animal experiments performed in the course of my doctoral studies in Heidelberg were approved by the Animal Protection Officer at the German Cancer Research Center (DKFZ) and by the regional council according to the German Animal Protection Law. In general, mice were kept in groups of five or less in specific pathogen-free individually ventilated cages with permanent access to enrichment, food, and drinking water in the Center for Preclinical Research of the DKFZ. For subcutaneous and intratumoral injections, 1 mL syringes and hollow 26 G needles were used. After tumor implantation, mice were checked daily for signs of illness, tumor diameters were assessed every two to three days by caliper measurement, and mouse weights were measured once weekly. Termination criteria resulting in immediate sacrifice of the respective animal were defined as tumor volume (calculated by largest diameter x smallest diameter^2 x 0.5) > 1000 mm^3, tumor

diameter > 15 mm, tumor ulceration, weight loss of > 20% within one week, or other signs of severe illness such as ill-kempt fur, hunched posture, heavy breathing, or apathy.

Tumor model

For analysis of MV-BiTE *in vivo*, 1×10^6 B16-CD20-CD46 cells of low passage number were washed twice with DPBS, resuspended in 100 µL DPBS, and injected subcutaneously into the right flank of six- to eight-week-old female C57BL/6 mice. Treatment was initiated when tumors had reached average volumes of 35-40 mm³ for survival experiments and 60-70 mm³ for mechanistic analyses. Mice were stratified into treatment groups to achieve similar distribution of tumor sizes and similar average volumes per group. After stratification, the experimenter was blinded to intervention until the experiment ended, including during treatments, tumor measurements, and sample analyses. Mice were treated by five intratumoral injections with indicated viruses or control treatments on consecutive days.

MV immunization and serum neutralization assay

Prime-boost vaccination of naïve C57BL/6 mice was performed 16 and 9 days prior to tumor implantation, respectively. At both time points, animals received intraperitoneal injections of 1×10^6 ciu of highly purified MV-NIS. A previously described *in vitro* neutralization assay[155] was performed with minor modifications to confirm presence of neutralizing antibodies against measles virus in the blood of immunized mice before start of the survival experiment. From the saphenous veins of pre-immunized and naïve control mice, blood was drawn into heparin-coated tubes and centrifuged for 10 min at 10,000 x g and 4°C for serum isolation. Sera were transferred to clean microcentrifuge tubes and heat inactivated by incubation in a 56°C water bath for 30 min. In a 96-well plate, 20 µL of serum were added to the wells of the first column containing 80 µL Opti-MEM to achieve a five-fold dilution. After mixing by pipetting, serial two-fold dilutions were prepared by transferring 50 µL from each well to the next column containing 50 µL Opti-MEM per well. When finished, 50 µL were discarded from each well of the last row to equalize volumes. Subsequently, 50 µL Opti-MEM containing 50 ciu of unmodified MV were added to each well and incubated for 1 h at 37°C, 5% CO2. Next, 2×10^4 Vero cells in 100 µL DMEM were added to each well and incubation was continued for 72 h at 37°C, 5% CO2 before presence of syncytia was assessed via light microscopy.

Ex vivo analysis

For survival analyses, tumor growth was followed until termination criteria were reached. For mechanistic analyses, mice were sacrificed at indicated time points, i.e. one day after the last treatment for flow cytometry, reverse transcription quantitative real time polymerase chain reaction (RT-qPCR) analysis of FoxP3 and T-bet expression, and targeted transcriptome analyses and directly after the first and the last treatment and one, two, and five days after the last treatment, respectively, for time course analysis of MV-N and BiTE expression.

Subcutaneous tumors were explanted and partitioned using a scalpel. Tumor samples to be analyzed by flow cytometry on the same day were kept in DPBS on ice, and for RNA analyses in

RNAlater RNA Stabilizing Reagent for up to seven days at 4°C, then transferred to -20°C in case of longer storage.

For flow cytometry analysis, single cell suspensions were prepared by passing tumors through 100 µm cell strainers into 50 mL tubes containing 10 mL DPBS. Cells were counted as described above and 2×10^6 cells per sample were resuspended in 100 µL DPBS, 1% FBS and incubated subsequently with mouse Fc block, specific antibodies, and DAPI as described above. Single stain controls, isotype controls, and fluorescence minus one (FMO) controls were prepared for compensation and gating. Samples were analyzed in 300 µL DPBS, 1% FBS, in flow tubes on a BD LSR II cytometer.

For RT-qPCR and targeted transcriptome analysis, total RNA was isolated from tumors using Qiagen RNeasy Mini Kit according to the manufacturer's instructions. All steps were carried out at room temperature. In brief, 30 mg tumor samples were disrupted in 600 µL Buffer RLT in 1.5 mL microcentrifuge tubes with a pestle (schuett-biotec), followed by homogenization. For this, tumor samples were loaded onto QIAshredder homogenizer columns placed in 2 mL microcentrifuge tubes and centrifuged for 2 min at 16,000 x g. Columns were removed and tubes were centrifuged for 3 min at 16,000 x g. Supernatants were transferred to clean tubes and an equal volume of 70% ethanol was added. Samples were mixed by pipetting up and down, transferred to RNeasy spin columns on 2 mL collection tubes, and centrifuged at 8,000 x g for 15 s. Flow-throughs were discarded and columns were washed thrice by adding 700 µL Buffer RW1 once and 500 µL Buffer RPE twice, with centrifugation steps as before and discarding of flow-throughs in between. The last washing step was performed with centrifugation for 2 min at 8,000 x g, followed by 1 min at 8,000 x g in a fresh collection tube to eliminate residual RPE buffer. RNA was eluted in 30 µL RNase-free H_2O into a clean 1.5 mL collection tube by centrifugation for 1 min at 8,000 x g.

Complementary DNA (cDNA) was synthesized from mRNA using the Maxima H Minus First Strand cDNA Synthesis Kit according to the manufacturer's instructions. Briefly, 500 ng RNA were mixed with 100 pmol of oligo(dT)18 primers and 1 µL dNTP mix containing 10mM of each dATP, dGTP, dCTP, and dTTP in a final volume of 14.5 µL nuclease-free H_2O. 4 µL 5x RT Buffer, 0.5 µL RiboLock RNase Inhibitor, and 200 U Maxima H Minus Reverse Transcriptase were added to a final volume of 20 µL. The reaction mix was mixed carefully by flicking the tube, centrifuged shortly to collect all liquid at the bottom of the tube, and incubated for 30 min at 50°C. The product containing cDNA was then stored at -20°C until further processing.

qPCR reactions were set up in triplicates in LightCycler 480 Multiwell Plate 96 plates containing 1 µL of cDNA synthesis product, each primer of the respective target-specific primer pair at a final concentration of 0.2 µM, and 10 µL Power SYBR Green PCR Master Mix in a final volume of 20 µL per well. Control samples without template and of reverse transcription reaction mixes lacking reverse transcriptase were included for each run. Reactions were performed on a cobas z 480 instrument. Each run started with an initial denaturation step for 10 min at 95°C. Forty cycles followed, consisting of denaturation for 5 s at 95°C, annealing and extension for 1 min at 55°C (for T-bet), 60°C (for BiTEs, FoxP3, and L13a), or 62°C (for MV-N), and fluorescence detection for 5 s at 77°C (for T-bet, FoxP3, and L13a), 78°C (for MV-N), 80°C (for mCD3xCEA BiTE), or 84°C (for mCD3xCD20 BiTE). Data analysis was performed using LightCycler 480 Software version 1.5.

For targeted transcriptome analysis using NanoString nCounter technology[156], RNA samples containing 100 ng RNA in 1 µL H_2O were prepared and submitted to the nCounter Core Facility

Heidelberg for further processing. RNA quality was assessed using Agilent Bioanalyzer 2100 and Qubit system and 25 ng RNA per sample were hybridized with the Mouse CodeSet Immunology Panel. Hybridized RNA was quantified on nCounter SPRINT Profiler and data was obtained from the nCounter Core Facility. Data was analyzed using nSolver 4.0 software and Advanced Analysis package after normalization of raw data to a pre-defined set of reference genes included in the Mouse CodeSet Immunology Panel.

2.2.3 CAR T cell methods

Production of retroviral vectors

Chimeric antigen receptor (CAR)-encoding retroviral vectors for transduction of human T cells were produced by transient transfection of 293GP cells. For this, $6x10^6$ cells were seeded in 10 mL DMEM, 10% FBS on a 10 cm dish and incubated overnight at 37°C, 5% CO2. The next day, 1.5 mL Opti-MEM containing 4.5 µg plasmid encoding RD114 envelope protein (pLTR-RD114A) and 9 µg CAR-encoding transfer plasmid (pMSGV1-Ha1-4.117scFv-28Z for second generation or pMSGV1-Ha1-4.117scFv-28-BBZ for third generation anti-PSCA CAR) and 1.5 mL Opti-MEM containing 60 µL Lipofectamine 2000 transfection reagent were prepared in 15 mL tubes and incubated separately for 5 min at room temperature. After transferring the plasmid-containing mix into the tube containing the transfection reagent and pipetting up and down once, the final transfection mix was incubated for 20 min at room temperature. During incubation, medium on the 293GP cells was replaced with 10 mL of fresh DMEM, 10% FBS. The transfection mix was carefully added dropwise to the cells to avoid mechanic detachment. After incubation for 6-8 h at 37°C, 5% CO2, medium on the cells was replaced with 10 mL DMEM, 10% FBS, 1% penicillin/streptomycin solution (Pen/Strep) and incubation was continued. Forty-eight hours post transfection, supernatant was harvested, passed into a 15 mL tube through a 0.45 µm filter using a syringe, and stored at -80°C. Ten milliliters of fresh DMEM, 10% FBS, 1% Pen/Strep were added to the cells and incubation was continued for 24 h before supernatant was harvested, filtered, and stored as before.

Retroviral transduction of human T cells

Human PBMCs were derived from peripheral blood as described in 2.2.1 and resuspended at $1x10^6$ cells/ mL in X-VIVO 15 medium supplemented with 5% human serum, 1% anti-biotic/anti-mycotic solution (ABAM), and 50 IU/ mL IL-2 (from here on referred to as T cell medium, TCM). To a non-tissue culture-treated (NTC) 24-well plate, 1 mL medium containing cells was added per well. Cells were stimulated by adding 0.5 µg/mL OKT3 antibody, followed by incubation for two days at 37°C, 5% CO2. On day two post stimulation, two NTC 6-well plates were prepared for transduction by incubation with 1.5 mL DPBS containing 20 µg/ mL RetroNectin per well for each virus construct for 2 h at room temperature. Subsequently, RetroNectin solution was removed and stored at -20°C to be re-used up to three times. Plates were blocked for 30 min at room temperature with 2 mL DPBS, 2% bovine serum albumin (BSA) per well. Following removal of BSA solution, wells were washed with 2 mL DPBS, and 2 mL of filtered supernatant from retrovirus production were added to the respective wells. Both plates were centrifuged at 2,000 x g and 32°C for 2 h. One plate was used directly for transduction and the other one was stored at 4°C in an autoclaving bag overnight for a second transduction on the following day.

For transduction, stimulated T cells were pooled from the 24-well plate, counted, and resuspended at $5x10^5$ cells/ mL in fresh TCM. To designated wells on the prepared 6-well plate, 4 mL of cell suspension, i.e. $4x10^6$ cells per well, were added. Excess cell suspension was cultured in a T25 NTC flask as untransduced T cell control (UT). In general, T cells were sub-cultured twice a week and kept at densities between $3x10^5$ and $3x10^6$ cells per mL. The plate containing cells and virus was centrifuged for 10 min at 1,000 x g and 32°C to collect the cells at well bottoms and subsequently incubated at 37°C, 5% CO2 overnight. The next day, cells were transferred to the previously prepared plate to increase transduction efficiency. Cells were collected at the bottom of the wells as before and again incubated at 37°C, 5% CO2 overnight. Following transduction, on day four post stimulation, cells were transferred from the 6-well plate to 15 mL tubes, spun down for 5 min at 300 x g, resuspended at $1x10^6$ cells/ mL in fresh TCM, and incubated in NTC cell culture flasks at 37°C, 5% CO2.

Flow cytometry analysis of CAR expression by human T cells

Three days after transfer of transduced cells to culture flasks and directly before use in an experiment, CAR expression by human T cells was analyzed via flow cytometry using Protein L, which binds immunoglobulin light chains, including unstained, single-stained, and UT samples as controls. For this, $2x10^5$ cells per sample were washed twice with DPBS, 2% BSA to remove residual TCM, which would interfere with staining using Protein L due to presence of immunoglobulins in human serum. All centrifugation steps were performed at 300 x g and 4°C for 5 min. Cell were then incubated with 1 µL Protein L-Biotin in a total volume of 300 µL DPBS, 2% BSA for 30 min on ice. After washing twice with DPBS, 2% BSA, Protein L-bound cells were stained with 1 µL streptavidin in 100 µL DPBS for 30 min on ice. Cells were then washed once with DPBS, 2% BSA, resuspended in 500 µL DPBS, 2% BSA, 0.2 µg/ mL DAPI, and acquired in flow tubes using a BD LSR II flow cytometer.

Impedance-based cell viability assay

CAR T cell-mediated cytotoxicity was analyzed using impedance measurement via the xCELLigence RTCA MP system (ACEA Biosciences Inc.) as a surrogate for viability of adherent target cells. For this, following a background measurement with 50 µL medium only per well, $1x10^4$ human pancreatic adenocarcinoma (HPAC) cells or PC05 cells in 50 µL cell type-specific medium per well were added to an appropriate 96-well plate, placed in the instrument, and incubated overnight at 37°C, 5% CO2 to allow attachment to the well bottom. The next day, 10 µL TCM or indicated virus suspensions were added to respective wells and incubated at 37°C, 5% CO2 for 2 h. All samples were set up in three technical replicates. Following incubation, 90 µL TCM or indicated T cell suspensions were added to the respective wells and incubation was continued for three to five days. Impedance measurements were performed automatically every five minutes, starting directly after cell seeding and paused when plates were taken out to add virus or effector cells, and values were normalized to the time point after last addition to the wells.

In vivo analysis of MV and CAR T cell combinations

A pilot experiment investigating combination treatments of intratumoral MV or MV-BiTE application with adoptive transfer of UT or CAR T cells in immunodeficient mice bearing human xenograft tumors was performed at H. Lee Moffitt Cancer Center and Research Institute, Tampa, FL, USA in the course of my research visit in Dr. Daniel Abate-Daga's laboratory. All experimental procedures were approved by the Institutional Animal Care and Use Committee (IACUC) at the University of South Florida. Mice were housed under specific pathogen-free conditions in accordance with IACUC standards at the H. Lee Moffitt Cancer Center and Research Institute. $2x10^6$ HPAC cells were implanted subcutaneously in six- to eight-week-old female NOD.Cg-$Prkdc^{scid}$ $Il2rg^{tm1Wjl}$/SzJ (NSG) mice obtained from The Jackson Laboratory (Bar Harbor, ME, USA). When tumors had reached an average volume of 40 mm^3, they were treated by intratumoral injections of $1x10^6$ unmodified MV or MV encoding CEA-targeting BiTE (MV-hCD3xCEA) or medium only in a volume of 100 µL on four consecutive days. One day later, mice received $1x10^6$ PSCA2 CAR-expressing human T cells or the corresponding amount of untransduced T cells in 100 µL DPBS via tail vein injection by expert staff of the animal facility at Moffitt. Mice treated with T cells received $2.2x10^5$ IU recombinant human IL-2 in 200 µL DPBS intraperitoneally on the day of T cell injection and the two following days, respectively. Tumor volumes were measured every two to three days and animals were sacrificed 30 days post T cell transfer to prevent potential onset of graft-versus-host disease. Throughout the experiment, animals were monitored every day and no signs of illness were observed. Spleens were explanted, single cell suspensions of splenocytes were prepared and analyzed for human CD3 expression by flow cytometry as described in 2.2.1.

T cell labeling with iron oxide nanoparticles

Human T cells obtained from human peripheral blood and stimulated as described above (2.2.3) were labeled with superparamagnetic iron oxide nanoparticles CLIO-FITC or ferumoxytol[*] in NTC 24-well and 6-well plates, respectively. For labeling with CLIO-FITC to be analyzed via flow cytometry, $1x10^6$ cells in 250 µL RPMI, 10 ng/mL IL-2 were used per well. For ferumoxytol labeling and later magnetic resonance imaging (MRI), $4x10^6$ cells in 1 mL medium were used. Heparin was added to a final concentration of 20 IU/mL and mixed by gentle swirling of the plate. Next, protamine sulfate was added at a final concentration of 30 µg/mL, or of 60 µg/mL for comparison, followed by swirling the plate, before nanoparticles were added to a final iron concentration of 100 µg/mL. After swirling the plate, cells were incubated for 4 h at 37°C, 5% CO2 before an equal volume of RPMI, 10 ng/mL IL-2, 20% FBS was added to each well. Incubation was continued overnight. Cells were then collected, washed once with DPBS and twice with DPBS, 10 IU/mL heparin, and resuspended in 300 µL DPBS, 0.2 µg/mL DAPI in a flow tube for analysis using an LSR II flow cytometer, or in 50 µL DPBS for 3D T2*-weighted MRI in a capillary phantom using a 9.4T small animal imaging system (BioSpec94/20 USR, Bruker BioSpin MRI GmbH)[†].

---

[*]both kindly provided by Dr. Dr. Michael Breckwoldt, Heidelberg University Hospital
[†]performed by Manuel Fischer, Heidelberg University Hospital

2.2.4 Statistical analyses

All statistical analyses were performed using GraphPad PRISM software version 6.04 (GraphPad Software). For statistical analyses of column data with one independent variable, one-way ANOVA was performed and p values were adjusted for multiple comparisons by Tukey test. Two-way ANOVA with p values adjusted for multiple comparisons by Sidak test was used to statistically analyze grouped data with two independent variables. Statistical comparisons of Kaplan-Meier survival curves were conducted using Mantle-Cox log-rank test with adjustment of p values for multiple comparisons via Bonferroni correction.

3 Results

The hypothesis underlying the present study is that efficacy of T cell re-direction immunotherapies against solid tumors can be enhanced by combination with oncolytic measles virotherapy. We furthermore hypothesized local antitumor activity of bispecific T cell engagers (BiTEs) encoded by oncolytic measles viruses (MV). To test these hypotheses, in the first part of the project, a novel syngeneic murine tumor cell line expressing human antigens allowing for measles virus entry and BiTE binding was generated, as well as BiTE-encoding MV (MV-BiTE) vectors. Kinetics of MV-BiTE replication and cytotoxicity were analyzed *in vitro* and binding specificities and functionality of virus-encoded BiTEs were investigated. MV-BiTE efficacy *in vivo* was assessed by survival and mechanistic analyses in immunocompetent mice using the novel solid tumor model.[†] In the second part of the project, the expression of chimeric antigen receptors (CARs) by T cells as an alternative strategy to re-direction via BiTEs was investigated. Combinations of MV with CAR-expressing human T cells were investigated *in vitro* and in an adoptive cell transfer experiment in immunodeficient mice bearing human cancer xenografts. T cell labeling with iron oxide nanoparticles was developed for *in vivo* monitoring by magnetic resonance imaging. Finally, a mathematical model describing dynamics of MV and T cell re-direction combination therapies was designed for future *in silico* experimentation to help identify parameters crucial for treatment success and thus guide further research.

3.1 *in vitro* analyses of MV-BiTE

3.1.1 Generation of recombinant MV-BiTE

Oncolytic measles vaccine virus (MV) genomes encoding bispecific T cell engagers (BiTEs) for re-direction of T cells to tumor surface antigens were designed and generated prior to start of my PhD studies. This thesis focuses on viruses encoding BiTEs that target CD20-expressing tumor cells[‡]. Unmodified MV and vectors encoding BiTEs against carcinoembryonic antigen (CEA)[§] were used for control purposes throughout the present study.

Viruses with BiTE specificity for human and murine CD3 were generated using scFv sequences derived from clones OKT3 and 145-2C11, respectively. BiTE inserts preceded by Kozak and immunoglobulin kappa leader sequences were introduced into the additional transcription unit (ATU) downstream of the *H* open reading frame and contained sequences encoding influenza hemagglutinin peptide and hexa-histidine tags (Fig. 5).

3.1.2 Generation of a tumor model susceptible for MV-BiTE

To test anti-tumor efficacy of MV-BiTE in a syngeneic solid tumor model, murine melanoma cells stably expressing human antigens for BiTE binding and viral entry were generated. Parental B16 cells and B16 cells stably expressing the BiTE target antigen human CD20[143] (B16-CD20)

[†]Main findings of the present thesis and of Dr. Tobias Speck's dissertation have been published together[150].

[‡]These viruses were cloned in the course of my master's thesis project[149].

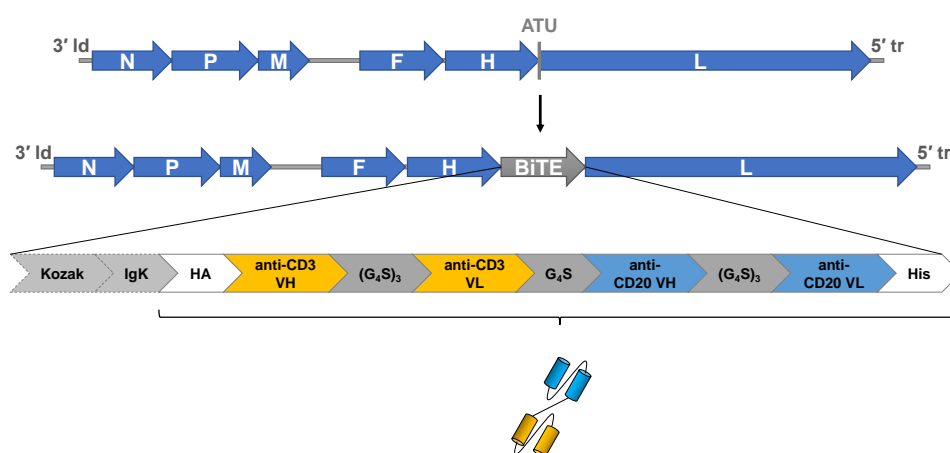[§]generated and analyzed by Tobias Speck[151]

Figure 5: Schematic representation of BiTE-encoding oncolytic measles virus (MV-BiTE) genome. An additional transcription unit (ATU) downstream of the *H* open reading frame (ORF) within the measles virus genome (upper panel) was used to insert bispecific T cell engager (BiTE)-encoding sequences via the reverse genetics system. The inserts include Kozak and Immunoglobulin kappa leader (Igκ) sequences preceding the BiTE-encoding sequence for efficient translation and secretion, respectively, and BiTE-associated protein tags for purification and detection purposes (lower panel, shown exemplarily for CD20-targeting BiTE). HA – influenza hemagglutinin peptide tag, VH – variable heavy chain, VL – variable light chain, G4S – flexible peptide linker (four glycines followed by one serine), His – hexa-histidine tag.

were transduced with lentiviruses encoding the measles virus entry receptor human CD46 isoform BC1[157], followed by single cell sorting of CD46-positive clones (Fig. 6A). The cell lines B16-CD46 and B16-CD20-CD46 were established from clonal colonies #4 and #2D, respectively, which exhibited similar duplication times compared to parental cell lines and were selected according to CD46 expression and MV susceptibility (Fig. 6B). Forty-eight hours post inoculation with an MV encoding enhanced green fluorescent protein (MV-ld-eGFP-H-mCD3xCD20), formation of large, fluorescent, multinucleated syncytia was observed for B16-CD20-CD46 cells in contrast to B16-CD20 cells. Following inoculation at a multiplicity of infection (MOI) of 1, few B16-CD20-CD46 cells remained at the plate bottom due to cell lysis, while for an MOI of 0.1, a dense layer of infected and uninfected cells was observed, indicating MOI-dependent MV susceptibility of the cell line.

3.1.3 MV-BiTE kinetics *in vitro*

MV-BiTE viruses were successfully rescued and propagated. Kinetics of viral replication and tumor cell lysis were determined for Vero producer cells and murine B16 cell lines by one-step growth curve infection experiments and XTT cell viability assays, respectively, and compared to unmodified virus (Fig. 7A,B). Viral progeny titers obtained from Vero cells peaked between 10^5 and 10^6 cell infectious units (ciu)/mL between 24 and 36 h after inoculation with unmodified oncolytic measles virus (MV) or MV encoding BiTEs targeting human (h) or murine (m) CD3 and CD20 or CEA (MV-hCD3xCD20, MV-hCD3xCEA, MV-mCD3xCD20, MV-mCD3xCEA, respectively). Correspondingly, Vero cell viability relative to uninfected (mock) decreased rapidly
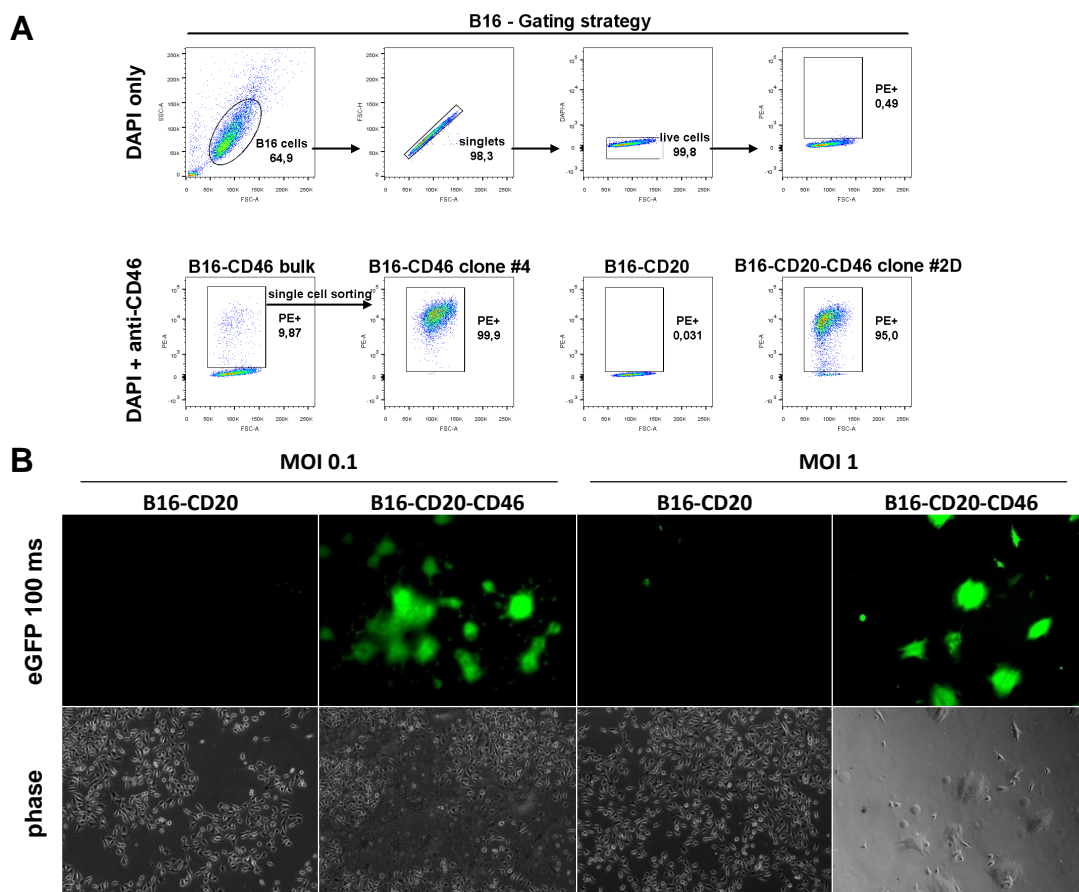
Figure 6: Generation of a murine melanoma cell line stably expressing human CD46 for measles virus entry. A. Flow cytometry analysis with phycoerythrin (PE)-labeled anti-CD46 antibody. Upper panel - general gating strategy shown for unstained sample of B16 cells incubated with DAPI. Lower panel – CD46 expression of selected samples. From left to right: B16 cells transduced with CD46-encoding lentiviral vector (LV-CD46) ("B16-CD46 bulk"), clonal cell line obtained after single cell sorting for CD46 expression ("B16-CD46 clone #4"), B16 cells stably expressing human CD20 antigen ("B16-CD20"), and a single cell clone selected for CD46 expression from B16-CD20 cells transduced with LV-CD46 ("B16-CD20-CD46 clone #2D"). B. MV susceptibility of B16-CD20 cells stably expressing human CD46. CD46-negative B16-CD20 cells and B16-CD20-CD46 clones expressing human CD46 as verified by flow cytometry were inoculated with eGFP-encoding MV at indicated multiplicities of infection (MOIs). eGFP expression was analyzed 48 h post inoculation. Shown are fluorescence microscopy and phase contrast images for B16-CD20 cells and the most susceptible B16-CD20-CD46 clone 2D.
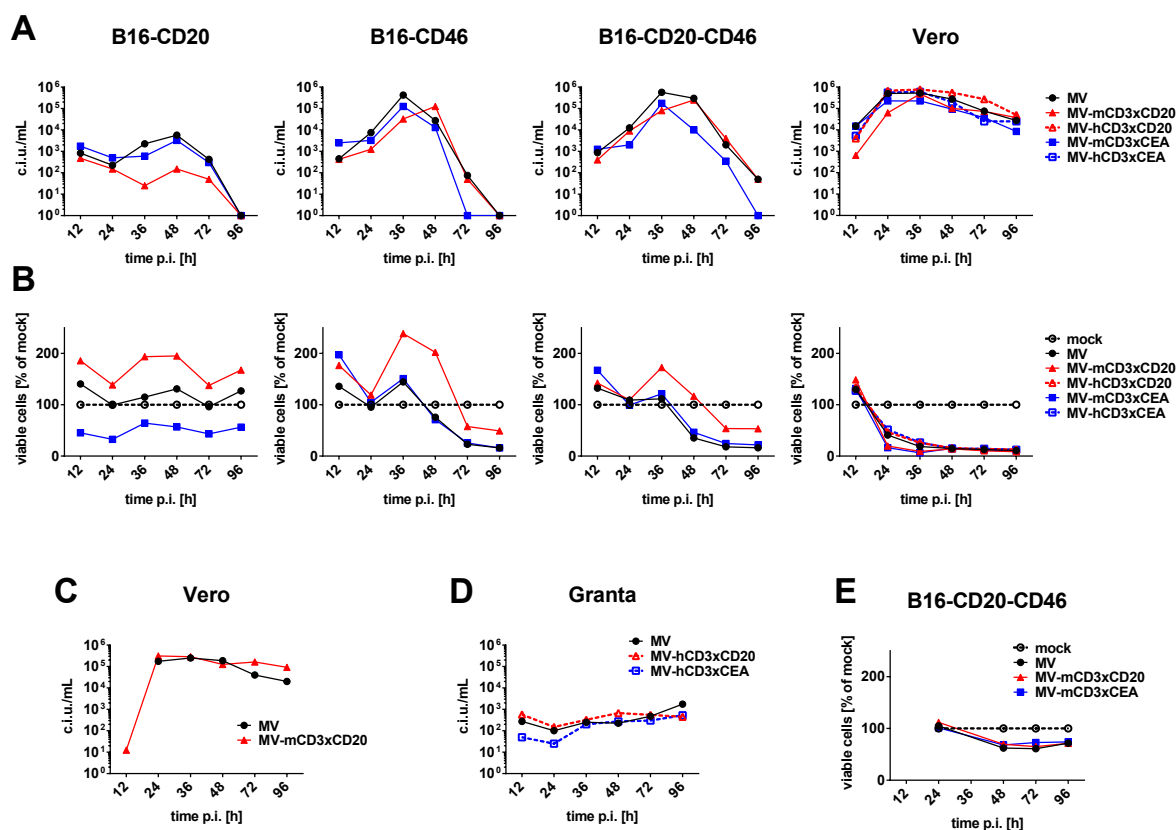
Figure 7: MV-BiTE replication and cytotoxicity kinetics *in vitro*. Indicated cell types were inoculated with medium only (mock) or indicated viruses at a multiplicity of infection of 1. For one-step growth curve experiments, cells were scraped into the supernatant at indicated time points viral progeny titers were determined by titration assay on Vero cells (A, C, D). XTT assay was performed to analyze virus-mediated cytotoxicity (B, E).

between 12 and 36 h post inoculation, with only minor differences between viruses. For B16-CD20 cells not expressing the MV receptor CD46, inoculation with MV, MV-mCD3xCD20, and MV-mCD3xCEA, respectively, yielded lower titers for each time point, with maxima around 10^3 ciu/mL at 12 and 48 h post inoculation. B16-CD20 cell viability was stable over 96 h post inoculation, at approximately 150, 100, and 50 % of mock for MV-mCD3xCD20, MV, and MV-mCD3xCEA, respectively. For both B16-CD46 and B16-CD20-CD46, progeny titers of MV and MV-mCD3xCEA peaked around 10^5 ciu/mL after 36 h, and relative cell viability dropped close to 0% after 72 h. MV-mCD3xCD20 reached similar maximal progeny titers after 48 h and induced reduction in cell viability to approximately 50 % after 72 h. In further experiments on Vero cells (Fig. 7C), human mantle cell lymphoma Granta-519 cells (Fig. 7D), and B16-CD20-CD46 cells (Fig. 7E), only minor differences between MV-mCD3xCD20 and other viruses were observed.

3.1.4 Functionality of MV-encoded BiTEs

BiTEs were isolated and purified by affinity exchange chromatography as described* from supernatants of MV-BiTE-infected Vero cells (henceforth referred to as virus-derived BiTEs, vBiTEs), yielding approximately 1-3 µg protein per mL supernatant. Binding of vBiTEs to target antigen-expressing cells was analyzed by flow cytometry. More than 95 % of human mantle cell lymphoma Granta-519 cells, which express high levels of endogenous CD20, were PE-positive after incubation with anti-CD20 antibody or mCD3xCD20 vBiTE followed by PE-conjugated anti-HA tag antibody (Fig. 8A). 22.5 % of B16-CD20-CD46 cells were PE-positive after subsequent incubation with hCD3xCD20 and anti-HA-PE antibody, while only background binding of hCD3xCD20 vBiTE to parental B16 cells was detected (0.36 % PE-positive) (Fig. 8B). vBiTE binding to immune effector cells was analyzed using FITC-labeled anti-His tag antibody[†] (Fig. 8C). Approximately 40 % of murine splenocytes were bound by vBiTEs specific for murine CD3 (mCD3xCD20, mCD3xCEA), in contrast to hCD3-targeting vBiTEs hCD3xCD20 and hCD3xCEA (1,71 and 1,88 % FITC-positive, respectively). After incubation with hCD3xCEA vBiTE, FITC signals were detected for 57.1 % of human peripheral blood mononuclear cells (PBMCs), compared to 1.21 % observed for mCD3xCEA. For CD20-specific vBiTEs, the values were approximately 10 % higher (71.9 % and 9.8 % for hCDxCD20 and mCD3xCD20, respectively). These results indicate antigen-specific cell binding by vBiTEs.

vBiTE functionality was assessed in co-cultures of tumor cells and immune effector cells via lactate dehydrogenase release assay. After 24 h, approximately 50 % specific lysis of B16-CD20[‡] and B16-CD20-CD46 cells was achieved in the presence of 100 and 500 ng/mL hCD3xCD20 vBiTE obtained from independent Vero cell infections and subsequent purifications, respectively (Fig. 9A). Compared to parental B16 cells not expressing the BiTE target antigen CD20, significantly higher lysis was observed at vBiTE concentrations of 1 and 0.5 ng/mL, respectively, and above. For Granta-519 cells, between 80 and 100 % specific lysis was observed for hCD3xCD20 vBiTE concentrations of 10 to 1000 ng/mL in presence of PBMCs, which was significantly higher compared to mCD3xCD20 control vBiTE. Specific lysis of B16-CD20-CD46 cells co-incubated with murine T cells increased with mCD3xCD20 vBiTE concentration (Fig. 9B). In three experiments with independently produced vBiTE samples, around 15 % specific lysis was achieved at vBiTE concentrations of 1 µg/mL. At 100 ng/mL, lysis was also significantly higher compared to B16-CD46 cells not expressing CD20. This indicates vBiTE concentration-dependent induction of surface antigen-specific tumor cell lysis by resting, polyclonal immune cells and thus functionality of virus-encoded BiTEs.

3.1.5 Preparation of appropriate controls for *in vivo* experimentation

Due to generation of MV-BiTE from crude cell lysates, BiTEs expressed by infected cells during virus production were present in virus suspensions, requiring appropriate controls for assessing efficacy *in vivo*. Therefore, the BiTE level present in virus suspension was assessed by vBiTE titration on Granta-519 cells, which express high levels of endogenous CD20. In a final volume of 50 µL, cells were incubated with 10 µL OptiMEM containing $1x10^5$ ciu MV-mCD3xCD20,

---

*established during master's thesis work[149] and published in a video protocol in the course of my doctoral project[134]

[†]experiment performed during my master's thesis work[149]

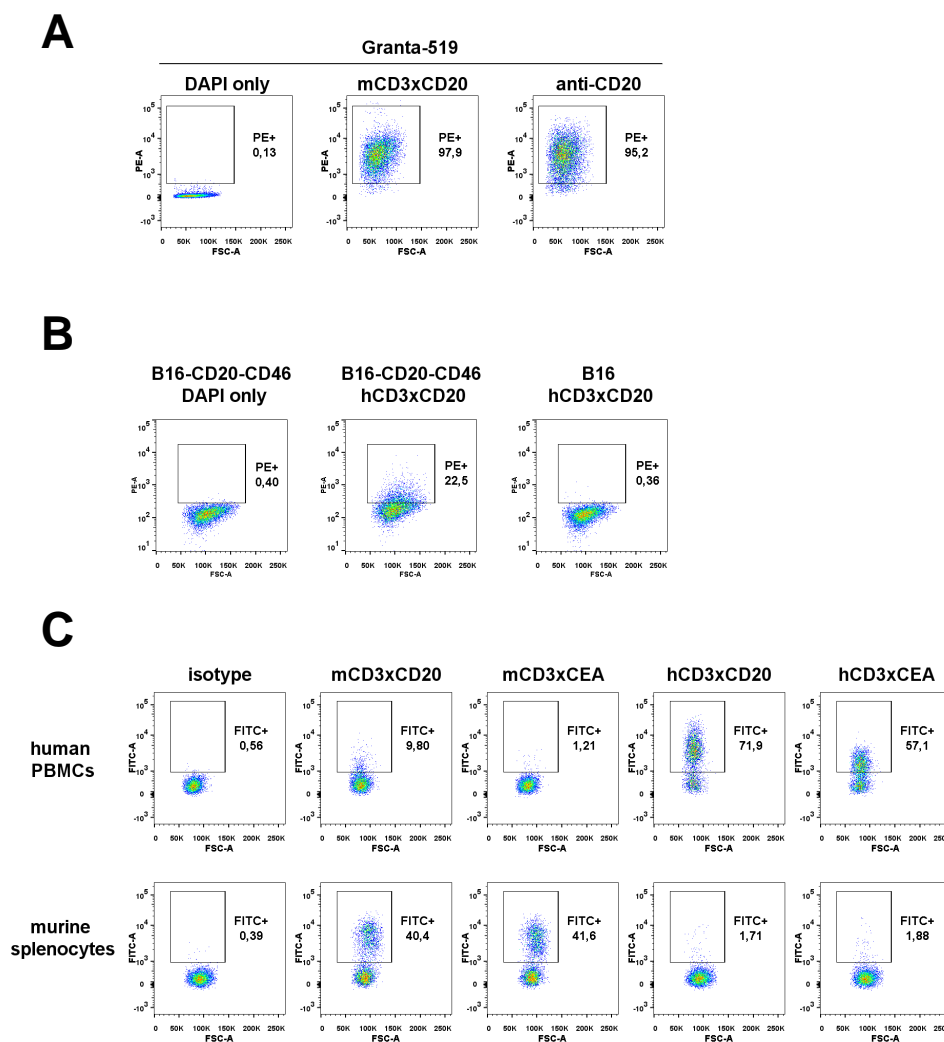[‡]experiment performed during my master's thesis work[149]

Figure 8: Binding of MV-encoded BiTEs to target cells *in vitro*. BiTEs were purified from the supernatant of MV-BiTE-infected Vero cells (vBiTEs) and binding to target cells was determined via flow cytometry using fluorophore-labeled antibodies specific for BiTE-associated peptide tags. PE – phycoerythrin, FITC – fluorescein isothiocyanate. A. Binding of mCD3xCD20 vBiTE to human mantel cell lymphoma cells (Granta-519). Endogenous CD20 expression was verified using PE-conjugated anti-human CD20 antibody (right panel). B. Binding of hCD3xCD20 vBiTE to murine melanoma cells expressing human antigens (B16-CD20-CD46). Parental B16 cells not expressing human antigens served as negative control (right panel). C. Binding of vBiTEs of different specificities to human (top) and murine (bottom) immune cells. PBMCs – peripheral blood mononuclear cells.
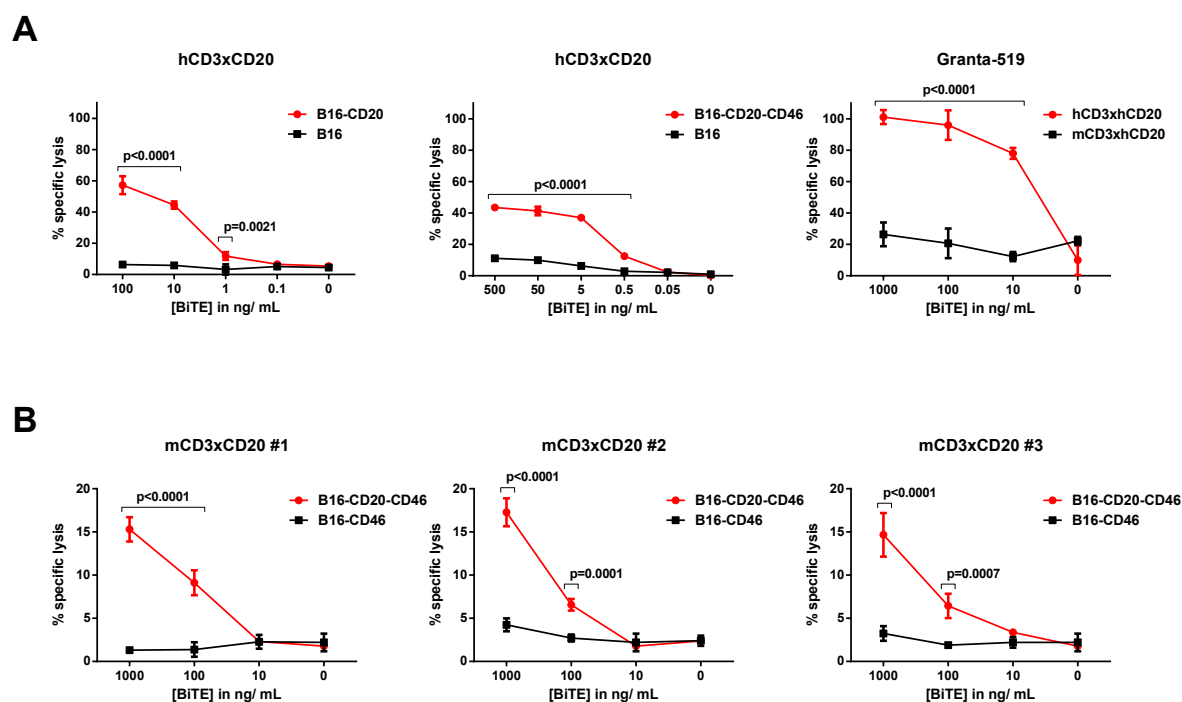
Figure 9: BiTE-mediated cytotoxicity _in vitro_. Indicated target tumor cells were co-incubated with (A) unstimulated human peripheral blood mononuclear cells (PBMCs) or (B) primary murine T cells for 24 and 48 hours, respectively, at effector-to-target cell ratios of 50:1. Relative target cell lysis in the presence of vBiTEs at indicated concentrations was determined by LDH release assay. Cells not expressing the relevant vBiTE target antigen (left and middle panels in the top row and all panels in the bottom row) or vBiTE of irrelevant specificity (upper right panel) served as controls. Shown are means ± standard deviation. Two-way ANOVA was performed for statistical analysis and p values were adjusted for multiple comparisons using Sidak test.

corresponding to a titer of $1x10^7$ ciu/mL, or different concentrations of mCD3xCD20 vBiTE and binding was determined by flow cytometry. For the mCD3xCD20 vBiTE concentration of 21.725 µg/mL, observed binding was comparable to the virus sample (Fig. 10A). Accordingly, the amount of BiTE present in one MV-mCD3xCD20 dose for *in vivo* treatment, i.e. 100 µL at a titer of $1x10^7$ ciu/mL, corresponds to approximately 2.17 µg vBiTE.

To dissect potential mechanisms of action, we tested an approach to inhibit replicative potential of MV-BiTE while maintaining a suspension of similar composition and BiTE level. To achieve this, the impact of ultraviolet (UV) C irradiation on viral replication and BiTE binding was assessed by titration assay and flow cytometry analysis of irradiated MV-BiTE samples in parallel. UV doses of 0.25 and 0.5 J/cm^2 resulted in titer reduction by five orders of magnitude and in complete abrogation of viral replication, respectively, while mean fluorescence intensity of signals detected in the flow cytometry-based BiTE binding assay with Granta-519 cells was reduced by approximately 10 and 20 % (Fig. 10B). This indicates feasibility of UV irradiation at a dose that completely inhibits viral replication without abrogating BiTE binding.

In order to assess the impact of viral replication on treatment outcome *in vivo*, irradiation schedules were adjusted to achieve viral titer reduction of two orders of magnitude (partial UV inactivation, pUV) and complete abrogation of viral replication (complete UV inactivation, cUV), respectively. Replication kinetics were analyzed on B16-CD20-CD46 cells by a one-step growth curve experiment (Fig. 10C). Cells were inoculated with MV-mCD3xCD20 at a multiplicity of infection of 1 and respective amounts of pUV- and cUV-treated virus. Viral progeny titers were measured at indicated time points by titration assay on Vero cells. Progeny titers peaked at 48 h post inoculation with MV-mCD3xCD20 between $2x10^4$ and $4x10^4$ ciu/mL. pUV-irradiated samples only yielded detectable progeny of approximately $1x10^2$ and $2x10^2$ ciu/mL at 48 and 72 h post inoculation, respectively, while no infectious progeny was detected after cUV irradiation. These results confirm partial and complete inhibition of viral replication by pUV and cUV irradiation schedules, respectively. Therefore, these schedules were used to prepare controls for subsequent *in vivo* studies.

For comparison of BiTE expression kinetics, de novo BiTE synthesis by Vero cells and B16-CD20-CD46 cells following inoculation with MV-mCD3xCD20 *in vitro* was monitored by ELISA of cell-free supernatants (Fig. 10D). For both cell lines, relative BiTE levels reached a maximum of 4-fold over medium after 72 h before decreasing to approximately 2-fold at 96 h. When inoculated with pUV- or cUV-inactivated virus, no increase in BiTE levels in the supernatant of B16-CD20-CD46 cells was observed, indicating absence of de novo synthesis of MV-encoded BiTEs in the tumor model *in vitro* upon UV irradiation, even at a dose that still allows for reduced viral replication.

3.2 Anti-tumor efficacy of MV-BiTE in immunocompetent mice

3.2.1 Tumor growth *in vivo*

To assess therapeutic efficacy of MV-BiTE treatment, C57BL/6 mice bearing subcutaneous B16-CD20-CD46 tumors received intratumoral injections of carrier fluid, vBiTE, control viruses, MV-BiTE, or UV-irradiated MV-BiTE, respectively, on five consecutive days. Tumor growth in individual mice was measured in three independent experiments (Fig. 11A-C). For mice receiving
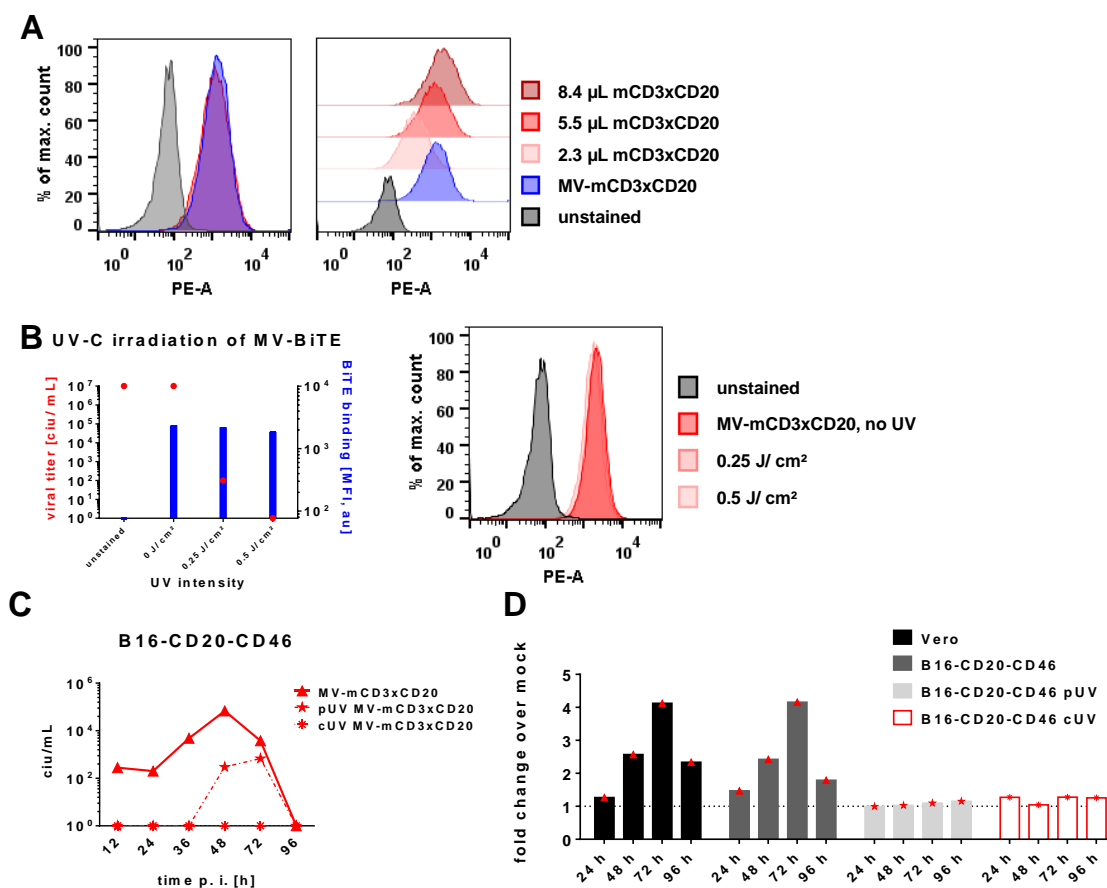
Figure 10: Effects of UV-C irradiation on MV-BiTE *in vitro*. A. Titration of vBiTE versus MV-BiTE suspension. Granta-519 cells were inoculated with 10 µL of OptiMEM containing 1×10^5 ciu MV-BiTE or indicated volumes of mCD3xCD20 vBiTE. Binding of BiTEs present in the viral suspension and purified vBiTE was determined using a phycoerythrin (PE)-labeled antibody targeting BiTE-associated HA-tag. B. Effects of ultraviolet C (UV-C) radiation on MV-BiTE titers and BiTE binding. Viral suspension of MV encoding mCD3xCD20 BiTE was irradiated at indicated intensities. Viral titers were assessed by titration assay (left y-axis on left panel) and binding of BiTEs to Granta-519 cells was analyzed with anti-HA-PE antibody (right y-axis and right panel). MFI – mean fluorescence intensity, au – arbitrary units. C. Effect of UV-C irradiation on MV-BiTE replication. B16-CD20-CD46 cells were inoculated with MV-BiTE at a multiplicity of infection of 1 and equal amounts of viral suspensions previously irradiated at two different intensities to achieve partial (pUV) or complete (cUV) inactivation. Viral progeny titers were assessed at indicated time points by titration assay on Vero cells. D. Effect of MV-BiTE irradiation on de novo production of BiTEs. Vero or B16-CD20-CD46 cells were inoculated with mCD3xCD20-encoding MV at a multiplicity of infection of 1 or equal amounts of partially (pUV) or completely (cUV) inactivated virus suspension as indicated. At indicated time points, cell-free supernatants were harvested and levels of CD20-specific BiTE were assessed by ELISA. Values were normalized to medium only (mock).
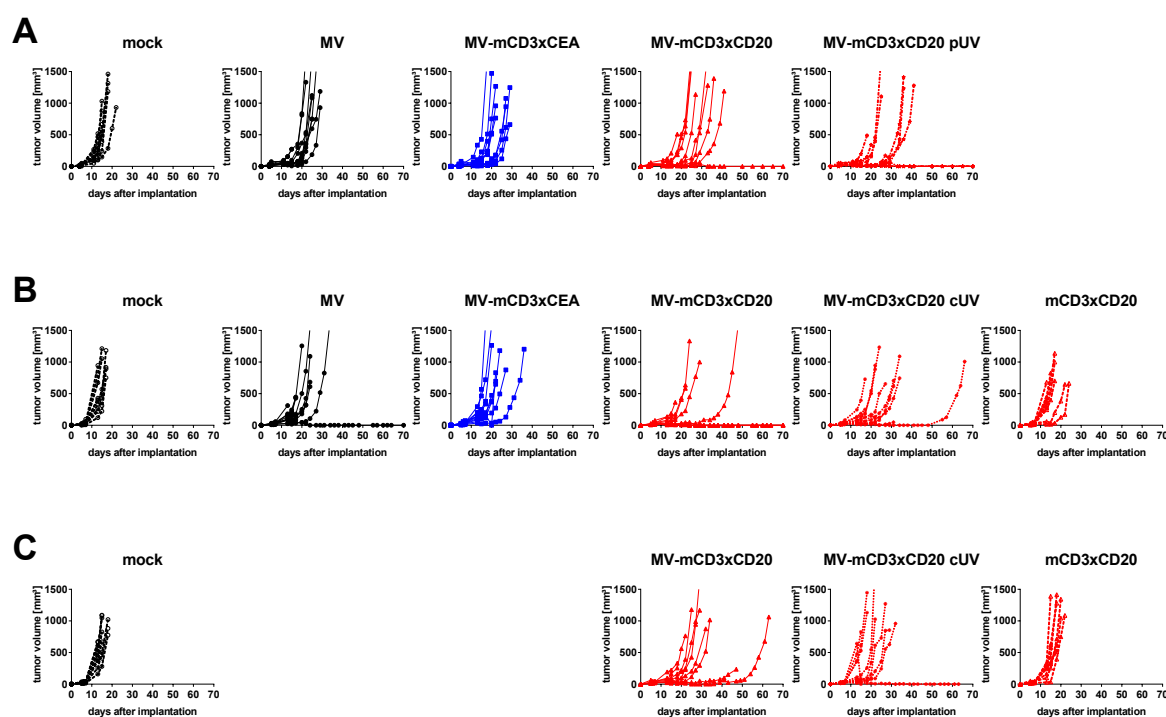
Figure 11: Effect of MV-BiTE treatment on tumor growth in immunocompetent mice. B16-CD20-CD46 tumor cells were implanted subcutaneously into C57BL/6 mice on day 0. When tumors had reached average volumes of 40 mm^3, animals received indicated treatments by intratumoral injection on five consecutive days. Shown are tumor volumes over time of individual mice in three independent experiments (A-C). mock – carrier fluid, MV – unmodified oncolytic measles virus, MV-mCD3xCEA – virus encoding mCD3xCEA control BiTE, MV-mCD3xCD20 – virus encoding mCD3xCD20 BiTE, pUV and cUV – virus partially and completely inactivated by ultraviolet irradiation, respectively, mCD3xCD20 – purified vBiTE.

carrier fluid only (mock) and mCD3xCD20 vBiTE alone, respectively, tumors progressed rapidly and the majority of mice had to be sacrificed between 10 and 20 days post tumor implantation. Delayed tumor growth was observed following treatment with unmodified measles virus (MV) and MV-mCD3xCEA, respectively, and most animals reached termination criteria between days 20 and 30. In the MV treatment group, a complete tumor remission was observed in one animal (Fig. 11B). Mice treated with MV-mCD3xCD20 exhibited even more delayed tumor growth, with no apparent differences between non-irradiated and partially (pUV) and completely (cUV) UV-inactivated virus. While the majority of those animals did not survive more than 40 days post tumor implantation, individual mice from each group survived more than 60 days in each of the independent experiments, and several complete tumor remissions were observed (see 3.2.3).

3.2.2 Survival analyses

Survival was prolonged significantly for mice treated with unmodified MV and MV-mCD3xCEA, respectively, compared to mock treatment, as assessed by Kaplan-Meier analysis of two independent experiments (Fig. 12A and B). Median survival was 16.5 and 15 days, respectively, for the mock
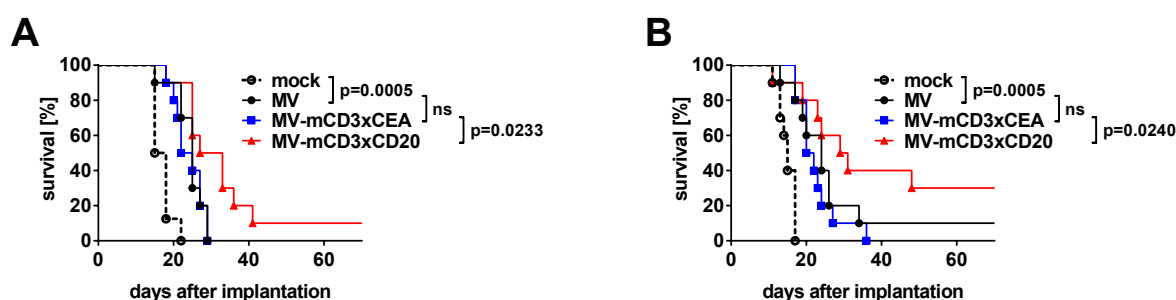
Figure 12: MV-BiTE efficacy *in vivo*. C57BL/6 mice bearing established subcutaneous B16-CD20-CD46 tumors received intratumoral treatments with carrier fluid (mock) or indicated viruses on five consecutive days. Animals were examined daily and sacrificed when termination criteria were reached. Kaplan-Meier survival plots are shown. Statistical analysis was performed by Mantle-Cox log-rank test with p values adjusted for multiple comparisons by Bonferroni correction. A: n = 8 for mock; B: n = 9 for mock and MV-mCD3xCD20, respectively; n = 10 for each other group.

groups, 25 and 24 days for MV and 23.5 and 21 days for MV encoding CEA-specific control BiTE. Compared to those treatment groups, survival was significantly prolonged in mice treated with MV encoding the tumor-targeting mCD3xCD20 BiTE, reaching a median of 30 days in both experiments and resulting in one and three mice, respectively, in complete tumor remission more than 40 days post tumor implantation.

vBiTE treatment alone had a marginal effect on survival compared to mock treatment, with a median survival of 16 and 18 days versus 16.5 and 15 days in two experiments, respectively (Fig. 13A and B). MV-mCD3xCD20 treatment was significantly more effective than vBiTE therapy in both experiments, while neither complete (cUV) nor partial (pUV) inhibition of virus replication significantly impaired treatment outcome. A median survival of 30 and 29 days was observed for MV-BiTE treatment compared to 30 and 25 days for the cUV groups, respectively (Fig. 13A and B). pUV treatment yielded a median survival of 33 days versus 30 days for non-irradiated MV-BiTE (Fig. 13C). Similarly, complete inactivation of unmodified MV did not significantly abrogate efficacy in an independent experiment (Fig. 13D). Medians of survival determined for MV cUV and MV groups were 20 and 23.5 days, respectively. This indicates that *in vivo* replication is not a major determinant of therapeutic efficacy.

Regarding the presence of MV-neutralizing antibodies in the population, effects of pre-vaccination on therapeutic efficacy was investigated. Median survival was 23.5 days in naïve mice and 25 days in pre-immunized mice upon treatment with unmodified MV, and 21 days in naïve mice and 48 days in pre-immunized mice for MV-BiTE (Fig. 14). In the mock-treated group, median survival was 12 days. Thus, in MV-immune mice, efficacy of intratumoral MV and MV-mCD3xCD20 treatments was not impaired compared to MV-naïve animals. One non-immunized mouse from the MV-BiTE treatment group and three MV-immune animals, one treated with MV and two with MV-BiTE, went into complete remission following treatment. These results indicate that pre-vaccination did not abrogate efficacy of intratumoral virus treatment.
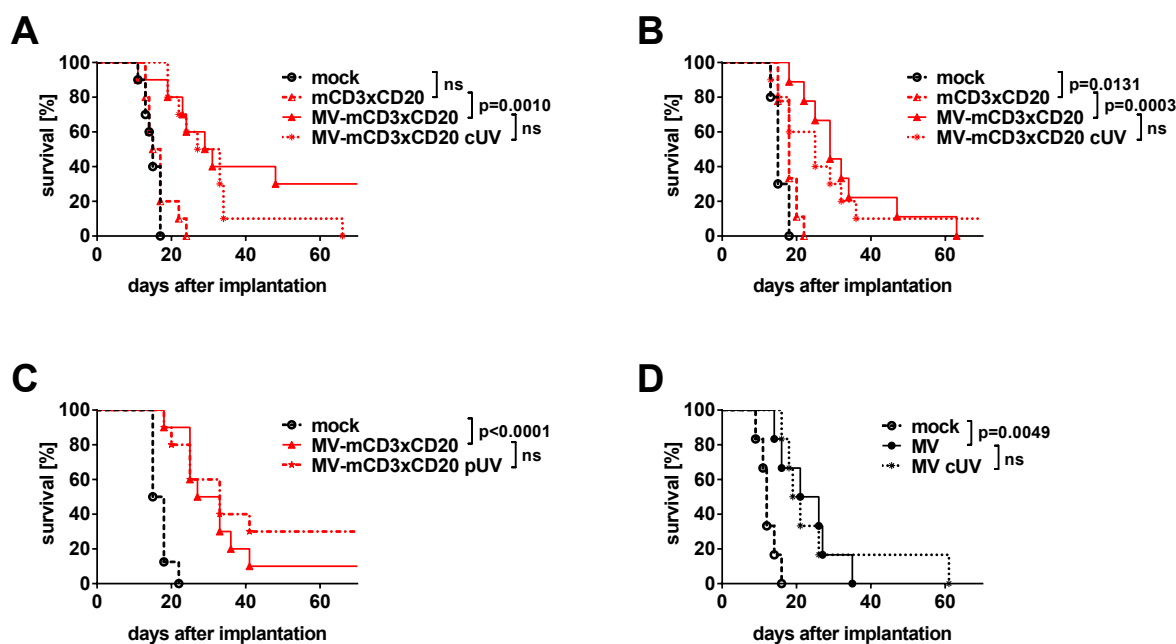
Figure 13: Treatment efficacy of vBiTE and UV-inactivated viruses *in vivo*. C57BL/6 mice bearing established subcutaneous B16-CD20-CD46 tumors received intratumoral injections of indicated regimens on five consecutive days: mock – carrier fluid, mCD3xCD20 – purified vBiTE specific for murine CD3 and human CD20 antigen, MV-mCD3xCD20 – BiTE-encoding MV, cUV – completely UV-inactivated, pUV – partially UV-inactivated. Animals were examined daily and sacrificed when termination criteria were reached. Kaplan-Meier survival plots are shown. Statistical analysis was performed by Mantle-Cox log-rank test with p values adjusted for multiple comparisons by Bonferroni correction. Data shown in panels A and C were obtained from the same experiments as displayed in Figures 12 B and A, respectively (i.e., corresponding mock and MV-mCD3xCD20 survival curves are identical). A: n = 9 for both mock and MV-mCD3xCD20, n = 10 for each other group; B: n = 9 for both MV-mCD3xCD20 and mCD3xCD20, n = 10 for each other group; C: n = 8 for mock, n = 10 for each other group; D: n = 6 for each group.
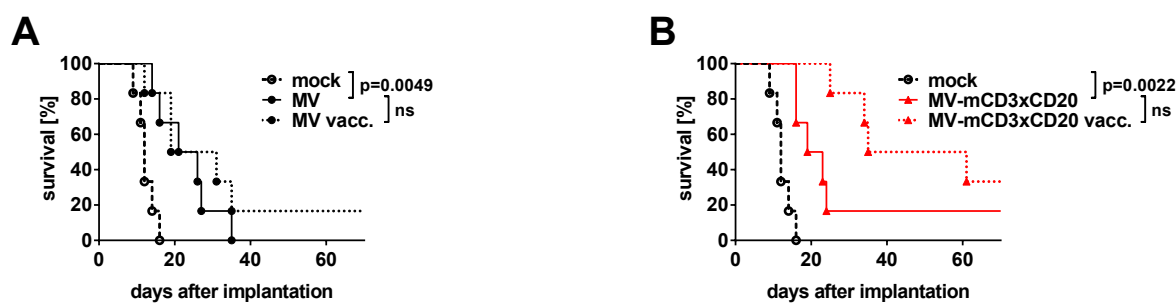
Figure 14: MV-BiTE efficacy in MV-immunized mice. B16-CD20-CD46 tumors were implanted subcutaneously into MV-naïve C57BL/6 mice and mice previously immunized with highly purified MV (MV-NIS) by prime-boost vaccination, i.e. two intraperitoneal injections. MV immunity was verified by serum neutralization assay. When tumor volumes reached an average of 40 mm³, mice received intratumoral injections of (A) unmodified MV, (B) MV encoding mCD3xCD20 BiTE, or carrier fluid only (mock) on five consecutive days. Kaplan-Meier survival plots are shown. Statistical analysis was performed by Mantle-Cox log-rank test with p values adjusted for multiple comparisons by Bonferroni correction. Data of both panels were derived from one experiment (i.e., mock survival curves are identical). vacc. – vaccinated, MV-immune animals. n = 6 for each group.

3.2.3 Tumor re-challenge

To investigate anti-tumor immunity in C57BL/6 mice in long-term tumor remission after virus treatment of subcutaneous B16-CD20-CD46 tumors, the animals were subjected to tumor re-challenge by injection of $1x10^5$ B16 cells into the contralateral flank. Mice naïve to both tumor and MV served as implantation controls. From the survival experiments shown in Figures 12 and 13, nine animals in total had gone into complete remission and survived more than 70 days after first tumor implantation. Six out of eight mice previously treated with MV-BiTE and the one survivor that had received unmodified MV rejected engraftment, while all six naïve mice developed tumors (Fig. 15, lower three bars). In a second re-challenge experiment, surviving mice from the vaccination experiment shown in Fig. 14 were re-challenged, yielding one out of three rejections for MV-BiTE survivors and one out of one for MV, versus no rejections by the four naïve control mice (upper three bars). In all survival experiments performed in the course of this study, two of 44 B16-CD20-CD46 tumor-bearing mice treated with unmodified MV showed complete tumor remission (4.55%) and both rejected engraftment of B16 tumors upon re-challenge. For a total of 71 animals treated with MV-mCD3xCD20, eleven complete tumor remissions were observed (16.90%). Of these animals, seven did not develop tumors after injection with B16 cells (63.64% of all re-challenged mice, 9.86% of all treated mice). This indicates long-term anti-tumor immune protection in a subset of mice after tumor treatment with MV-BiTE.

3.2.4 Mechanistic analyses of MV-BiTE ex vivo

To identify mechanisms of efficacy in the B16-CD20-CD46 model, tumor-bearing C57BL/6 mice were treated with carrier fluid only (mock), MV encoding control BiTE (MV-mCD3xCEA), or MV-mCD3xCD20 on five consecutive days by intratumoral injection.
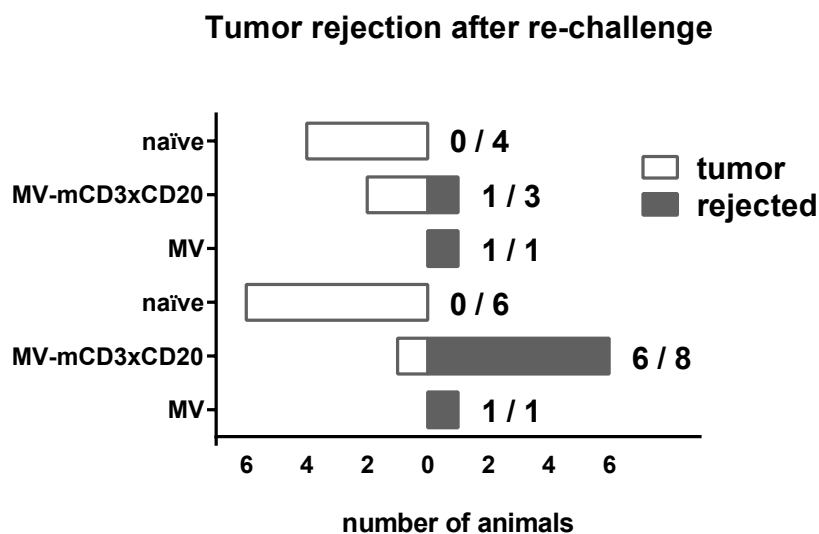
Tumor rejection after re-challenge

Figure 15: Long-term immune protection in MV-BiTE-treated mice. In two separate experiments, C57BL/6 mice in long-term remission after treatment of subcutaneous B16-CD20-CD46 tumors with indicated viruses and naïve animals, respectively, were injected subcutaneously with 1×10^5 B16 cells and tumor engraftment was monitored. The three lower bars display data for re-challenge of mice from the survival experiments shown in Figs. 12 and 13 and the upper bars show data for mice from the MV-immunization experiment (Fig. 14).

Kinetics of viral gene expression *in vivo* were assessed by RT-qPCR analysis of bulk RNA isolated from tumors explanted at designated time points. mRNA levels of MV-N and mCD3xCD20 and mCD3xCEA BiTEs, respectively, were highest for the first two measured time points, i.e. directly after the first and the fifth intratumoral treatment (Fig. 16). While similar levels were detected one and two days after the last treatment, values were close to baseline after five days.

To assess immunological consequences of MV-BiTE therapy, mice were sacrificed one day after the last treatment, tumors were explanted and partitioned for cytometric and bulk RNA analyses. The relative abundance of tumor-infiltrating lymphocyte subsets following treatment was analyzed by flow cytometry and compared between treatment groups. A significantly increased ratio of CD3+ cells to CD20+ tumor cells of all live cells was observed for MV-mCD3xCD20-treated mice compared to both other groups (Fig. 17A). In addition, the ratio of CD8+ (cytotoxic) to CD4+ (helper) T cells was significantly increased (Fig. 17B). For both virus treatment groups, a trend towards increased expression of the activation marker CD69 on CD3+ T cells was observed (Fig. 17C), whereas significantly lower levels of the inhibitory molecule CTLA-4 were detected (Fig. 17D). Compared to mock, CD4+CD25+ double positive cells were reduced among the CD3+ populations after virus treatment, although significance was reached only for MV-mCD3xCD20 (Fig. 17E). The general composition of tumor-infiltrating lymphocyte compartments indicates induction of an effector T cell phenotype upon MV-BiTE treatment.

RT-qPCR of bulk RNA revealed a two-fold increase in *Foxp3* mRNA levels after treatment with MV-mCD3xCD20 compared to mock, while expression of Tbet mRNA was increased by factor 100 (Figure 18A). Targeted transcriptome analysis showed a significant increase in the ratio of *Cd8a* versus *Foxp3* expression (Fig. 18B). Compared to MV-mCD3xCEA treatment, obtained
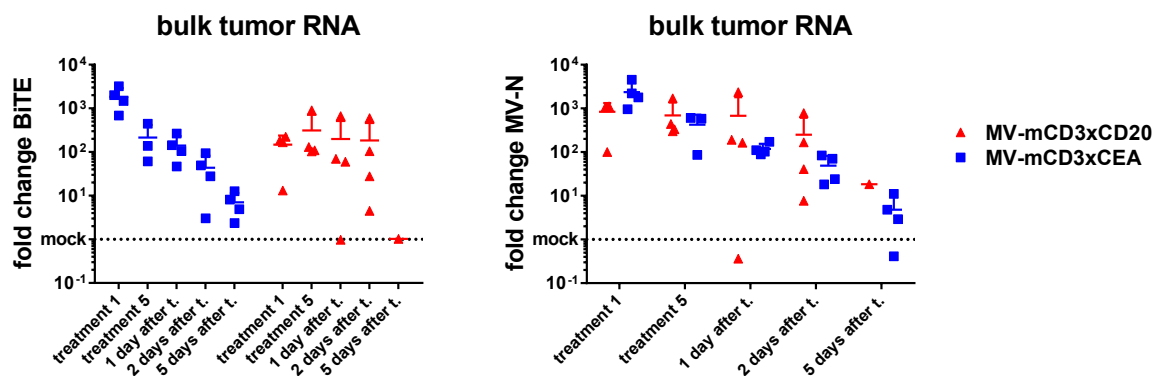
Figure 16: Intratumoral expression levels of viral mRNA over time. Subcutaneous B16-CD20-CD46 tumors in C57BL/6 mice were injected with carrier fluid only (mock), MV encoding CEA- and CD20-specific BiTE, respectively, on five consecutive days. At indicated time points, mice from each group were sacrificed (n = 3 for MV-CD3xCEA treatment 5, n = 1 for MV-CD3xCD20 5 days after t., n = 4 for every other time point), tumors were explanted, whole RNA was extracted and analyzed by RT-qPCR. Shown are means + standard deviation of fold change over the average of the respective mock group. Treatment 1/5 – directly after the first/fifth treatment, respectively; t. – treatment.

values were also higher for the MV-mCD3xCD20-treated group, with significance reached for *T-bet* levels and the *Cd8a/Foxp3* ratio, but not for *Foxp3* expression. These data indicate a shift from a regulatory to an effector T cell phenotype.

Targeted transcriptome analysis using a commercially available set of murine immune-related genes (NanoString CodeSet Immunology Panel) was performed to identify treatment-induced changes in the immune transcriptome that potentially represent determinants of therapeutic success. A gene expression heat map was generated by agglomerative clustering including T cell activation, differentiation, and proliferation genes pre-defined in the Advanced Analysis package of nSolver 4.0 software (Fig. 19). T cell-related genes were found to be differentially expressed in tumors from different treatment groups. The cluster with the lowest relative expression of indicated genes exclusively contained samples from the mock group, whereas highest relative expression was observed for MV-mCD3xCD20-treated animals. Individual analysis further revealed upregulated expression of genes associated with T cell inhibition and exhaustion, such as PDCD1 and CD274 which encode the immune checkpoint proteins programmed cell death protein 1 (PD-1) and programmed death-ligand 1 (PD-L1), respectively.

3.3 Combining oncolytic measles viruses and CAR T cells

Re-direction of resting, polyclonal endogenous T cells in the context of oncolytic measles virotherapy was investigated by MV-BiTE treatment in the B16-CD20-CD46 model. Ectopic expression of a chimeric antigen receptor (CAR) represents another method of re-direction, in this case of ex vivo expanded and stimulated T cells, that has been approved for hematological malignancies but lacks efficacy in solid tumors. As CAR T cell therapy has both advantages and
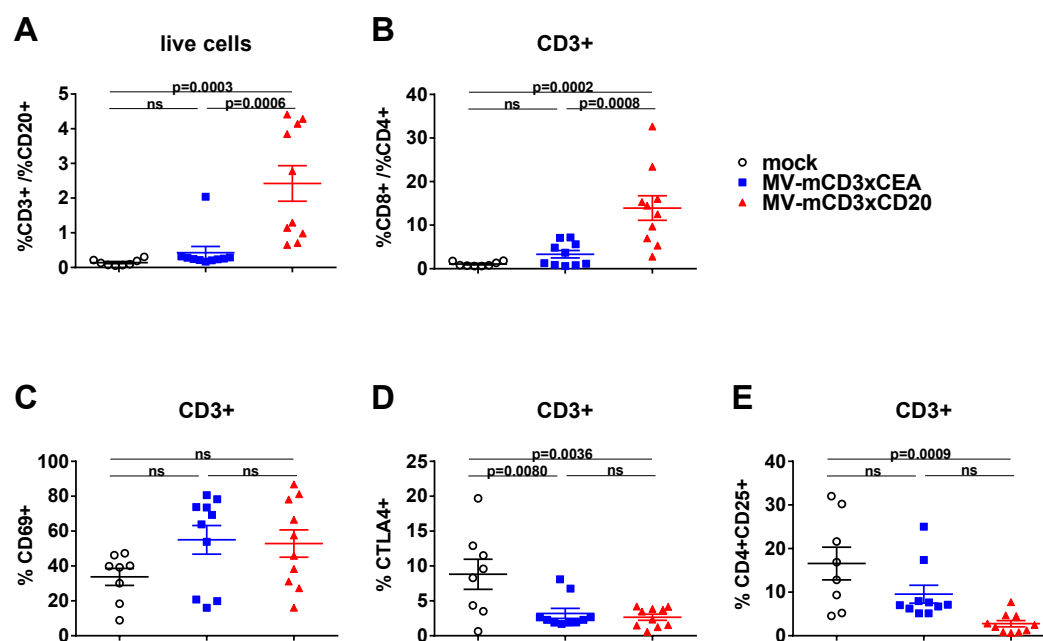
Figure 17: Tumor-infiltrating lymphocytes after MV-BiTE treatment. C57BL/6 mice bearing established subcutaneous B16-CD20-CD46 tumors received intratumoral injections of carrier fluid only (mock), MV encoding mCD3xCEA control BiTE (MV-mCD3xCEA) or MV encoding CD20-specific BiTE (MV-mCD3xCD20) on five consecutive days. One day after the last treatment, tumors were explanted and single cell suspensions were prepared, stained for the indicated markers and analyzed by flow cytometry. Populations on which gating was performed are indicated above panels. Exemplary data from one of two independent experiments is shown. Statistical analysis was performed by one-way ANOVA with p values adjusted for multiple comparisons by Tukey test. ns – not significant. n = 8 for mock, n = 10 for both other groups.
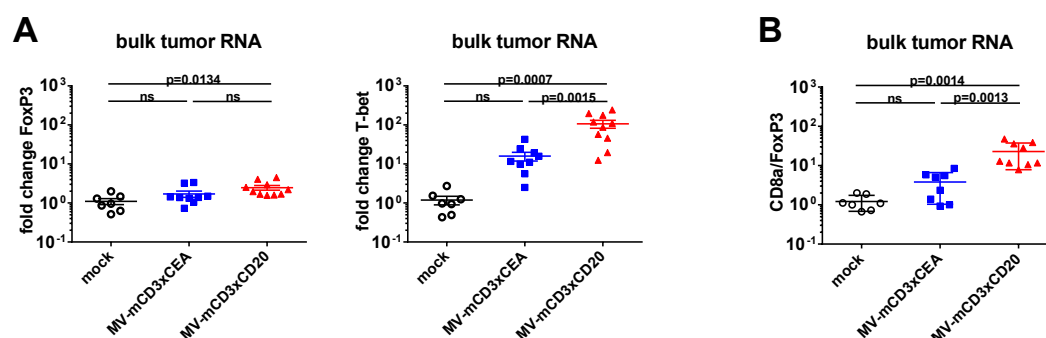
Figure 18: Expression levels of T cell transcription factors after MV-BiTE treatment.
C57BL/6 mice bearing established subcutaneous B16-CD20-CD46 tumors received intratumoral
injections of carrier fluid only (mock), MV encoding mCD3xCEA control BiTE (MV-mCD3xCEA)
or MV encoding CD20-specific BiTE (MV-mCD3xCD20) on five consecutive days. One day after
the last treatment, tumors were explanted and whole RNA was extracted. A. Expression levels
of mRNA encoding transcription factors FoxP3 and T-bet were determined by RT-qPCR and
normalized to L13A mRNA. Fold changes over the average value of the respective mock-treated
group are shown. n = 7 for mock, n = 8 for MV-mCD3xCEA, n = 10 for MV-mCD3xCD20. B.
In a separate experiment, extracted RNA was subjected to targeted transcriptome analysis and
ratios of *Cd8a* and *Foxp3* mRNA expression levels were calculated. n = 7 for mock, n = 8 for
MV-mCD3xCEA, n = 9 for MV-mCD3xCD20. Shown are mean ± standard deviation. Statistical
analysis was performed by one-way ANOVA with p values adjusted for multiple comparisons by
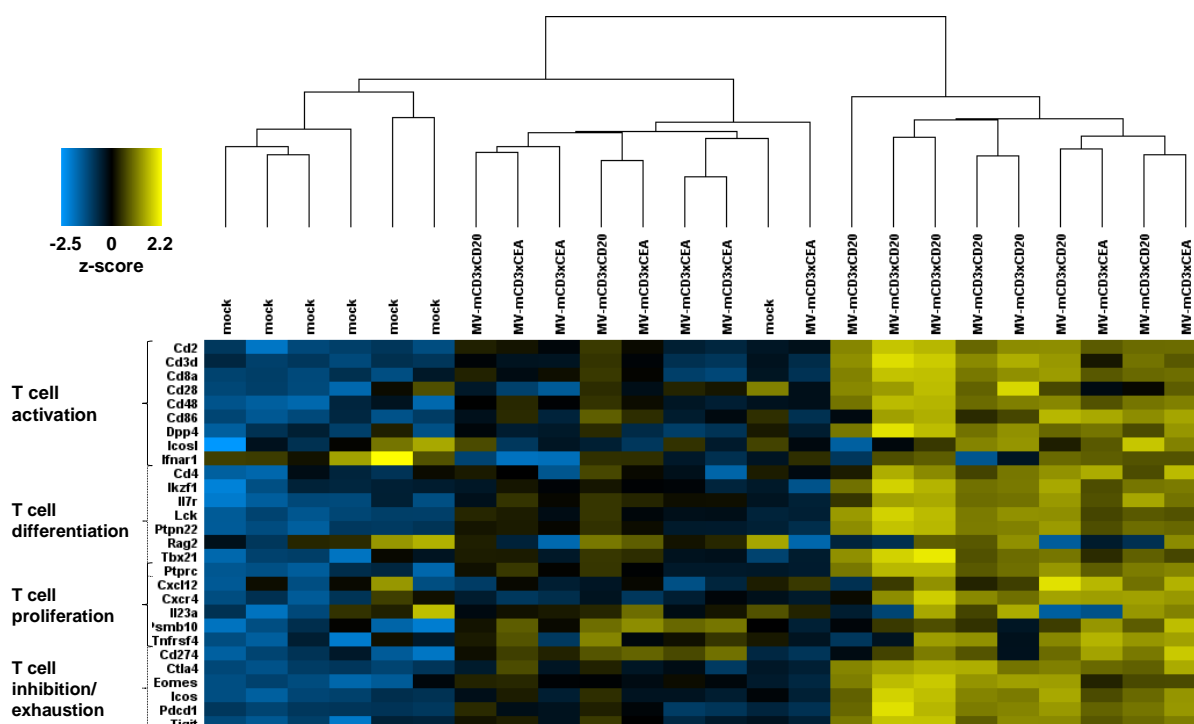Tukey test. ns – not significant.

Figure 19: Expression levels of T cell-associated genes after MV-BiTE treatment.
C57BL/6 mice bearing established subcutaneous B16-CD20-CD46 tumors received intratumoral injections of carrier fluid only (mock), MV encoding mCD3xCEA control BiTE (MV-mCD3xCEA) or MV encoding CD20-specific BiTE (MV-mCD3xCD20) on five consecutive days. One day after the last treatment, tumors were explanted and whole RNA was extracted and subjected to targeted transcriptome analysis. Data was derived from the same experiment as shown in Figure 18B. Expression was normalized to internal reference genes and scaled for equal variance of each gene. Color coding corresponds to indicated z-scores representing relative fold change of gene expression. Agglomerative clustering analysis was performed for selected T cell-related genes using nSolver 4.0 software.

disadvantages compared to BiTE treatment, potential of combination with MV was investigated for this therapeutic approach as well.

CAR vectors were provided by Dr. Daniel Abate-Daga, Department of Immunology, H. Lee Moffitt Cancer Center and Research Institute, Tampa, FL, USA* Two previously published CARs targeting prostate stem cell antigen (PSCA) as a model antigen were used in this study. The second generation CAR, PSCA2 contains a CD28 co-stimulatory domain only, while the third generation CAR, PSCA3, contains both CD28 and 4-1BB co-stimulatory domains[158].

To achieve re-direction to PSCA-expressing cells, ex vivo stimulated human T cells were transduced with CAR-encoding retroviral vectors. CAR expression was verified by flow cytometry, reproducibly yielding high percentages of CAR-positive cells (Fig. 20A). No selection of CAR-expressing cells was applied prior to performing experiments. Therefore, CAR-negative T cells were still present in the CAR T cell suspension. Accordingly, numbers of untransduced human T cells (UT) to be used as controls were always calculated according to the amount of total T cells, not CAR T cells, present in respective samples.

The PSCA-expressing human pancreatic adenocarcinoma cell line HPAC was used as a solid tumor model for CAR T cell therapy. As determined by flow cytometry, HPAC cells were also bound by carcinoembryonic antigen (CEA)-specific vBiTE (Fig 20B), additionally allowing analyses of MV-BiTE efficacy in the CAR tumor model.

The influence of designated MV and T cell combinations on HPAC cell viability over time was determined via impedance measurement. Continuous growth over three days was observed for untreated HPAC cells seeded on a 96-well plate (Fig. 20C, left panel). Incubation for 2 h with MV-hCD3xCEA and MV-hCD3xCD20, respectively, at a multiplicity of infection of 1 induced reduction in cell viability after 48 h. Addition of UT did not affect viability after 24 h but led to reduced growth at 48 and 72 h (middle panel). When inoculated with MV encoding non-targeting control BiTE hCD3xCD20 prior to addition of UT, growth was reduced at 24 and 48 h and no increase in cell viability was observed at 72 h compared to the 48 h time point. When addition of UT was preceded by inoculation with MV-hCD3xCEA, no viable cells were detected after 24 h. The same outcome was observed for incubation with PSCA2 CAR T cells, irrespective of inoculation with virus (right panel). These results indicate effective T cell re-direction by both approaches.

For efficacy analysis in a pilot experiment *in vivo*, NSG mice bearing subcutaneous HPAC tumors received intratumoral treatment with carrier fluid only (mock), unmodified MV, or MV-hCD3xCEA (MV-BiTE) on four consecutive days, followed by a single intravenous injection of UT or CAR T cells and subsequent intraperitoneal application of IL-2. Tumor growth did not differ significantly between different treatment groups (Fig. 20D). However, irrespective of T cell application, a trend towards delayed growth upon virus treatment compared to mock was observed. Tumor growth was also reduced upon CAR T cell treatment (right panel) compared to without application of T cells (left) and to UT treatment (middle), respectively. Before onset of potential graft-versus-host-disease, the experiment was terminated 34 days post treatment initiation. Spleens were explanted from sacrificed animals and analyzed by flow cytometry. No CD3-positive events were detected (data not shown), indicating lack of persistence of adoptively transferred T cells in the immunodeficient hosts.

---

*I learned methods of CAR T cell therapy, including isolation, expansion, transduction and application of T cells, during a research visit to Dr. Abate-Daga's laboratory between May 16 and August 18, 2017, in the course of my thesis work.
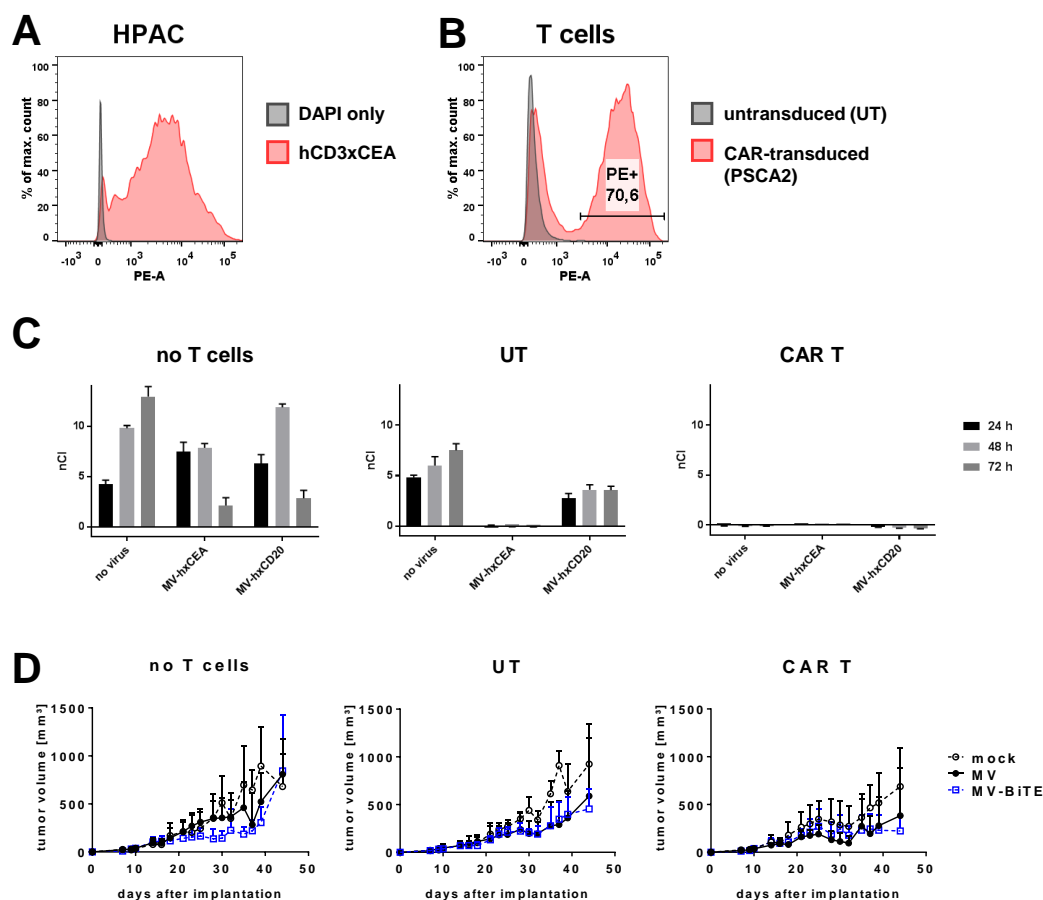
Figure 20: Combining CAR T cell and oncolytic measles virotherapy. A. Expression of BiTE target antigen by the human pancreatic adenocarcinoma cell line HPAC. Binding of CEA-specific vBiTE to HPAC cells was analyzed by flow cytometry using a phycoerythrin (PE)-labeled antibody targeting the BiTE-associated HA-tag. B. Chimeric antigen receptor (CAR) expression on human T cells. Ex vivo stimulated human T cells were transduced with a lentiviral vector encoding prostate stem cell antigen-specific CAR of the second generation (PSCA2). Three days after transduction, cell surface expression of CARs was analyzed via binding of protein L conjugated to biotin, which was in turn detected using phycoerythrin (PE)-labeled streptavidin. C. Cytotoxic potential of T cell re-direction by CARs and BiTE-encoding oncolytic measles viruses *in vitro*. HPAC cells were seeded on a 96-well plate. After 24 h, adherent cells were inoculated with medium only (no virus) or oncolytic measles viruses encoding hCD3xCEA or hCD3xCD20 BiTE at a multiplicity of infection of 1 for 2 h. Then, medium only (no T cells), untransduced, stimulated human T cells (UT), or T cells expressing PSCA2 (CAR T) were added and cell viability was analyzed over time via impedance measurement. Values were normalized to the first measurement after adding T cells (normalized cell index, nCI). Shown are mean + standard deviation of three technical replicates for each condition at indicated time points. D. CAR T and MV-BiTE combination *in vivo*. Established subcutaneous HPAC tumors in immunodeficient NSG mice received intratumoral injections of carrier fluid only (mock), unmodified MV, or MV encoding hCD3xCEA BiTE (MV-BiTE) on four consecutive days, followed by a single intravenous injection of carrier fluid (no T cells), untransduced, stimulated human T cells (UT), or PSCA-specific CAR T cells (CAR T) on the next day. Recombinant human IL-2 was applied intraperitoneally for three days to support T cell engraftment. Group means + standard deviation of tumor volumes are shown (n = 4 for each mock group, n = 5 for each other condition).

3.3.1 T cell labeling ex vivo

Regarding the lack of information on the fate of injected T cells *in vivo*, non-invasive T cell tracking would be a useful tool to analyze homing, distribution, and persistence in individual animals over time. To achieve detection of T cells by magnetic resonance imaging (MRI), labeling with iron oxide nanoparticles was evaluated as a potential method. Direct incubation with fluorophore-labeled nanoparticles alone yielded a labeling efficiency of 16.8% of live T cells determined by flow cytometry (Fig. 21A, lower left panel). Using a previously published protocol for nanoparticle labeling of various cell types with heparin and protamine[159], labeling of more than 75% of live cells was achieved (lower middle panel). However, protocol optimization was necessary because high protamine concentrations were associated with increased toxicity (upper right panel).

MRI was performed to assess labeling of T cells with the non-fluorescent nanoparticle ferumoxytol. Dark spots indicating field inhomogeneities as induced by iron oxide nanoparticles were detected in samples containing T cells incubated with heparin, protamine, and ferumoxytol, but not for T cells with heparin and protamine alone (Fig. 21B). Confocal microscopy revealed presence of fluorescently labeled nanoparticles within cells upon labeling with heparin and protamine (Fig. 21C).

3.3.2 Combining CAR T cells and MV encoding checkpoint inhibitors

While mouse survival was prolonged and a proportion of complete remissions was observed upon MV-BiTE treatment (Figs. 12-14), there remained a potential to further increase efficacy, and an upregulation of genes associated with T cell inhibition and exhaustion was observed (Fig. 19). To address these issues and to further enhance the repertoire of immunomodulatory approaches for supporting T cell re-direction immunotherapies, potential of MV-encoded checkpoint inhibitors in CAR T cell treatment was investigated *in vitro*. When co-cultured with PSCA-specific CAR T cells, an effector-to-target cell ratio-dependent reduction in viability of patient-derived PC05 cells was observed, compared to incubation with untransduced human T cells (Fig. 22, upper panel). CAR T cell-mediated killing was enhanced by MV encoding anti-PD-1 antibodies Pembrolizumab (middle panel) and Nivolumab (lower panel) as compared to MV encoding control immunoglobulin.

3.4 Mathematical modeling of T cell-based MV-immunotherapies

The complex consequences of oncolytic measles virotherapy and the availability of alternative approaches for T cell re-direction require careful consideration of potential combination regimens. Mathematical modeling provides a tool for exploring complex biological mechanisms at reduced experimental cost. An appropriately designed model fitted to relevant experimental data can support the identification of crucial therapeutic parameters and allow *in silico* prediction of treatment outcomes. For a rational evaluation of the potential combinations of oncolytic measles viruses with BiTE and CAR T cell therapies investigated in this study, a mathematical model describing the interactions of tumor cells, oncolytic viruses, and the immune cell compartment was therefore conceived in collaboration with Drs. Daniel Santiago and Heiko Enderling at the Integrated Mathematical Oncology Department, H. Lee Moffitt Cancer Center and Research
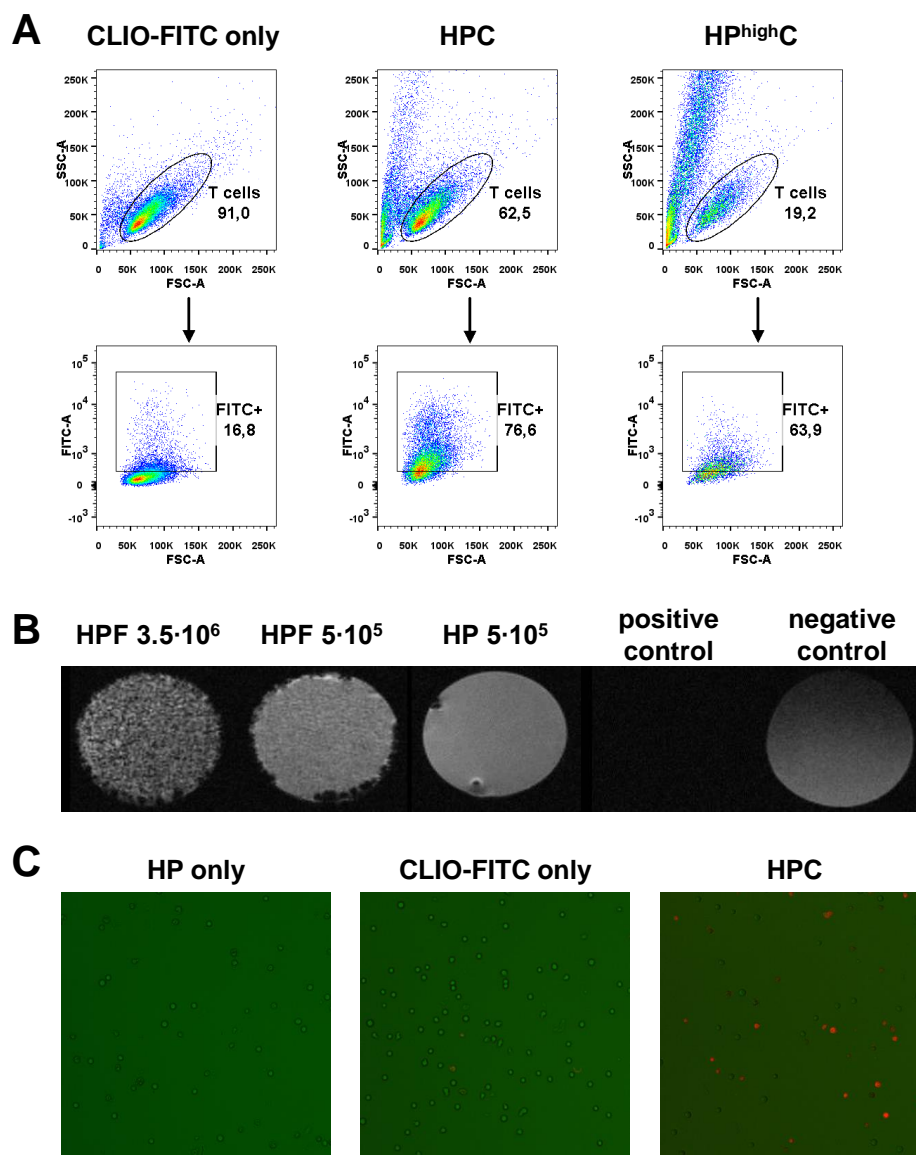
Figure 21: T cell labeling with iron oxide nanoparticles. A. Efficiency of T cell labeling with nanoparticles ex vivo. Stimulated human T cells were incubated with fluorescein isothiocyanate (FITC)-labeled iron oxide nanoparticles at 100 µg iron/mL (CLIO-FITC only), or additionally with 20 IU/mL heparin and 30 µg/mL protamine (HPC) or 20 IU/mL heparin and 60 µgL/mL protamine (HPhighC). FITC fluorescence was analyzed by flow cytometry. B. *in vitro* magnetic resonance imaging (MRI) of T cells labeled with iron oxide nanoparticles. Indicated numbers of pre-stimulated human T cells incubated with heparin and protamine only (HP) or additionally with ferumoxytol (HPF) were transferred to capillaries of a phantom and T2*-weighted images were acquired. H_2O and ferumoxytol diluted 1:100 in H_2O served as negative and positive controls, respectively. C. Intracellular detection of iron oxide nanoparticles. Stimulated human T cells were incubated with heparin and protamine (HP), CLIO-FITC, or heparin, protamine and CLIO-FITC (HPC) overnight. FITC fluorescence was analyzed by confocal microscopy. For better visualization, contrast and brightness were equally adjusted for all presented images.
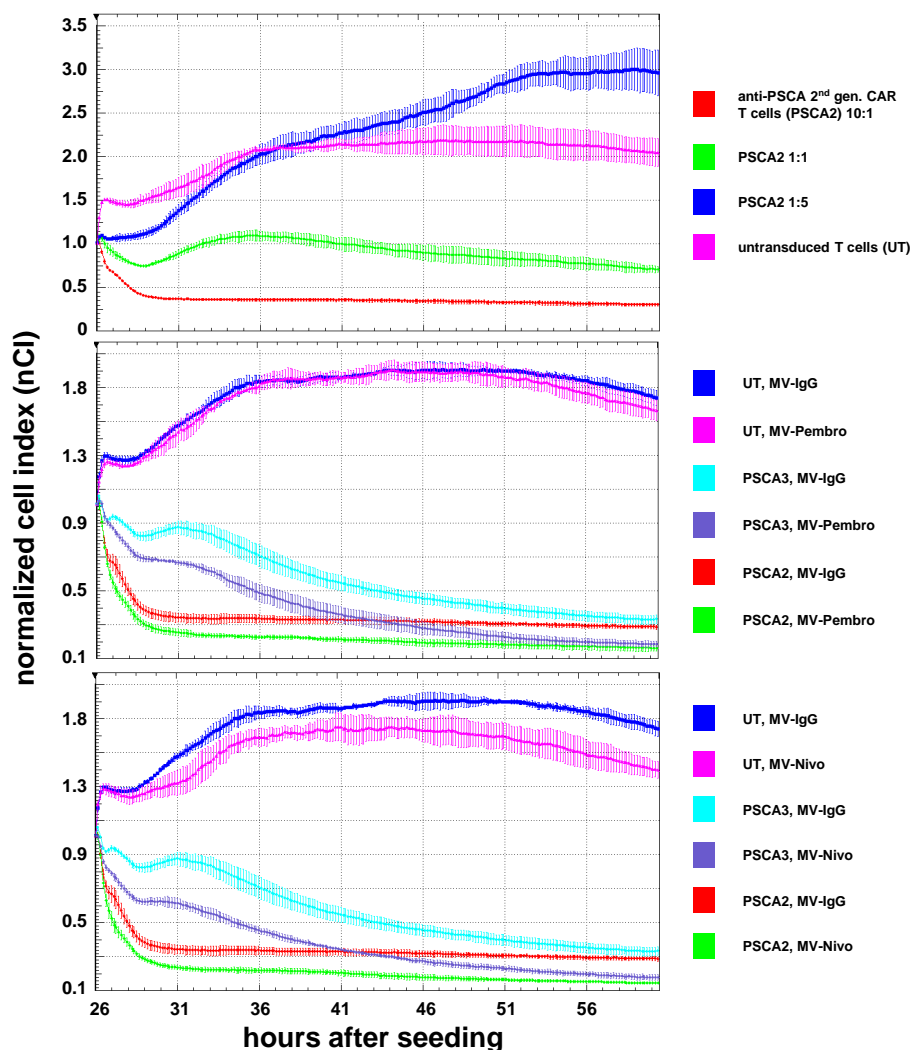
Figure 22: Combination of CAR T cells and checkpoint antibody-encoding MV against primary human tumor cell cultures. Human pancreatic carcinoma cells PC05 were seeded on a 96-well plate with electrodes at the bottom and incubated overnight. Carrier fluid only (upper panel) or oncolytic measles viruses encoding control immunoglobulin G4 (MV-IgG) or an anti-PD1 antibody, either Pembrolizumab (MV-Pembro, middle panel) or Nivolumab (MV-Nivo, bottom panel), at a multiplicity of infection of 1 were added to the respective wells. After 2 h of incubation, untransduced human T cells (UT) or T cells expressing a PSCA-specific CAR of the second (PSCA2) or third generation (PSCA3) were added to indicated samples and cell viability was analyzed over time via impedance measurement. Values were normalized to the first measurement after adding T cells (normalized cell index, nCI). Shown are mean + standard deviation of three technical replicates for each condition.
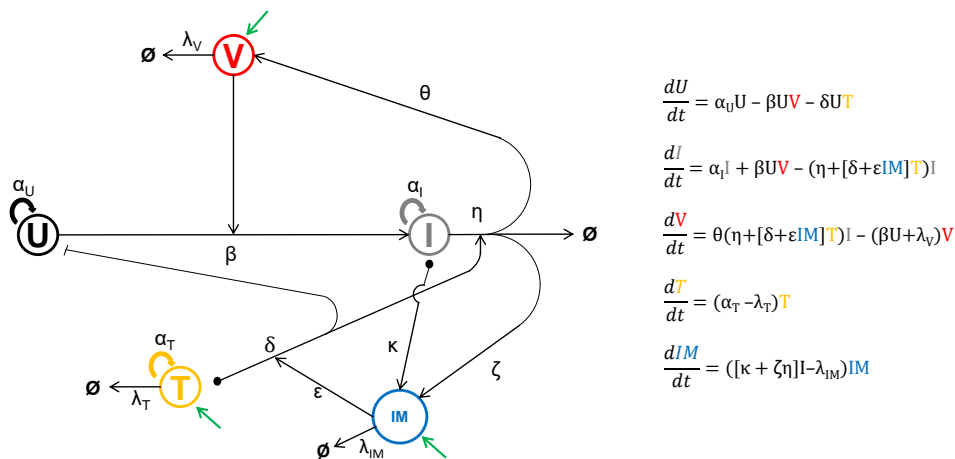
Figure 23: Mathematical modeling of oncolytic measles immunovirotherapy of cancer. The schematic on the left visualizes a model of the interplay between uninfected (U) and infected (I) tumor cells, (CAR) T cells (T), oncolytic virus (V), and virus-encoded immunomodulators (IM) in the context of tumor immunovirotherapy. This model is represented mathematically by the ordinary differential equations shown on the right. α – net growth rates, β – infection rate, δ – tumor cell killing by T cells, ε – immunomodulatory enhancement of T cell cytotoxicity, ζ –release of IM due to oncolysis of infected cells, η – death rate of infected cells, ϑ – release of viral progeny upon oncolysis, $\varkappa$ –secretion of IM by live infected cells, λ – rates of cell death, virus and IM degradation, respectively, $\varnothing$ – exit from the experimental system, green arrows – input by therapeutic intervention (injection).

Institute, Tampa, FL, USA* (Fig. 23). The general model, which can be expanded to include e.g. further immune cell compartments, signaling molecules, or therapeutic agents, if necessary, was restricted to a set of ordinary differential equations describing changes of five key variables over time.

Transfer of uninfected, i.e. virus-susceptible tumor cells (U) to an infected tumor cell compartment (I) corresponds to the amount of virus present (V) and the attributed rate of infection (β). Death of infected cells is associated with the release of viral progeny as well as of virus-encoded immunomodulators (IM) such as BiTEs or checkpoint inhibitors, which in turn can affect activity of T cells (T), resulting in reduction of both U and I. Parameters describing the respective activities and rates of effects have to be derived experimentally. For this, *in vitro* and *in vivo* experiments described in this thesis can inform on virus replication, infection, and cytolysis, T cell activity and persistence, and immunomodulatory parameters of BiTEs or other MV-encoded transgenes. Further model-guided data acquisition and subsequent fitting to the model is required for computing outcomes of additional combination treatments and schedules *in silico* for future identification of optimal conditions.

---

4 Discussion

Based on both pre-clinical and clinical evidence of T cell-mediated tumor regression upon oncolytic virotherapy (reviewed in[160]) and shortcomings of BiTE and CAR T cell re-direction approaches in the treatment of solid tumors in terms of safety and efficacy (reviewed in[32]), we proposed a mechanism of action of combined oncolytic immunotherapy in which virus-mediated tumor debulking and local inflammation support tumor-directed T cell responses. We furthermore hypothesized that virus-mediated tumor-directed expression of a BiTE could achieve tumor-restricted activity.

Attenuated measles vaccine viruses have beneficial properties for use as oncolytic agents, including a natural oncotropism, an excellent safety profile, fusogenicity, high immunogenicity, and genetic modifiability (reviewed in[94]). Therefore, to test our hypotheses, we engineered oncolytic measles viruses encoding BiTE constructs concomitantly targeting human model tumor antigens CD20 or carcinoembryonic antigen (CEA), respectively, and human or murine CD3 (MV-BiTE).

In this study, immune-mediated efficacy of MV-BiTE was demonstrated in a solid tumor model in immunocompetent mice and tools to further investigate combination immunotherapies based on MV and T cell re-direction strategies were developed.

4.1 A novel murine solid tumor model to study MV-BiTE

Due to lack of an appropriate existing mouse model to investigate efficacy and mechanism of action of MV-BiTE in immunocompetent hosts, we had to first generate a novel syngeneic murine solid tumor model allowing for measles virus entry and BiTE binding. In melanoma patients, promising results were achieved by T cell-mediated immunotherapies, including adoptive cell transfer[19], checkpoint inhibition[161,162], oncolytic virotherapy[87,88], and oncolytic virotherapy in combination with checkpoint inhibition[91,92]. For this first proof-of-concept study of MV-BiTE, we therefore decided to use a melanoma model. The murine B16 cell line, derived from a melanoma spontaneously formed in a wild-type C57BL/6 mouse, provides a well-established model in cancer immunotherapy research that is characterized by low T cell infiltration and therefore especially suited for studies on experimental therapies aiming at inducing T cell responses (reviewed in[163]). B16-CD20 cells stably expressing human CD20 had been generated previously in the lab146. By lentiviral transduction of B16-CD20 cells, we generated a B16-derived cell line expressing the human antigens CD20 and CD46 as BiTE target and measles virus entry receptor, respectively, for subsequent studies on MV-BiTE efficacy. While careful consideration of appropriate targets is absolutely essential for the clinical development of novel therapeutics regarding both efficacy and safety, we decided to use CD20 as a model antigen in this proof-of-concept study mainly due to availability of sequences of both the antigen and an appropriate scFv[164]. CD20 is a transmembrane protein expressed on most stages of B cell differentiation[165] and frequently found to be expressed on B cell malignancies[166]. It is the target of several approved therapeutics including rituximab, the first approved monoclonal antibody for cancer treatment[167,168]. CD20 was also reported to be expressed on a subset of melanoma cells with stem cell-like properties[169], yielding promising results when targeted therapeutically in mice[170] and human patients[171].

Cell surface expression of human antigens and susceptibility to measles virus were verified for B16-CD20-CD46 cells by flow cytometry and infection experiments, respectively. Kinetics of viral replication and virus-mediated cytotoxicity were comparable between MV-BiTE and unmodified MV, despite insertion of a transgene of approximately 1,600 nt. Expression of human CD46 on murine B16 cells increased titers of viral progeny by two orders of magnitude, to a similar level as observed in Vero MV producer cells. However, progeny titers peaked later compared to Vero cells and declined within four days, indicating post-entry restriction and limited permissiveness of mouse cells for MV. While CD46 cell surface density may be one factor[130,172], host cell-intrinsic factors are known to limit replication of measles vaccine strain viruses in mouse cells[173]. Accordingly, viral cell lysis after inoculation lagged behind on CD46-expressing B16 cells compared to Vero cells. Without expression of human CD46, no decline in B16 cell viability was observed upon inoculation with measles viruses.

4.2 Analyses of MV-BiTE *in vitro*

Importantly, we were able to isolate functional BiTEs from the supernatant of virus-infected Vero cells, as evidenced by flow cytometry-based cell binding assay, cell-mediated cytotoxicity assay, and target antigen-specific ELISA, which is not trivial for a negative strand RNA vector. Binding of BiTEs to target cells was antigen-specific. Observed percentages of peripheral blood mononuclear cells (PBMCs) bound by BiTEs specific for CD3 and CD20 correspond to literature values of relative T and B cell levels, respectively[174]. Target antigen-specific, BiTE concentration-dependent lysis of tumor cells by immune effector cells *in vitro* was demonstrated by lactate dehydrogenase assay. Compared to human PBMCs, a longer co-incubation time and higher BiTE concentrations were required for murine T cells and lower overall values of relative specific lysis were observed, indicating limitations of this assay for primary mouse immune cells. Despite sub-optimal culture conditions yielding relatively high background LDH release by murine T cells, BiTE-mediated target cell lysis was demonstrated for three independently produced BiTE suspensions. Thus, specificity and functionality of BiTEs expressed by virus-infected cells was shown *in vitro*.

Production of good manufacturing practice (GMP)-grade MV is possible in bioreactors[95], but not routinely performed in the academic setting. Therefore, virus suspensions were produced from crude lysates of infected cells, resulting in the presence of cellular proteins and BiTEs at relatively high levels of approximately 2 µg/mL, as estimated by protein analyses[150]. While this allows for introduction of MV-encoded BiTEs into murine tumors without having to rely entirely on de novo synthesis of the transgene by mouse cells, it represents a crucial limitation for animal experiments which required careful consideration of appropriate controls.

4.3 MV-BiTE efficacy in immunocompetent mice

B16-CD20-CD46 cells engrafted in immunocompetent C57BL/6 mice and formed subcutaneous tumors at the site of injection despite the expression of foreign antigens. This model was used to investigate efficacy of MV-BiTE following the established schedule of five intratumoral virus injections on consecutive days[146].

Intratumoral treatment with suspensions of unmodified MV and MV encoding a control BiTE, both also produced from crude cell lysates and thus of similar composition as MV-BiTE, prolonged survival of mice bearing subcutaneous B16-CD20-CD46 tumors compared to mock treatment, but were significantly less effective than MV encoding BiTEs specific for the tumor target antigen CD20. This was not due simply to the injection of CD20-targeting BiTE molecules present in the virus suspension, as intratumoral injection of an equivalent amount of purified BiTE alone had little effect. The analysis of viral gene expression kinetics revealed a decrease in BiTE and MV-N mRNA levels to baseline within five days after treatment. Moreover, previous UV irradiation of MV-BiTE and unmodified MV to decrease replicative capacity did not abrogate efficacy of either treatment, indicating that viral replication *in vivo* was not a main driver of anti-tumor efficacy in this model. However, UV irradiation may have influenced not only viral replication, but also the molecular composition of the virus suspension, potentially leading to higher immunogenicity e.g. via danger-associated molecular patterns. For the murine paramyxovirus Sendai, anti-tumor efficacy after UV inactivation was observed and shown to rely on an interferon response induced upon recognition of disrupted viral RNA via intracellular retinoic acid inducible gene I (RIG-I) (reviewed in[175]). In addition, for an oncolytic vaccinia virus, inactivation of viral gene expression and replication increases immune-mediated anti-tumor efficacy[176]. As this depends on inactivation of a gene involved in preventing antiviral host cell responses to sensing of viral DNA, the same mechanism cannot account for RNA viruses such as MV. Still, although highly speculative, a similar mechanism may have masked a decrease in anti-tumor efficacy based on reduced lytic replication of irradiated MV. Nevertheless, our findings indicate that non-replicating MV-BiTE can induce durable tumor remissions, providing a potential approach to increase safety of oncolytic virotherapy. Furthermore, in a more permissive tumor, increased lytic replication may facilitate enhanced therapeutic efficacy of MV-BiTE as compared to the B16-CD20-CD46 model.

In immunodeficient NSG mice bearing subcutaneous CEA-expressing human colorectal carcinoma tissue sphere culture xenografts, intratumoral injections of MV encoding a CEA-targeting BiTE in combination with transfer of unstimulated human PBMCs resulted in prolonged survival, compared to both monotherapies alone[150,151]. High levels of sustained viral gene expression were observed in virus-treated tumors. Although MV-BiTE efficacy in both models cannot be directly compared, this provides evidence for enhanced virus replication in a more permissive model, associated with anti-tumor activity of transferred PBMCs. Importantly, in this model that allows for expression of high BiTE levels, no BiTE was detected in peripheral blood. However, MV-BiTE pharmacodynamics and potential toxicities would need to be analyzed in more relevant models prior to future clinical development. Transgenic mice expressing human CD46 in all nucleated cells in a similar pattern as in humans are available for biodistribution studies and can also be used for efficacy analyses, and toxicity studies are often performed in macaques, which more closely mimic the human organism[93,177].

Efficacy of MV encoding anti-CEA BiTE was furthermore assessed in C57BL/6 mice bearing subcutaneous murine colon carcinoma MC38-CEA tumors stably expressing human CEA as a BiTE target antigen[150,151]. Notably, MC38-CEA cells lack expression of an MV entry receptor and thus are less susceptible to MV infection than B16-CD20-CD46 cells. MC38-CEA-CD46 cells expressing human CD46 were generated analogously to B16-CD20-CD46, but ulcerated quickly when injected subcutaneously into C57BL/6 mice and were frequently rejected. Due to the origin from a murine colon carcinoma induced by chemical carcinogens[178], parental MC38 cells have a high mutational load[179] and tumors show high baseline levels of T cell infiltration. A previous study reporting loss of MC38 tumorigenicity after transduction with a retroviral

vector encoding murine IL-12 indicates potential for T cell-mediated rejection upon expression of foreign genes[180]. In a subcutaneous MC38 model, previous work in our lab has shown high rates of T cell-mediated complete tumor remissions following treatment with an IL-12-encoding MV[181]. Therefore, also without exogenous expression of IL-12, expression of two foreign antigens may tip the balance of tumor immunosurveillance in C57BL/6 mice in favor of anti-tumor T cell responses and thus facilitate rejection of MC38-CEA-CD46 tumors. Therefore, MC38-CEA cells not expressing human CD46 were used. Interestingly, treatment with both MV encoding a CEA-targeting BiTE or a CD20-targeting control BiTE, respectively, induced high rates of tumor remission in this model, indicating that in this immunologically "hot" tumor model, neither viral replication nor specific BiTE activity were required for inducing anti-tumor immunity. This adds to the conclusion that viral replication is not necessarily required for anti-tumor efficacy and that immune-mediated mechanisms of action dominate in the models studied.

Previous studies with immunocompetent C57BL/6 mice have been performed in the lab using MV re-targeted to human CEA or CD20 ectopically expressed on the surface of MC38 or B16 cells, respectively. In the MC38-CEA model, MV encoding GM-CSF yielded promising results compared to control viruses, including delayed tumor growth, prolonged overall survival, complete tumor remissions, and long-term immune protection[143]. However, this approach was not successful in the B16 model. MV encoding checkpoint inhibitors showed prolonged overall survival in the B16-CD20 model, but no durable complete tumor remissions were observed[146]. T cell infiltration into B16 tumors was still limited upon combination treatment with MV and checkpoint inhibition, indicating that an alternative strategy aiming at inducing activation and proliferation of T cells, such as BiTE-mediated re-direction, could achieve improved treatment outcome.

With regards to the high prevalence of measles immunity in the general population, we analyzed the impact of MV-immunization on treatment outcome in the B16-CD20-CD46 model. To this end, we pre-immunized C57BL/6 mice with highly purified MV-NIS. Immunization was confirmed via ex vivo serum neutralization assay. This did not result in reduced efficacy of treatment with MV-BiTE and unmodified MV, respectively, compared to MV-naïve mice, which may be attributed at least in part to the intratumoral route of administration. This has translational implications as these results indicate that MV-immune individuals may still benefit from MV-BiTE treatment despite the presence of neutralizing antibodies in serum, but this requires further investigations. Interestingly, a recent study demonstrated increased efficacy of oncolytic reovirus in presence of neutralizing antibodies via a monocyte-dependent mechanism[182]. This challenged the former paradigm of neutralizing antibodies being a hindrance to oncolytic virotherapy, which had led to the development of several approaches to achieve antibody escape, including immunosuppressive pre-conditioning[183], virus shielding[184], usage of cell carriers[185-190], mutation of known antibody epitopes[85], and envelope exchange[85,155,191-193]. We observed a statistically non-significant trend towards prolonged survival and increased occurrence of complete tumor remissions in MV-immunized versus naïve mice. Based on these observations, a new project was initiated in the lab in which we are investigating potential roles of neutralizing antibodies and immune cells such as monocytes in the delivery of MV as evidenced for oncolytic reovirus.

Considering the observed median survival of mock-treated mice of below 20 days, the subcutaneous B16-CD20-CD46 tumor model is fairly aggressive. Nevertheless, in approximately 5% and 17% of all C57BL/6 mice treated with unmodified MV and MV-BiTE in the course of this study, respectively, complete tumor remissions were observed. Re-challenge experiments with parental B16 cells not expressing the foreign antigens CD20 and CD46 demonstrated long-term systemic immune protection in a subset of these animals. Importantly, this furthermore indicated immune

responses against endogenous B16 antigens upon MV-BiTE treatment and thus antigen spread, supporting our initial hypothesis of achieving anti-tumor protection by combining T cell re-targeting and antigen-agnostic vaccination by MV.

4.4 Mechanisms of action of MV-BiTE

Long-term immune control implies a T cell-mediated mechanism of action. Therefore, we analyzed tumor-infiltrating lymphocytes by flow cytometry. Upon MV-BiTE treatment, increased T cell infiltration into the tumor and high CD8+ to CD4+ T cell ratios were observed, indicating a strong cytotoxic T cell response. T cells were activated by treatment with both MV-BiTE and MV encoding a control BiTE, respectively, as evidenced by a trend towards higher proportions of T cells expressing the activation marker CD69. Relative abundances of T_{regs} and of T cells positive for the co-inhibitory molecule CTLA-4 were reduced upon MV-BiTE treatment, and a TH1-skewed pro-inflammatory cytokine response was indicated by 100-fold upregulation of the transcription factor T-bet[194]. NanoString targeted transcriptome analysis revealed strong clustering of different treatment groups according to relative expression of T cell-related genes, with MV-BiTE treatment yielding highest expression levels. This included not only genes associated with T cell activation, differentiation, and proliferation, but also with T cell inhibition and exhaustion. Although the proportion of CD3+ T cells expressing CTLA-4 was reduced according to flow cytometry data, overall expression levels of *Ctla-4* were elevated compared to mock treatment, which may be explained by the increase in absolute numbers of tumor-infiltrating T cells. These data provide a rationale for future combination with checkpoint blockade antibodies, which might further prolong survival and increase incidence of complete tumor remissions compared to MV-BiTE treatment alone.

Furthermore, the data represent a resource for exploratory rather than simply descriptive analyses, yielding several target genes which may be associated with efficacy, including CXCL9 and CXCL10, among others. Validation of these targets and investigation of potential mechanisms is the aim of another recently started research project in the lab. However, so far only a correlation of T cell responses and MV-BiTE efficacy was demonstrated, and efficacy and mechanistic analyses were not performed in the same animals. To validate a causative connection between observed T cell responses and efficacy, depletion experiments will be performed in the future. For this, mice will receive antibodies targeting individual subpopulations of immune cells, including CD8+ T cells, CD4+ T cells, and natural killer (NK) cells, respectively, prior to tumor cell implantation and throughout the experiment. In addition, the role of dendricitc cells (DCs) may be evaluated in BatF3-knockout mice[195,196], and macrophage depletion can be achieved by injection of liposomes containing clodronate[197,198]. In these settings, MV-BiTE treatment will be compared to unmodified MV and mock treatment, respectively, to evaluate the relative contributions of these cell types to efficacy. Based on the present data, we hypothesize that efficacy will rely mainly on CD8+ T cells via direct BiTE-mediated and TCR-specific cytotoxicity, but to smaller degree also on CD4+ T cells via cytokine release and BiTE-mediated induction of apoptosis in tumor cells and possibly on DCs via T cell priming.

Regarding the characteristics of the T cell response upon MV-BiTE treatment, T cell receptor sequencing, together with cloning of identified TCRs and antigen stimulation assays, can provide insights into the clonality and specificity of the T cell compartment[199]. With this method, we aim to address various questions, including whether known B16 antigens might play a role in

tumor recognition. We propose that several clones, rather than one single clone, drive anti-tumor efficacy due to MV-induced antigen spread. Presence or absence of clones with a particular specificity might be decisive for treatment success. Furthermore, studies showed that CAR T cells with original specificity for viral antigens are especially effective in mediating anti-tumor responses[200-202]. We therefore hypothesize that virus-specific T cells re-directed by BiTEs may have added to the efficacy observed in pre-immunized mice.

Oncolytic viruses are a unique class of novel immunotherapeutics especially suited for combination therapies[203-206]. Similar to our approach, other researchers have proposed[207-210] and investigated combinations of oncolytic viruses with tumor-targeting BiTEs[211-213] or CARs[214-218] or both BiTEs and CARs[219]. Anti-tumor efficacy of the mentioned combinations was observed in various solid tumor models. Yu and colleagues were the first to test a BiTE-encoding oncolytic virus *in vivo*. In xenograft experiments in immunodeficient mice with intratumoral PBMCs, they reported anti-tumor efficacy of a vaccinia virus encoding an anti-EphA2 BiTE[211,220]. Oncolytic adenoviruses encoding BiTEs targeting EGFR[212] and EpCAM[213], respectively, showed efficacy in an immunodeficient mouse model with transfer of immune cells and in cancer biopsies ex vivo, respectively. Wing et al. used the anti-EGFR BiTE-encoding adenovirus in combination with folate receptor alpha (FRα)-targeted CAR T cells, showing BiTE-mediated CAR T cell re-direction *in vitro* and increased anti-tumor efficacy compared to the respective monotherapies in immunodeficient mice[219]. Further studies used oncolytic viruses as a vector for tumor-targeted delivery of immunotherapeutic transgenes, including chemokines[218], checkpoint inhibitors[215], or both cytokines and checkpoint inhibitors[214], to support CAR T cell efficacy in immunodeficient models. Additionally, the use of CAR T cells as carriers for oncolytic viruses has shown promising results *in vitro*[221]. Recently, two groups have reported anti-tumor properties of oncolytic adenoviruses encoding a BiTE targeting cancer-associated fibroblasts[222,223], thereby expanding the repertoire of potential targets beyond tumor cells alone.

This multitude of recent studies illustrates the current interest in such combination approaches and the versatility of the field. In one recent study, efficacy of combination treatment with murine mesothelin-targeted CAR T cells and an oncolytic adenovirus encoding the cytokines TNFα and IL-2 was observed in a syngeneic mouse model of pancreatic ductal adenocarcinoma[216]. However, to our knowledge, no other study has yet shown efficacy of combining oncolytic viruses and T cell re-direction immunotherapies in an organism with an intact immune system, i.e. an immunocompetent mouse model. Rather, experiments were performed in immunodeficient mice, which is a highly artificial model that additionally has limitations regarding lack of cytokines and thus T cell homing and persistence, and in patient-derived ascites fluids containing a clinically relevant composition of human tumor and immune cells and cytokines but lacking three-dimensional structures of a solid tumor, associated vasculature and lymphoid organs, and organismic compartmentalization in general. In the present study, we provide evidence for efficacy of a BiTE-encoding oncolytic virus in an immunocompetent model for the first time.

4.5 Combining oncolytic measles virotherapy with CAR T cells

CAR T cells as a defined effector cell population can serve as a simplified model to investigate the impact of oncolytic viruses on T cell distribution, activity, and persistence *in vivo*. For combination experiments with oncolytic measles viruses, we used an established model of CAR T cell therapy of pancreatic carcinoma. Patients diagnosed with pancreatic carcinoma have a

median overall survival of only approximately six months, also because diagnosis often occurs at a late stage of the disease when tumors progress rapidly[224]. Limited treatment options are available, especially by immunotherapeutic approaches, due to dense stroma and strong immunosuppression. CAR constructs targeting prostate stem cell antigen (PSCA) have been shown to be effective in a mouse xenograft model of pancreatic cancer158. However, PSCA expression on normal tissues prevents direct translation to clinical application due to potentially severe on-target off-tumor effects[225]. Therefore, novel approaches are desperately needed for safe and effective treatment of pancreatic carcinoma, with combination of CAR T cell therapy with oncolytic virotherapy as one strategy.

Identification of highly specific target antigens such as claudin 18.2 in gastric and pancreatic cancer[226-230] represents a potential way to achieve efficient targeting at relatively low risk of side effects. Targeting of several target antigens by different components of a combination treatment regimen can promote higher specificity and thus increased efficacy without compromising safety. Several approaches have been reported of multi-specific antibody (reviewed in[231,232]) and CAR constructs[233,234], respectively, to address both intra-patient and inter-patient heterogeneities. Trivalent CAR T cells targeting HER2, IL13Rα2, and EphA2 were effective against glioblastoma xenografts in immunodeficient mice[233], and CAR T cells simultaneously targeting CD19, CD20, and CD22 showed tumor cell killing in patient-derived B-ALL cells *in vitro*[234]. Further studies investigated the use of modular CARs to decouple cytotoxic potential and antigen specificity[235-238]. The UniCAR platform uses T cells expressing a CAR lacking a targeting moiety and targeting modules binding to the inert CAR T cells for re-direction. This allows for simultaneous targeting and for switching CAR specificity during treatment and might potentially benefit from a combination with tumor-restricted expression of targeting modules by oncolytic viruses. Reported UniCAR-targeted antigens tested in immunodeficient mouse models include CD33 and CD123 in an acute myeloid leukemia (AML) model[238], CD19 in a B-ALL model[235], and EGFR in epithelial cancer models[236,237]. The potential of modulating specificity on various levels via pre- and post-entry targeting of MV and additionally choosing appropriate BiTE and/or CAR targets provides flexibility to the combination platform investigated in this study. Antigen escape frequently occurs in the treatment of CD19-positive hematological malignancies by BiTEs and CARs, causing relapses. While targeting several antigens concomitantly may help to overcome this limitation of antigen-specific treatments, importantly, MV-mediated immune activation and antigen-agnostic vaccination as described above may represent another strategy to effectively prevent antigen escape.

HPAC cells provided an ideal model target for testing both CAR- and BiTE-mediated T cell re-direction as well as measles virus-induced oncolysis due to simultaneous expression of PSCA, CEA, and CD46 surface antigens. Both targeting of PSCA by CARs and of CEA by MV-encoded BiTEs achieved rapid eradication of tumor cells *in vitro* within one day, while virus-mediated cytotoxicity was observed after two days. Nevertheless, a pilot experiment in NSG mice bearing subcutaneous tumors did not result in statistically significant differences between tested monotherapies and combination treatments. Although this might be due to small group sizes resulting in low statistical power of this experiment, treatment dosing and scheduling were probably not optimal. MV treatment on four consecutive days was followed by T cell injection according to the standard protocols. A suboptimal T cell dose of 10% of the dose known to be curative in the model[158] was intentionally chosen to be able to observe a possible benefit of additional MV treatment. Combination with checkpoint inhibition may improve efficacy, as observed in a co-culture assay with PSCA-specific CAR T cells and patient-derived human pancreatic tumor cells *in vitro*. Tumor

cells lysis by CAR T cells depended on the effector-to-target cell ratio and was accelerated when tumor cells had previously been inoculated with MV encoding checkpoint inhibitors, compared to MV encoding control IgG. A higher initial T cell number might also improve outcome in the NSG, as no T cells persisted 30 days post injection. For future experiments, we tested T cell labeling with iron oxide nanoparticles for detection by MRI, as non-invasive longitudinal tracking would provide a useful tool to monitor T cells *in vivo*. High labeling efficiencies were achieved and labeled T cells were detected via MRI *in vitro*. In future experiments, immunohistochemistry will be performed on labeled T cells to identify nanoparticle distribution, and viability and functionality of labeled T cells will be assessed *in vitro*. Subsequently, detection of T cells labeled with iron oxide nanoparticles by magnetic resonance imaging will be assessed *in vivo*, comparing different injection routes and T cell doses. These data can be used for treatment optimization.

4.6 Mathematical modeling

Exhaustive testing of alternative treatment schedules to identify a potentially successful experimental layout in terms of order and dosing of treatments would not have been feasible. Although the complex dynamics of combination immunotherapy and oncolytic virotherapy are drastically simplified and "all models are wrong by definition"[239], mathematical models provide the possibility to identify crucial treatment parameters and generate novel hypotheses (reviewed in[240,241]). A previously published mathematical model describing oncolytic virotherapy in combination with immune checkpoint inhibition, for example, indicates an optimal dose of an immune checkpoint inhibitor that, if exceeded, results in reduced anti-tumor efficacy due to enhanced anti-viral immune responses[242]. The authors concluded that such levels of checkpoint inhibition should be avoided in clinical trials, indicating the potential of mathematical modeling for translational research. Other models have been developed to analyze combinations of oncolytic viruses with radiotherapy[243], a proteasome inhibitor[244], or transfer of dendritic cells[245], among others.

To cope with the multitude of potential treatment combinations and to be able to optimize treatment schedules without exhaustive empirical testing, a mathematical model of MV and T cell combination treatments was conceived in this study and will be further developed in the future following a general approach to mathematical modeling of oncolytic virotherapy[246]. As a next step, the model needs to be calibrated by fitting to experimental data. Results from this thesis will be used and additional parameters will be derived by appropriate experiments, if necessary. Subsequently, validation of the model will be performed by predicting experimental outcomes and comparing these to experimentally derived results. If necessary, the complexity of the model can be increased or reduced. For example, additional immune cell compartments can be added or the parameter describing virus replication might be removed. Finally, *in silico* studies will be performed to provide new insights and guide rational development of treatment regimens.

4.7 Conclusion and outlook

The present thesis provides, for the first time, proof-of-concept for combination immunotherapy with a BiTE-encoding oncolytic virus in an immunocompetent mouse model. Our data furthermore provide a rationale for future combination of MV-BiTE therapy with immune checkpoint inhibition. A model for simultaneous targeting of distinct tumor surface antigens by MV, BiTEs, and CARs

was established and pilot experiments *in vitro* and in immunodeficient mice indicated functionality of tumor targeting. Furthermore, CAR T cell activity against pancreatic tumor cultures was increased by MV-encoded checkpoint inhibitors. Finally, we established a protocol for T cell labeling with iron oxide nanoparticles for future *in vivo* tracking via magnetic resonance imaging and a mathematical model to perform *in silico* studies to predict outcome of experimental combination treatment schedules.

In the future, immune cell depletion experiments will be performed in the B16-CD20-CD46 model to evaluate the relative contributions of distinct immune cell subsets to MV-BiTE efficacy. Furthermore, TCR sequencing will be applied to analyze clonality of tumor-reactive T cells. Based on targeted transcriptome analysis data, combination treatment with checkpoint inhibition will be performed to further improve efficacy of MV-BiTE in this model. Nanoparticle uptake by T cells will be validated by immunohistochemistry and viability and functionality of labeled T cells will be evaluated prior to assessing MRI-based detection *in vivo*. For calibration of the mathematical model, relevant parameters will be derived at required resolutions and model predictions will be validated experimentally before applying the model for hypothesis generation and treatment schedule optimization. This will support future development of combined oncolytic measles virus and T cell re-direction therapies to hopefully provide improved treatment options to cancer patients.

References

1 Malvezzi, M. et al. European cancer mortality predictions for the year 2019 with focus on breast cancer. Annals of oncology : official journal of the European Society for Medical Oncology, doi:10.1093/annonc/mdz051 (2019).

2 Weeks, J. C. et al. Patients' expectations about effects of chemotherapy for advanced cancer. The New England journal of medicine 367, 1616-1625, doi:10.1056/NEJMoa1204410 (2012).

3 Coley, W. B. II. Contribution to the Knowledge of Sarcoma. Annals of surgery 14, 199-220 (1891).

4 Ehrlich, P. Ueber den jetzigen Stand der Karzinomforschung. Nederlands Tijdschrift voor Geneeskunde 273-290 (1909).

5 Stutman, O. Tumor development after 3-methylcholanthrene in immunologically deficient athymic-nude mice. Science (New York, N.Y.) 183, 534-536 (1974).

6 Shankaran, V. et al. IFNgamma and lymphocytes prevent primary tumour development and shape tumour immunogenicity. Nature 410, 1107-1111, doi:10.1038/35074122 (2001).

7 Morales, A., Eidinger, D. & Bruce, A. W. Intracavitary Bacillus Calmette-Guerin in the treatment of superficial bladder tumors. The Journal of urology 116, 180-183 (1976).

8 Pettenati, C. & Ingersoll, M. A. Mechanisms of BCG immunotherapy and its outlook for bladder cancer. Nature reviews. Urology 15, 615-625, doi:10.1038/s41585-018-0055-4 (2018).

9 Apetoh, L. et al. Toll-like receptor 4-dependent contribution of the immune system to anticancer chemotherapy and radiotherapy. Nature medicine 13, 1050-1059, doi:10.1038/nm1622 (2007).

10 Balachandran, V. P. et al. Imatinib potentiates antitumor T cell responses in gastrointestinal stromal tumor through the inhibition of Ido. Nature medicine 17, 1094-1100, doi:10.1038/nm.2438 (2011).

11 Gotwals, P. et al. Prospects for combining targeted and conventional cancer therapy with immunotherapy. Nature reviews. Cancer 17, 286-301, doi:10.1038/nrc.2017.17 (2017).

12 Gajewski, T. F., Schreiber, H. & Fu, Y. X. Innate and adaptive immune cells in the tumor microenvironment. Nature immunology 14, 1014-1022, doi:10.1038/ni.2703 (2013).

13 Chen, D. S. & Mellman, I. Oncology meets immunology: the cancer-immunity cycle. Immunity 39, 1-10, doi:10.1016/j.immuni.2013.07.012 (2013).

14 Rosenberg, S. A. et al. Use of tumor-infiltrating lymphocytes and interleukin-2 in the immunotherapy of patients with metastatic melanoma. A preliminary report. The New England journal of medicine 319, 1676-1680, doi:10.1056/NEJM198812223192527 (1988).

15 Dudley, M. E. et al. Cancer regression and autoimmunity in patients after clonal repopulation with antitumor lymphocytes. Science (New York, N.Y.) 298, 850-854, doi:10.1126/science.1076514 (2002).

16 Delorme, E. J. & Alexander, P. Treatment of Primary Fibrosarcoma in the Rat with Immune Lymphocytes. Lancet 2, 117-120 (1964).

17 Fernandez-Cruz, E., Woda, B. A. & Feldman, J. D. Elimination of syngeneic sarcomas in rats by a subset of T lymphocytes. The Journal of experimental medicine 152, 823-841 (1980).

18 Rosenberg, S. A., Spiess, P. & Lafreniere, R. A new approach to the adoptive immunotherapy of cancer with tumor-infiltrating lymphocytes. Science (New York, N.Y.) 233, 1318-1321 (1986).

19 Rosenberg, S. A. & Restifo, N. P. Adoptive cell transfer as personalized immunotherapy for human cancer. Science (New York, N.Y.) 348, 62-68, doi:10.1126/science.aaa4967 (2015).

20 Pardoll, D. M. The blockade of immune checkpoints in cancer immunotherapy. Nature reviews. Cancer 12, 252-264, doi:10.1038/nrc3239 (2012).

21 Sharma, P. & Allison, J. P. The future of immune checkpoint therapy. Science (New York, N.Y.) 348, 56-61, doi:10.1126/science.aaa8172 (2015).

22 Wei, S. C., Duffy, C. R. & Allison, J. P. Fundamental Mechanisms of Immune Checkpoint Blockade Therapy. Cancer discovery 8, 1069-1086, doi:10.1158/2159-8290.CD-18-0367 (2018).

23 Chen, L. Co-inhibitory molecules of the B7-CD28 family in the control of T-cell immunity. Nature reviews. Immunology 4, 336-347, doi:10.1038/nri1349 (2004).

24 Freeman, G. J. et al. Engagement of the PD-1 immunoinhibitory receptor by a novel B7 family member leads to negative regulation of lymphocyte activation. The Journal of experimental medicine 192, 1027-1034 (2000).

25 Dong, H. et al. Tumor-associated B7-H1 promotes T-cell apoptosis: a potential mechanism of immune evasion. Nature medicine 8, 793-800, doi:10.1038/nm730 (2002).

26 Hargadon, K. M., Johnson, C. E. & Williams, C. J. Immune checkpoint blockade therapy for cancer: An overview of FDA-approved immune checkpoint inhibitors. International immunopharmacology 62, 29-39, doi:10.1016/j.intimp.2018.06.001 (2018).

27 Couzin-Frankel, J. Breakthrough of the year 2013. Cancer immunotherapy. Science (New York, N.Y.) 342, 1432-1433, doi:10.1126/science.342.6165.1432 (2013).

28 Platten, M. & Offringa, R. Cancer immunotherapy: exploiting neoepitopes. Cell research 25, 887, doi:10.1038/cr.2015.66 (2015).

29 Kreiter, S. et al. Erratum: Mutant MHC class II epitopes drive therapeutic immune responses to cancer. Nature 523, 370, doi:10.1038/nature14567 (2015).

30 Sahin, U. et al. Personalized RNA mutanome vaccines mobilize poly-specific therapeutic immunity against cancer. Nature 547, 222-226, doi:10.1038/nature23003 (2017).

31 Tran, E. et al. T-Cell Transfer Therapy Targeting Mutant KRAS in Cancer. The New England journal of medicine 375, 2255-2262, doi:10.1056/NEJMoa1609279 (2016).

32 Slaney, C. Y., Wang, P., Darcy, P. K. & Kershaw, M. H. CARs versus BiTEs: A Comparison between T Cell-Redirection Strategies for Cancer Treatment. Cancer discovery 8, 924-934, doi:10.1158/2159-8290.CD-18-0297 (2018).

33 Baeuerle, P. A. & Reinhardt, C. Bispecific T-cell engaging antibodies for cancer therapy. Cancer research 69, 4941-4944, doi:10.1158/0008-5472.CAN-09-0547 (2009).

34 Klinger, M., Benjamin, J., Kischel, R., Stienen, S. & Zugmaier, G. Harnessing T cells to fight cancer with BiTE(R) antibody constructs–past developments and future directions. Immunological reviews 270, 193-208, doi:10.1111/imr.12393 (2016).

35 Frankel, S. R. & Baeuerle, P. A. Targeting T cells to tumor cells using bispecific antibodies. Current opinion in chemical biology 17, 385-392, doi:10.1016/j.cbpa.2013.03.029 (2013).

36 Krishnamurthy, A. & Jimeno, A. Bispecific antibodies for cancer therapy: A review. Pharmacology & therapeutics 185, 122-134, doi:10.1016/j.pharmthera.2017.12.002 (2018).

37 Offner, S., Hofmeister, R., Romaniuk, A., Kufer, P. & Baeuerle, P. A. Induction of regular cytolytic T cell synapses by bispecific single-chain antibody constructs on MHC class I-negative tumor cells. Molecular immunology 43, 763-771, doi:10.1016/j.molimm.2005.03.007 (2006).

38 Loffler, A. et al. A recombinant bispecific single-chain antibody, CD19 x CD3, induces rapid and high lymphoma-directed cytotoxicity by unstimulated T lymphocytes. Blood 95, 2098-2103 (2000).

39 Bargou, R. et al. Tumor regression in cancer patients by very low doses of a T cell-engaging antibody. Science (New York, N.Y.) 321, 974-977, doi:10.1126/science.1158545 (2008).

40 Haas, C. et al. Mode of cytotoxic action of T cell-engaging BiTE antibody MT110. Immunobiology 214, 441-453, doi:10.1016/j.imbio.2008.11.014 (2009).

41 Mack, M., Gruber, R., Schmidt, S., Riethmuller, G. & Kufer, P. Biologic properties of a bispecific single-chain antibody directed against 17-1A (EpCAM) and CD3: tumor cell-dependent T cell stimulation and cytotoxic activity. Journal of immunology (Baltimore, Md. : 1950) 158, 3965-3970 (1997).

42 Münz, M. et al. Abstract 4841: Lysis of cancer cells by highly purified T regulatory cells engaged via an EpCAM/CD3-bispecific BiTE antibody. Cancer research 72, 4841-4841, doi:10.1158/1538-7445.am2012-4841 (2012).

43 Nagele, V. et al. Changes in clinical laboratory parameters and pharmacodynamic markers in response to blinatumomab treatment of patients with relapsed/refractory ALL. Experimental hematology & oncology 6, 14, doi:10.1186/s40164-017-0074-5 (2017).

44 Hoffmann, P. et al. Serial killing of tumor cells by cytotoxic T cells redirected with a CD19-/CD3-bispecific single-chain antibody construct. International journal of cancer 115, 98-104, doi:10.1002/ijc.20908 (2005).

45 Johnson, L. A. & June, C. H. Driving gene-engineered T cell immunotherapy of cancer. Cell research 27, 38-58, doi:10.1038/cr.2016.154 (2017).

46 June, C. H. & Sadelain, M. Chimeric Antigen Receptor Therapy. The New England journal of medicine 379, 64-73, doi:10.1056/NEJMra1706169 (2018).

47 June, C. H., O'Connor, R. S., Kawalekar, O. U. & Ghassemi, S. CAR T cell immunotherapy for human cancer. 359, 1361-1365, doi:10.1126/science.aar6711 (2018).

48 Yang, Y. et al. CD4 CAR T Cells Mediate CD8-like Cytotoxic Anti-Leukemic Effects Resulting in Leukemic Clearance and Are Less Susceptible to Attenuation By Endogenous TCR Activation Than CD8 CAR T Cells. Blood 126, 100-100 (2015).

49 Davenport, A. J. et al. Chimeric antigen receptor T cells form nonclassical and potent immune synapses driving rapid cytotoxicity. Proceedings of the National Academy of Sciences of the United States of America 115, E2068-E2076, doi:10.1073/pnas.1716266115 (2018).

50 Mueller, K. T. et al. Cellular kinetics of CTL019 in relapsed/refractory B-cell acute lymphoblastic leukemia and chronic lymphocytic leukemia. Blood 130, 2317-2325, doi:10.1182/blood-2017-06-786129 (2017).

51 Mueller, K. T. et al. Clinical Pharmacology of Tisagenlecleucel in B-cell Acute Lymphoblastic Leukemia. Clinical cancer research : an official journal of the American Association for Cancer Research 24, 6175-6184, doi:10.1158/1078-0432.CCR-18-0758 (2018).

52 Xu, Y. et al. Closely related T-memory stem cells correlate with in vivo expansion of CAR.CD19-T cells and are preserved by IL-7 and IL-15. Blood 123, 3750-3759, doi:10.1182/blood-2014-01-552174 (2014).

53 Sadelain, M., Riviere, I. & Riddell, S. Therapeutic T cell engineering. Nature 545, 423-431, doi:10.1038/nature22395 (2017).

54 Guest, R. D. et al. The role of extracellular spacer regions in the optimal design of chimeric immune receptors: evaluation of four different scFvs and antigens. Journal of immunotherapy 28, 203-211 (2005).

55 James, S. E. et al. Antigen sensitivity of CD22-specific chimeric TCR is modulated by target epitope distance from the cell membrane. Journal of immunology (Baltimore, Md. : 1950) 180, 7028-7038 (2008).

56 Eshhar, Z., Waks, T., Gross, G. & Schindler, D. G. Specific activation and targeting of cytotoxic lymphocytes through chimeric single chains consisting of antibody-binding domains and the gamma or zeta subunits of the immunoglobulin and T-cell receptors. Proceedings of the National Academy of Sciences of the United States of America 90, 720-724 (1993).

57 Krause, A. et al. Antigen-dependent CD28 signaling selectively enhances survival and proliferation in genetically modified activated human primary T lymphocytes. The Journal of experimental medicine 188, 619-626 (1998).

58 Maher, J., Brentjens, R. J., Gunset, G., Riviere, I. & Sadelain, M. Human T-lymphocyte cytotoxicity and proliferation directed by a single chimeric TCRzeta /CD28 receptor. Nature biotechnology 20, 70-75, doi:10.1038/nbt0102-70 (2002).

59 Abate-Daga, D. & Davila, M. L. CAR models: next-generation CAR modifications for enhanced T-cell function. Molecular therapy oncolytics 3, 16014, doi:10.1038/mto.2016.14 (2016).

60 Hartmann, J., Schussler-Lenz, M., Bondanza, A. & Buchholz, C. J. Clinical development of CAR T cells-challenges and opportunities in translating innovative treatment concepts. EMBO molecular medicine 9, 1183-1197, doi:10.15252/emmm.201607485 (2017).

61 Przepiorka, D. et al. FDA Approval: Blinatumomab. Clinical cancer research : an official journal of the American Association for Cancer Research 21, 4035-4039, doi:10.1158/1078-0432.CCR-15-0612 (2015).

62 Pulte, E. D. et al. FDA Supplemental Approval: Blinatumomab for Treatment of Relapsed and Refractory Precursor B-Cell Acute Lymphoblastic Leukemia. The oncologist 23, 1366-1371, doi:10.1634/theoncologist.2018-0179 (2018).

63 Jen, E. Y. et al. FDA Approval: Blinatumomab for Patients with B-cell Precursor Acute Lymphoblastic Leukemia in Morphologic Remission with Minimal Residual Disease. Clinical cancer research : an official journal of the American Association for Cancer Research 25, 473-477, doi:10.1158/1078-0432.CCR-18-2337 (2019).

64 Kantarjian, H. et al. Blinatumomab versus Chemotherapy for Advanced Acute Lymphoblastic Leukemia. The New England journal of medicine 376, 836-847, doi:10.1056/NEJMoa1609783 (2017).

65 Goebeler, M. E. et al. Bispecific T-Cell Engager (BiTE) Antibody Construct Blinatumomab for the Treatment of Patients With Relapsed/Refractory Non-Hodgkin Lymphoma: Final Results From a Phase I Study. Journal of clinical oncology : official journal of the American Society of Clinical Oncology 34, 1104-1111, doi:10.1200/JCO.2014.59.1586 (2016).

66 Nagorsen, D., Kufer, P., Baeuerle, P. A. & Bargou, R. Blinatumomab: a historical perspective. Pharmacology & therapeutics 136, 334-342, doi:10.1016/j.pharmthera.2012.07.013 (2012).

67 O'Leary, M. C. et al. FDA Approval Summary: Tisagenlecleucel for Treatment of Patients with Relapsed or Refractory B-cell Precursor Acute Lymphoblastic Leukemia. Clinical cancer research : an official journal of the American Association for Cancer Research 25, 1142-1146, doi:10.1158/1078-0432.CCR-18-2035 (2019).

68 Sharma, P., King, G. T., Shinde, S. S., Purev, E. & Jimeno, A. Axicabtagene ciloleucel for the treatment of relapsed/refractory B-cell non-Hodgkin's lymphomas. Drugs of today 54, 187-198, doi:10.1358/dot.2018.54.3.2776625 (2018).

69 Brudno, J. N. & Kochenderfer, J. N. Recent advances in CAR T-cell toxicity: Mechanisms, manifestations and management. Blood reviews 34, 45-55, doi:10.1016/j.blre.2018.11.002 (2019).

70 Sotillo, E. et al. Convergence of Acquired Mutations and Alternative Splicing of CD19 Enables Resistance to CART-19 Immunotherapy. Cancer discovery 5, 1282-1295, doi:10.1158/2159-8290.CD-15-1020 (2015).

71 Kelly, E. & Russell, S. J. History of oncolytic viruses: genesis to genetic engineering. Molecular therapy : the journal of the American Society of Gene Therapy 15, 651-659, doi:10.1038/sj.mt.6300108 (2007).

72 Miest, T. S. & Cattaneo, R. New viruses for cancer therapy: meeting clinical needs. Nature reviews. Microbiology 12, 23-34, doi:10.1038/nrmicro3140 (2014).

73 Russell, S. J., Peng, K. W. & Bell, J. C. Oncolytic virotherapy. Nature biotechnology 30, 658-670, doi:10.1038/nbt.2287 (2012).

74 Dock, G. The influence of complicating diseases upon leukaemia. Am. J. Med. Sci. 127, 563–592 (1904).

75 Weller, T. H., Robbins, F. C. & Enders, J. F. Cultivation of poliomyelitis virus in cultures of human foreskin and embryonic tissues. Proceedings of the Society for Experimental Biology and Medicine. Society for Experimental Biology and Medicine 72, 153-155 (1949).

76 Lerner, B. H. Sins of omission–cancer research without informed consent. The New England journal of medicine 351, 628-630, doi:10.1056/NEJMp048108 (2004).

77 Hoster, H. A., Zanes, R. P., Jr. & Von Haam, E. Studies in Hodgkin's syndrome; the association of viral hepatitis and Hodgkin's disease; a preliminary report. Cancer research 9, 473-480 (1949).

78 Moore, A. E., Rhoads, C. P. & Southam, C. M. Homotransplantation of human cell lines. Science (New York, N.Y.) 125, 158-160 (1957).

79 Southam, C. M. Homotransplantation of human cell lines. Bulletin of the New York Academy of Medicine 34, 416-423 (1958).

80 Martuza, R. L., Malick, A., Markert, J. M., Ruffner, K. L. & Coen, D. M. Experimental therapy of human glioma by means of a genetically engineered virus mutant. Science (New York, N.Y.) 252, 854-856 (1991).

81 Workenhe, S. T. & Mossman, K. L. Oncolytic virotherapy and immunogenic cancer cell death: sharpening the sword for improved cancer treatment strategies. Molecular therapy : the journal of the American Society of Gene Therapy 22, 251-256, doi:10.1038/mt.2013.220 (2014).

82 Keller, B. A. & Bell, J. C. Oncolytic viruses-immunotherapeutics on the rise. Journal of molecular medicine 94, 979-991, doi:10.1007/s00109-016-1453-9 (2016).

83 Lichty, B. D., Breitbach, C. J., Stojdl, D. F. & Bell, J. C. Going viral with cancer immunotherapy. Nature reviews. Cancer 14, 559-567, doi:10.1038/nrc3770 (2014).

84 Arulanandam, R. et al. VEGF-Mediated Induction of PRD1-BF1/Blimp1 Expression Sensitizes Tumor Vasculature to Oncolytic Virus Infection. Cancer cell 28, 210-224, doi:10.1016/j.ccell.2015.06.009 (2015).

85 Dyer, A. et al. Turning cold tumours hot: oncolytic virotherapy gets up close and personal with other therapeutics at the 11th Oncolytic Virus Conference. Cancer gene therapy 26, 59-73, doi:10.1038/s41417-018-0042-1 (2019).

86 Liu, B. L. et al. ICP34.5 deleted herpes simplex virus with enhanced oncolytic, immune stimulating, and anti-tumour properties. Gene therapy 10, 292-303, doi:10.1038/sj.gt.3301885 (2003).

87 Andtbacka, R. H. et al. Talimogene Laherparepvec Improves Durable Response Rate in Patients With Advanced Melanoma. Journal of clinical oncology : official journal of the American Society of Clinical Oncology 33, 2780-2788, doi:10.1200/jco.2014.58.3377 (2015).

88 Andtbacka, R. H. et al. Patterns of Clinical Response with Talimogene Laherparepvec (T-VEC) in Patients with Melanoma Treated in the OPTiM Phase III Clinical Trial. Annals of surgical oncology 23, 4169-4177, doi:10.1245/s10434-016-5286-0 (2016).

89 Zamarin, D. et al. Localized oncolytic virotherapy overcomes systemic tumor resistance to immune checkpoint blockade immunotherapy. Science translational medicine 6, 226ra232, doi:10.1126/scitranslmed.3008095 (2014).

90 Bourgeois-Daigneault, M. C. et al. Neoadjuvant oncolytic virotherapy before surgery sensitizes triple-negative breast cancer to immune checkpoint therapy. Science translational medicine 10, doi:10.1126/scitranslmed.aao1641 (2018).

91 Ribas, A. et al. Oncolytic Virotherapy Promotes Intratumoral T Cell Infiltration and Improves Anti-PD-1 Immunotherapy. Cell 170, 1109-1119.e1110, doi:10.1016/j.cell.2017.08.027 (2017).

92 Chesney, J. et al. Randomized, Open-Label Phase II Study Evaluating the Efficacy and Safety of Talimogene Laherparepvec in Combination With Ipilimumab Versus Ipilimumab Alone in Patients With Advanced, Unresectable Melanoma. Journal of clinical oncology : official journal of the American Society of Clinical Oncology 36, 1658-1667, doi:10.1200/JCO.2017.73.7379 (2018).

93 Russell, S. J. & Peng, K. W. Measles virus for cancer therapy. Current topics in microbiology and immunology 330, 213-241 (2009).

94 Aref, S., Bailey, K. & Fielding, A. Measles to the Rescue: A Review of Oncolytic Measles Virus. Viruses 8, doi:10.3390/v8100294 (2016).

95 Ungerechts, G. et al. Moving oncolytic viruses into the clinic: clinical-grade production, purification, and characterization of diverse oncolytic viruses. Molecular therapy. Methods & clinical development 3, 16018, doi:10.1038/mtm.2016.18 (2016).

96 Robinson, S. & Galanis, E. Potential and clinical translation of oncolytic measles viruses. Expert opinion on biological therapy 17, 353-363, doi:10.1080/14712598.2017.1288713 (2017).

97 Bankamp, B., Takeda, M., Zhang, Y., Xu, W. & Rota, P. A. Genetic characterization of measles vaccine strains. The Journal of infectious diseases 204 Suppl 1, S533-548, doi:10.1093/infdis/jir097 (2011).

98 Phan, M. V. T. et al. Complete Genome Sequences of Six Measles Virus Strains. Genome announcements 6, doi:10.1128/genomeA.00184-18 (2018).

99 Rota, P. A. et al. Measles. Nature reviews. Disease primers 2, 16049, doi:10.1038/nrdp.2016.49 (2016).

100 Parks, C. L. et al. Analysis of the noncoding regions of measles virus strains in the Edmonston vaccine lineage. Journal of virology 75, 921-933, doi:10.1128/jvi.75.2.921-933.2001 (2001).

101 Sidhu, M. S. et al. Rescue of synthetic measles virus minireplicons: measles genomic termini direct efficient expression and propagation of a reporter gene. Virology 208, 800-807, doi:10.1006/viro.1995.1215 (1995).

102 Kolakofsky, D. et al. Paramyxovirus RNA synthesis and the requirement for hexamer genome length: the rule of six revisited. Journal of virology 72, 891-899 (1998).

103 Kolakofsky, D., Roux, L., Garcin, D. & Ruigrok, R. W. Paramyxovirus mRNA editing, the "rule of six" and error catastrophe: a hypothesis. The Journal of general virology 86, 1869-1877, doi:10.1099/vir.0.80986-0 (2005).

104 Gutsche, I. et al. Structural virology. Near-atomic cryo-EM structure of the helical measles virus nucleocapsid. Science (New York, N.Y.) 348, 704-707, doi:10.1126/science.aaa5137 (2015).

105 Liston, P., DiFlumeri, C. & Briedis, D. J. Protein interactions entered into by the measles virus P, V, and C proteins. Virus research 38, 241-259 (1995).

106 Harty, R. N. & Palese, P. Measles virus phosphoprotein (P) requires the NH2- and COOH-terminal domains for interactions with the nucleoprotein (N) but only the COOH terminus for interactions with itself. The Journal of general virology 76 (Pt 11), 2863-2867, doi:10.1099/0022-1317-76-11-2863 (1995).

107 Cevik, B. et al. The phosphoprotein (P) and L binding sites reside in the N-terminus of the L subunit of the measles virus RNA polymerase. Virology 327, 297-306, doi:10.1016/j.virol.2004.07.002 (2004).

108 Suryanarayana, K., Baczko, K., ter Meulen, V. & Wagner, R. R. Transcription inhibition and other properties of matrix proteins expressed by M genes cloned from measles viruses and diseased human brain tissue. Journal of virology 68, 1532-1543 (1994).

109 Wild, T. F., Malvoisin, E. & Buckland, R. Measles virus: both the haemagglutinin and fusion glycoproteins are required for fusion. The Journal of general virology 72 (Pt 2), 439-442, doi:10.1099/0022-1317-72-2-439 (1991).

110 Galanis, E. et al. Use of viral fusogenic membrane glycoproteins as novel therapeutic transgenes in gliomas. Human gene therapy 12, 811-821, doi:10.1089/104303401750148766 (2001).

111 Singh, B. K. et al. Cell-to-Cell Contact and Nectin-4 Govern Spread of Measles Virus from Primary Human Myeloid Cells to Primary Human Airway Epithelial Cells. Journal of virology 90, 6808-6817, doi:10.1128/JVI.00266-16 (2016).

112 Shaffer, J. A., Bellini, W. J. & Rota, P. A. The C protein of measles virus inhibits the type I interferon response. Virology 315, 389-397 (2003).

113 Palosaari, H., Parisien, J. P., Rodriguez, J. J., Ulane, C. M. & Horvath, C. M. STAT protein interference and suppression of cytokine signal transduction by measles virus V protein. Journal of virology 77, 7635-7644 (2003).

114 Cattaneo, R., Rebmann, G., Baczko, K., ter Meulen, V. & Billeter, M. A. Altered ratios of measles virus transcripts in diseased human brains. Virology 160, 523-526 (1987).

115 Bluming, A. Z. & Ziegler, J. L. Regression of Burkitt's lymphoma in association with measles infection. Lancet 2, 105-106 (1971).

116 Hilleman, M. R. Current overview of the pathogenesis and prophylaxis of measles with focus on practical implications. Vaccine 20, 651-665 (2001).

117 Noyce, R. S. et al. Tumor cell marker PVRL4 (nectin 4) is an epithelial cell receptor for measles virus. PLoS pathogens 7, e1002240, doi:10.1371/journal.ppat.1002240 (2011).

118 Takeuchi, K., Miyajima, N., Nagata, N., Takeda, M. & Tashiro, M. Wild-type measles virus induces large syncytium formation in primary human small airway epithelial cells by a SLAM(CD150)-independent mechanism. Virus research 94, 11-16 (2003).

119 Tatsuo, H., Ono, N., Tanaka, K. & Yanagi, Y. SLAM (CDw150) is a cellular receptor for measles virus. Nature 406, 893-897, doi:10.1038/35022579 (2000).

120 Hsu, E. C., Iorio, C., Sarangi, F., Khine, A. A. & Richardson, C. D. CDw150(SLAM) is a receptor for a lymphotropic strain of measles virus and may account for the immunosuppressive properties of this virus. Virology 279, 9-21, doi:10.1006/viro.2000.0711 (2001).

121 Schneider-Schaulies, J., Meulen, V. & Schneider-Schaulies, S. Measles infection of the central nervous system. Journal of neurovirology 9, 247-252, doi:10.1080/13550280390193993 (2003).

122 Bellini, W. J. et al. Subacute sclerosing panencephalitis: more cases of this fatal disease are prevented by measles immunization than was previously recognized. The Journal of infectious diseases 192, 1686-1693, doi:10.1086/497169 (2005).

123 Enders, J. F., Katz, S. L., Milovanovic, M. V. & Holloway, A. Studies on an attenuated measles-virus vaccine. I. Development and preparations of the vaccine: technics for assay of effects of vaccination. The New England journal of medicine 263, 153-159, doi:10.1056/NEJM196007282630401 (1960).

124 Dabbagh, A. et al. Progress Toward Regional Measles Elimination - Worldwide, 2000-2016. MMWR. Morbidity and mortality weekly report 66, 1148-1153, doi:10.15585/mmwr.mm6642a6 (2017).

125 Patel, M. K. et al. Progress Toward Regional Measles Elimination - Worldwide, 2000-2015. MMWR. Morbidity and mortality weekly report 65, 1228-1233, doi:10.15585/mmwr.mm6544a6 (2016).

126 Davidkin, I., Jokinen, S., Broman, M., Leinikki, P. & Peltola, H. Persistence of measles, mumps, and rubella antibodies in an MMR-vaccinated cohort: a 20-year follow-up. The Journal of infectious diseases 197, 950-956, doi:10.1086/528993 (2008).

127 Dorig, R. E., Marcil, A., Chopra, A. & Richardson, C. D. The human CD46 molecule is a receptor for measles virus (Edmonston strain). Cell 75, 295-305 (1993).

128 Naniche, D. et al. Human membrane cofactor protein (CD46) acts as a cellular receptor for measles virus. Journal of virology 67, 6025-6032 (1993).

129 Nielsen, L., Blixenkrone-Moller, M., Thylstrup, M., Hansen, N. J. & Bolt, G. Adaptation of wild-type measles virus to CD46 receptor usage. Archives of virology 146, 197-208 (2001).

130 Anderson, B. D., Nakamura, T., Russell, S. J. & Peng, K. W. High CD46 receptor density determines preferential killing of tumor cells by oncolytic measles virus. Cancer research 64, 4919-4926, doi:10.1158/0008-5472.can-04-0884 (2004).

131 Riley-Vargas, R. C., Gill, D. B., Kemper, C., Liszewski, M. K. & Atkinson, J. P. CD46: expanding beyond complement regulation. Trends in immunology 25, 496-503, doi:10.1016/j.it.2004.07.004 (2004).

132 Nakatsu, Y., Takeda, M., Ohno, S., Koga, R. & Yanagi, Y. Translational inhibition and increased interferon induction in cells infected with C protein-deficient measles virus. Journal of virology 80, 11861-11867, doi:10.1128/JVI.00751-06 (2006).

133 Reutter, G. L., Cortese-Grogan, C., Wilson, J. & Moyer, S. A. Mutations in the measles virus C protein that up regulate viral RNA synthesis. Virology 285, 100-109, doi:10.1006/viro.2001.0962 (2001).

134 Heidbuechel, J. P. W. & Engeland, C. E. Paramyxoviruses for Tumor-targeted Immunomodulation: Design and Evaluation Ex Vivo. JoVE 143, e58651, doi:doi:10.3791/58651 (2019).

135 Billeter, M. A., Naim, H. Y. & Udem, S. A. Reverse genetics of measles virus and resulting multivalent recombinant vaccines: applications of recombinant measles viruses. Current topics in microbiology and immunology 329, 129-162 (2009).

136 Martin, A., Staeheli, P. & Schneider, U. RNA polymerase II-controlled expression of antigenomic RNA enhances the rescue efficacies of two different members of the Mononegavirales independently of the site of viral genome replication. Journal of virology 80, 5708-5715, doi:10.1128/jvi.02389-05 (2006).

137 Radecke, F. et al. Rescue of measles viruses from cloned DNA. The EMBO journal 14, 5773-5784 (1995).

138 Leber, M. F. et al. Enhanced Control of Oncolytic Measles Virus Using MicroRNA Target Sites. Molecular therapy oncolytics 9, 30-40, doi:10.1016/j.omto.2018.04.002 (2018).

139 Baertsch, M. A. et al. MicroRNA-mediated multi-tissue detargeting of oncolytic measles virus. Cancer gene therapy 21, 373-380, doi:10.1038/cgt.2014.40 (2014).

140 Leber, M. F. et al. MicroRNA-sensitive oncolytic measles viruses for cancer-specific vector tropism. Molecular therapy : the journal of the American Society of Gene Therapy 19, 1097-1106, doi:10.1038/mt.2011.55 (2011).

141 Msaouel, P. et al. Clinical Trials with Oncolytic Measles Virus: Current Status and Future Prospects. Current cancer drug targets 18, 177-187, doi:10.2174/1568009617666170222125035 (2018).

142 Russell, S. J. et al. Remission of disseminated cancer after systemic oncolytic virotherapy. Mayo Clinic proceedings 89, 926-933, doi:10.1016/j.mayocp.2014.04.003 (2014).

143 Grossardt, C. et al. Granulocyte-macrophage colony-stimulating factor-armed oncolytic measles virus is an effective therapeutic cancer vaccine. Human gene therapy 24, 644-654, doi:10.1089/hum.2012.205 (2013).

144 Iankov, I. D. et al. Expression of immunomodulatory neutrophil-activating protein of Helicobacter pylori enhances the antitumor activity of oncolytic measles virus. Molecular therapy : the journal of the American Society of Gene Therapy 20, 1139-1147, doi:10.1038/mt.2012.4 (2012).

145 Hutzler, S. et al. Antigen-specific oncolytic MV-based tumor vaccines through presentation of selected tumor-associated antigens on infected cells or virus-like particles. Scientific reports 7, 16892, doi:10.1038/s41598-017-16928-8 (2017).

146 Engeland, C. E. et al. CTLA-4 and PD-L1 checkpoint blockade enhances oncolytic measles virus therapy. Molecular therapy : the journal of the American Society of Gene Therapy 22, 1949-1959, doi:10.1038/mt.2014.160 (2014).

147 Veinalde, R. et al. Oncolytic measles virus encoding interleukin-12 mediates potent antitumor effects through T cell activation. Oncoimmunology 6, doi:10.1080/2162402x.2017.1285992 (2017).

148 Russell, S. J. & Barber, G. N. Oncolytic Viruses as Antigen-Agnostic Cancer Vaccines. Cancer cell 33, 599-605, doi:10.1016/j.ccell.2018.03.011 (2018).

149 Heidbuechel, J. P. W. Oncolytic Measles Virus Encoding AntiCD20/CD3 Bispecific T Cell Engager for the Treatment of B Cell Lymphoma M. Sc. thesis, Universität Heidelberg, (2016).

150 Speck, T. et al. Targeted BiTE expression by an oncolytic vector augments therapeutic efficacy against solid tumors. Clinical cancer research : an official journal of the American Association for Cancer Research, doi:10.1158/1078-0432.CCR-17-2651 (2018).

151 Speck, T. BiTE-armed oncolytic measles viruses for cancer immunovirotherapy Doctor of Natural Sciences thesis, Ruperto-Carola University of Heidelberg, Germany, (2018).

152 Ungerechts, G. et al. Lymphoma chemovirotherapy: CD20-targeted and convertase-armed measles virus can synergize with fludarabine. Cancer research 67, 10939-10947, doi:10.1158/0008-5472.can-07-1252 (2007).

153 Brinkmann, U. & Kontermann, R. E. The making of bispecific antibodies. mAbs 9, 182-212, doi:10.1080/19420862.2016.1268307 (2017).

154 Mack, M., Riethmuller, G. & Kufer, P. A small bispecific antibody construct expressed as a functional single-chain molecule with high tumor cell cytotoxicity. Proceedings of the National Academy of Sciences of the United States of America 92, 7021-7025 (1995).

155 Miest, T. S. et al. Envelope-chimeric entry-targeted measles virus escapes neutralization and achieves oncolysis. Molecular therapy : the journal of the American Society of Gene Therapy 19, 1813-1820, doi:10.1038/mt.2011.92 (2011).

156 Geiss, G. K. et al. Direct multiplexed measurement of gene expression with color-coded probe pairs. Nature biotechnology 26, 317-325, doi:10.1038/nbt1385 (2008).

157 Manchester, M., Liszewski, M. K., Atkinson, J. P. & Oldstone, M. B. Multiple isoforms of CD46 (membrane cofactor protein) serve as receptors for measles virus. Proceedings of the National Academy of Sciences of the United States of America 91, 2161-2165 (1994).

158 Abate-Daga, D. et al. A novel chimeric antigen receptor against prostate stem cell antigen mediates tumor destruction in a humanized mouse model of pancreatic cancer. Human gene therapy 25, 1003-1012, doi:10.1089/hum.2013.209 (2014).

159 Thu, M. S. et al. Self-assembling nanocomplexes by combining ferumoxytol, heparin and protamine for cell tracking by magnetic resonance imaging. Nature medicine 18, 463-467, doi:10.1038/nm.2666 (2012).

160 J, G. P. et al. Trial Watch: Oncolytic viro-immunotherapy of hematologic and solid tumors. Oncoimmunology 7, e1503032, doi:10.1080/2162402X.2018.1503032 (2018).

161 Wolchok, J. D. et al. Overall Survival with Combined Nivolumab and Ipilimumab in Advanced Melanoma. The New England journal of medicine 377, 1345-1356, doi:10.1056/NEJMoa1709684 (2017).

162 Hodi, F. S. et al. Improved survival with ipilimumab in patients with metastatic melanoma. The New England journal of medicine 363, 711-723, doi:10.1056/NEJMoa1003466 (2010).

163 Overwijk, W. W. & Restifo, N. P. B16 as a mouse model for human melanoma. Current protocols in immunology Chapter 20, Unit 20 21, doi:10.1002/0471142735.im2001s39 (2001).

164 Bucheit, A. D. et al. An oncolytic measles virus engineered to enter cells through the CD20 antigen. Molecular therapy : the journal of the American Society of Gene Therapy 7, 62-72 (2003).

165 Stashenko, P., Nadler, L. M., Hardy, R. & Schlossman, S. F. Characterization of a human B lymphocyte-specific antigen. Journal of immunology (Baltimore, Md. : 1950) 125, 1678-1685 (1980).

166 Einfeld, D. A., Brown, J. P., Valentine, M. A., Clark, E. A. & Ledbetter, J. A. Molecular cloning of the human B cell CD20 receptor predicts a hydrophobic protein with multiple transmembrane domains. The EMBO journal 7, 711-717 (1988).

167 Pierpont, T. M., Limper, C. B. & Richards, K. L. Past, Present, and Future of Rituximab-The World's First Oncology Monoclonal Antibody Therapy. Frontiers in oncology 8, 163, doi:10.3389/fonc.2018.00163 (2018).

168 Plosker, G. L. & Figgitt, D. P. Rituximab: a review of its use in non-Hodgkin's lymphoma and chronic lymphocytic leukaemia. Drugs 63, 803-843, doi:10.2165/00003495-200363080-00005 (2003).

169 Fang, D. et al. A tumorigenic subpopulation with stem cell properties in melanomas. Cancer research 65, 9328-9337, doi:10.1158/0008-5472.CAN-05-1343 (2005).

170 Schmidt, P. et al. Eradication of melanomas by targeted elimination of a minor subset of tumor cells. Proceedings of the National Academy of Sciences of the United States of America 108, 2474-2479, doi:10.1073/pnas.1009069108 (2011).

171 Pinc, A. et al. Targeting CD20 in melanoma patients at high risk of disease recurrence. Molecular therapy : the journal of the American Society of Gene Therapy 20, 1056-1062, doi:10.1038/mt.2012.27 (2012).

172 Yanagi, Y., Hu, H. L., Seya, T. & Yoshikura, H. Measles virus infects mouse fibroblast cell lines, but its multiplication is severely restricted in the absence of CD46. Archives of virology 138, 39-53 (1994).

173 Vincent, S. et al. Restriction of measles virus RNA synthesis by a mouse host cell line: trans-complementation by polymerase components or a human cellular factor(s). Journal of virology 76, 6121-6130 (2002).

174 Ponchel, F. et al. Changes in peripheral blood immune cell composition in osteoarthritis. Osteoarthritis and cartilage 23, 1870-1878, doi:10.1016/j.joca.2015.06.018 (2015).

175 Saga, K. & Kaneda, Y. Oncolytic Sendai virus-based virotherapy for cancer: recent advances. Oncolytic virotherapy 4, 141-147, doi:10.2147/ov.s66419 (2015).

176 Dai, P. et al. Intratumoral delivery of inactivated modified vaccinia virus Ankara (iMVA) induces systemic antitumor immunity via STING and Batf3-dependent dendritic cells. Science immunology 2, doi:10.1126/sciimmunol.aal1713 (2017).

177 Myers, R. M. et al. Preclinical pharmacology and toxicology of intravenous MV-NIS, an oncolytic measles virus administered with or without cyclophosphamide. Clinical pharmacology and therapeutics 82, 700-710, doi:10.1038/sj.clpt.6100409 (2007).

178 Corbett, T. H., Griswold, D. P., Jr., Roberts, B. J., Peckham, J. C. & Schabel, F. M., Jr. Tumor induction relationships in development of transplantable cancers of the colon in mice for chemotherapy assays, with a note on carcinogen structure. Cancer research 35, 2434-2439 (1975).

179 Efremova, M. et al. Targeting immune checkpoints potentiates immunoediting and changes the dynamics of tumor evolution. Nature communications 9, 32, doi:10.1038/s41467-017-02424-0 (2018).

180 Pajtasz-Piasecka, E. et al. Loss of tumorigenicity of murine colon carcinoma MC38/0 cell line after transduction with a retroviral vector carrying murine IL-12 genes. Folia biologica 50, 7-14 (2004).

181 Veinalde, R. et al. Oncolytic measles virus encoding interleukin-12 mediates potent antitumor effects through T cell activation. Oncoimmunology 6, e1285992, doi:10.1080/2162402x.2017.1285992 (2017).

182 Berkeley, R. A. et al. Antibody-Neutralized Reovirus Is Effective in Oncolytic Virotherapy. Cancer immunology research 6, 1161-1173, doi:10.1158/2326-6066.CIR-18-0309 (2018).

183 Peng, K. W. et al. Using clinically approved cyclophosphamide regimens to control the humoral immune response to oncolytic viruses. Gene therapy 20, 255-261, doi:10.1038/gt.2012.31 (2013).

184 Croyle, M. A. et al. PEGylation of a vesicular stomatitis virus G pseudotyped lentivirus vector prevents inactivation in serum. Journal of virology 78, 912-921 (2004).

185 Samson, A. et al. Intravenous delivery of oncolytic reovirus to brain tumor patients immunologically primes for subsequent checkpoint blockade. Science translational medicine 10, doi:10.1126/scitranslmed.aam7577 (2018).

186 Adair, R. A. et al. Cell carriage, delivery, and selective replication of an oncolytic virus in tumor in patients. Science translational medicine 4, 138ra177, doi:10.1126/scitranslmed.3003578 (2012).

187 Lilly, C. L. et al. Ex Vivo Oncolytic Virotherapy with Myxoma Virus Arms Multiple Allogeneic Bone Marrow Transplant Leukocytes to Enhance Graft versus Tumor. Molecular therapy oncolytics 4, 31-40, doi:10.1016/j.omto.2016.12.002 (2017).

188 Ong, H. T. et al. Systemically delivered measles virus-infected mesenchymal stem cells can evade host immunity to inhibit liver cancer growth. Journal of hepatology 59, 999-1006, doi:10.1016/j.jhep.2013.07.010 (2013).

189 Mader,E.K. et al. Mesenchymal stem cell carriers protect oncolytic measles viruses from antibody neutralization in an orthotopic ovarian cancer therapy model. Clinical cancer research 15, 7246–7255 (2009).

190 Ong, H. T., Hasegawa, K., Dietz, A. B., Russell, S. J. & Peng, K. W. Evaluation of T cells as carriers for systemic measles virotherapy in the presence of antiviral antibodies. Gene therapy 14, 324-333, doi:10.1038/sj.gt.3302880 (2007).

191 Engeland, C. E. et al. A Tupaia paramyxovirus vector system for targeting and transgene expression. The Journal of general virology 98, 2248-2257, doi:10.1099/jgv.0.000887 (2017).

192 Evgin, L. et al. Complement inhibition enables tumor delivery of LCMV glycoprotein pseudotyped viruses in the presence of antiviral antibodies. Molecular therapy oncolytics 3, 16027, doi:10.1038/mto.2016.27 (2016).

193 Hudacek, A. W., Navaratnarajah, C. K. & Cattaneo, R. Development of measles virus-based shielded oncolytic vectors: suitability of other paramyxovirus glycoproteins. Cancer gene therapy 20, 109-116, doi:10.1038/cgt.2012.92 (2013).

194 Constant, S. L. & Bottomly, K. Induction of Th1 and Th2 CD4+ T cell responses: the alternative approaches. Annual review of immunology 15, 297-322, doi:10.1146/annurev.immunol.15.1.297 (1997).

195 Hildner, K. et al. Batf3 deficiency reveals a critical role for CD8alpha+ dendritic cells in cytotoxic T cell immunity. Science (New York, N.Y.) 322, 1097-1100, doi:10.1126/science.1164206 (2008).

196 Spranger, S., Dai, D., Horton, B. & Gajewski, T. F. Tumor-Residing Batf3 Dendritic Cells Are Required for Effector T Cell Trafficking and Adoptive T Cell Therapy. Cancer cell 31, 711-723 e714, doi:10.1016/j.ccell.2017.04.003 (2017).

197 Weisser, S. B., van Rooijen, N. & Sly, L. M. Depletion and reconstitution of macrophages in mice. Journal of Visualized Experiments : JoVE, 4105, doi:10.3791/4105 (2012).

198 van Rooijen, N. & Hendrikx, E. Liposomes for specific depletion of macrophages from organs and tissues. Methods in molecular biology 605, 189-203, doi:10.1007/978-1-60327-360-2_13 (2010).

199 Heather, J. M., Ismail, M., Oakes, T. & Chain, B. High-throughput sequencing of the T-cell receptor repertoire: pitfalls and opportunities. Briefings in bioinformatics 19, 554-565, doi:10.1093/bib/bbw138 (2018).

200 Ahmed, N. et al. HER2-Specific Chimeric Antigen Receptor-Modified Virus-Specific T Cells for Progressive Glioblastoma: A Phase 1 Dose-Escalation Trial. JAMA oncology 3, 1094-1101, doi:10.1001/jamaoncol.2017.0184 (2017).

201 Terakura, S. et al. Generation of CD19-chimeric antigen receptor modified CD8+ T cells derived from virus-specific central memory T cells. Blood 119, 72-82, doi:10.1182/blood-2011-07-366419 (2012).

202 Savoldo, B. et al. Epstein Barr virus specific cytotoxic T lymphocytes expressing the anti-CD30zeta artificial chimeric T-cell receptor for immunotherapy of Hodgkin disease. Blood 110, 2620-2630, doi:10.1182/blood-2006-11-059139 (2007).

203 Bommareddy, P. K., Shettigar, M. & Kaufman, H. L. Integrating oncolytic viruses in combination cancer immunotherapy. Nature reviews. Immunology 18, 498-513, doi:10.1038/s41577-018-0014-6 (2018).

204 Twumasi-Boateng, K., Pettigrew, J. L., Kwok, Y. Y. E., Bell, J. C. & Nelson, B. H. Oncolytic viruses as engineering platforms for combination immunotherapy. Nature reviews. Cancer 18, 419-432, doi:10.1038/s41568-018-0009-4 (2018).

205 Achard, C. et al. Lighting a Fire in the Tumor Microenvironment Using Oncolytic Immunotherapy. EBioMedicine 31, 17-24, doi:10.1016/j.ebiom.2018.04.020 (2018).

206 Martin, N. T. & Bell, J. C. Oncolytic Virus Combination Therapy: Killing One Bird with Two Stones. Molecular therapy : the journal of the American Society of Gene Therapy 26, 1414-1422, doi:10.1016/j.ymthe.2018.04.001 (2018).

207 Ajina, A. & Maher, J. Prospects for combined use of oncolytic viruses and CAR T-cells. Journal for immunotherapy of cancer 5, 90, doi:10.1186/s40425-017-0294-6 (2017).

208 Scott, E. M., Duffy, M. R., Freedman, J. D., Fisher, K. D. & Seymour, L. W. Solid Tumor Immunotherapy with T Cell Engager-Armed Oncolytic Viruses. Macromolecular bioscience 18, doi:10.1002/mabi.201700187 (2018).

209 Crupi, M. J. F., Bell, J. C. & Singaravelu, R. Concise Review: Targeting cancer stem cells and their supporting niche using oncolytic viruses. Stem cells, doi:10.1002/stem.3004 (2019).

210 Guedan, S. & Alemany, R. CAR-T Cells and Oncolytic Viruses: Joining Forces to Overcome the Solid Tumor Challenge. Frontiers in immunology 9, 2460, doi:10.3389/fimmu.2018.02460 (2018).

211 Yu, F. et al. T-cell engager-armed oncolytic vaccinia virus significantly enhances antitumor therapy. Molecular therapy : the journal of the American Society of Gene Therapy 22, 102-111, doi:10.1038/mt.2013.240 (2014).

212 Fajardo, C. A. et al. Oncolytic Adenoviral Delivery of an EGFR-Targeting T-cell Engager Improves Antitumor Efficacy. Cancer research 77, 2052-2063, doi:10.1158/0008-5472.can-16-1708 (2017).

213 Freedman, J. D. et al. Oncolytic adenovirus expressing bispecific antibody targets T-cell cytotoxicity in cancer biopsies. 9, 1067-1087, doi:10.15252/emmm.201707567 (2017).

214 Rosewell Shaw, A. et al. Adenovirotherapy Delivering Cytokine and Checkpoint Inhibitor Augments CAR T Cells against Metastatic Head and Neck Cancer. Molecular therapy : the journal of the American Society of Gene Therapy 25, 2440-2451, doi:10.1016/j.ymthe.2017.09.010 (2017).

215 Tanoue, K. et al. Armed Oncolytic Adenovirus-Expressing PD-L1 Mini-Body Enhances Antitumor Effects of Chimeric Antigen Receptor T Cells in Solid Tumors. Cancer research 77, 2040-2051, doi:10.1158/0008-5472.CAN-16-1577 (2017).

216 Watanabe, K. et al. Pancreatic cancer therapy with combined mesothelin-redirected chimeric antigen receptor T cells and cytokine-armed oncolytic adenoviruses. JCI insight 3, doi:10.1172/jci.insight.99573 (2018).

217 Nishio, N. et al. Armed oncolytic virus enhances immune functions of chimeric antigen receptor-modified T cells in solid tumors. Cancer research 74, 5195-5205, doi:10.1158/0008-5472.CAN-14-0697 (2014).

218 Moon, E. K. et al. Intra-tumoral delivery of CXCL11 via a vaccinia virus, but not by modified T cells, enhances the efficacy of adoptive T cell therapy and vaccines. Oncoimmunology 7, e1395997, doi:10.1080/2162402X.2017.1395997 (2018).

219 Wing, A. et al. Improving CART-Cell Therapy of Solid Tumors with Oncolytic Virus-Driven Production of a Bispecific T-cell Engager. Cancer immunology research 6, 605-616, doi:10.1158/2326-6066.cir-17-0314 (2018).

220 Albelda, S. M. & Thorne, S. H. Giving oncolytic vaccinia virus more BiTE. Molecular therapy : the journal of the American Society of Gene Therapy 22, 6-8, doi:10.1038/mt.2013.271 (2014).

221 VanSeggelen, H., Tantalo, D. G., Afsahi, A., Hammill, J. A. & Bramson, J. L. Chimeric antigen receptor-engineered T cells as oncolytic virus carriers. Molecular therapy oncolytics 2, 15014, doi:10.1038/mto.2015.14 (2015).

222 Freedman, J. D. et al. An Oncolytic Virus Expressing a T-cell Engager Simultaneously Targets Cancer and Immunosuppressive Stromal Cells. Cancer research, doi:10.1158/0008-5472.CAN-18-1750 (2018).

223 de Sostoa, J. et al. Targeting the tumor stroma with an oncolytic adenovirus secreting a fibroblast activation protein-targeted bispecific T-cell engager. Journal for immunotherapy of cancer 7, 19, doi:10.1186/s40425-019-0505-4 (2019).

224 Kamisawa, T., Wood, L. D., Itoi, T. & Takaori, K. Pancreatic cancer. Lancet 388, 73-85, doi:10.1016/S0140-6736(16)00141-0 (2016).

225 Priceman, S. J. et al. Co-stimulatory signaling determines tumor antigen sensitivity and persistence of CAR T cells targeting PSCA+ metastatic prostate cancer. Oncoimmunology 7, e1380764, doi:10.1080/2162402X.2017.1380764 (2018).

226 Tureci, Mitnacht-Kraus, R., Woll, S., Yamada, T. & Sahin, U. Characterization of zolbetuximab in pancreatic cancer models. Oncoimmunology 8, e1523096, doi:10.1080/2162402X.2018.1523096 (2019).

227 Sahin, U. et al. A phase I dose-escalation study of IMAB362 (Zolbetuximab) in patients with advanced gastric and gastro-oesophageal junction cancer. Eur J Cancer 100, 17-26, doi:10.1016/j.ejca.2018.05.007 (2018).

228 Woll, S. et al. Claudin 18.2 is a target for IMAB362 antibody in pancreatic neoplasms. International journal of cancer 134, 731-739, doi:10.1002/ijc.28400 (2014).

229 Klamp, T. et al. Highly specific auto-antibodies against claudin-18 isoform 2 induced by a chimeric HBcAg virus-like particle vaccine kill tumor cells and inhibit the growth of lung metastases. Cancer research 71, 516-527, doi:10.1158/0008-5472.CAN-10-2292 (2011).

230 Sahin, U. et al. Claudin-18 splice variant 2 is a pan-cancer target suitable for therapeutic antibody development. Clinical cancer research : an official journal of the American Association for Cancer Research 14, 7624-7634, doi:10.1158/1078-0432.CCR-08-1547 (2008).

231 Runcie, K., Budman, D. R., John, V. & Seetharamu, N. Bi-specific and tri-specific antibodies-the next big thing in solid tumor therapeutics. Molecular medicine 24, 50, doi:10.1186/s10020-018-0051-4 (2018).

232 Jachimowicz, R. D., Borchmann, S. & Rothe, A. Multi-specific antibodies for cancer immunotherapy. BioDrugs : clinical immunotherapeutics, biopharmaceuticals and gene therapy 28, 331-343, doi:10.1007/s40259-014-0091-4 (2014).

233 Bielamowicz, K. et al. Trivalent CAR T cells overcome interpatient antigenic variability in glioblastoma. Neuro-oncology 20, 506-518, doi:10.1093/neuonc/nox182 (2018).

234 Fousek, K. et al. Targeting Primary Pre-B Cell Acute Lymphoblastic Leukemia and CD19-Negative Relapses Using Trivalent CAR T Cells. Blood 130, 4614-4614 (2017).

235 Bachmann, D. et al. Retargeting of UniCAR T cells with an in vivo synthesized target module directed against CD19 positive tumor cells. Oncotarget 9, 7487-7500, doi:10.18632/oncotarget.23556 (2018).

236 Albert, S. et al. From mono- to bivalent: improving theranostic properties of target modules for redirection of UniCAR T cells against EGFR-expressing tumor cells in vitro and in vivo. Oncotarget 9, 25597-25616, doi:10.18632/oncotarget.25390 (2018).

237 Albert, S. et al. A novel nanobody-based target module for retargeting of T lymphocytes to EGFR-expressing cancer cells via the modular UniCAR platform. Oncoimmunology 6, e1287246, doi:10.1080/2162402x.2017.1287246 (2017).

238 Cartellieri, M. et al. Switching CAR T cells on and off: a novel modular platform for retargeting of T cells to AML blasts. Blood cancer journal 6, e458, doi:10.1038/bcj.2016.61 (2016).

239 Box, G. E. P. Science and Statistics. Journal of the American Statistical Association 71, 791-799, doi:10.1080/01621459.1976.10480949 (1976).

240 Santiago, D. N. et al. Fighting Cancer with Mathematics and Viruses. Viruses 9, doi:10.3390/v9090239 (2017).

241 Wodarz, D. Computational modeling approaches to the dynamics of oncolytic viruses. Wiley interdisciplinary reviews. Systems biology and medicine 8, 242-252, doi:10.1002/wsbm.1332 (2016).

242 Friedman, A. & Lai, X. Combination therapy for cancer with oncolytic virus and checkpoint inhibitor: A mathematical model. 13, e0192449, doi:10.1371/journal.pone.0192449 (2018).

243 Dingli, D., Cascino, M. D., Josic, K., Russell, S. J. & Bajzer, Z. Mathematical modeling of cancer radiovirotherapy. Mathematical biosciences 199, 55-78, doi:10.1016/j.mbs.2005.11.001 (2006).

244 Kim, Y. et al. Complex role of NK cells in regulation of oncolytic virus-bortezomib therapy. Proceedings of the National Academy of Sciences of the United States of America 115, 4927-4932, doi:10.1073/pnas.1715295115 (2018).

245 Gevertz, J. L. & Wares, J. R. Developing a Minimally Structured Mathematical Model of Cancer Treatment with Oncolytic Viruses and Dendritic Cell Injections. Computational and mathematical methods in medicine 2018, 8760371, doi:10.1155/2018/8760371 (2018).

246 Heidbuechel, J. P. W., Abate-Daga, D., Engeland, C. E. & Enderling, H. Mathematical modeling of oncolytic virotherapy. in Oncolytic Viruses: Methods and Protocols. Methods in Molecular Biology (ed C. E. Engeland) (Springer Nature, in press).

Contributions

Not all experiments shown were performed by me, partly due to my research visit abroad. I am very thankful for the support I received and want to acknowledge the persons who supported this project with their work:

Birgit Hoyler performed the transductions of B16 and B16-CD20 cells with CD46-encoding lentiviruses (Fig. 6). Jessica Albert repeated the XTT assay on B16-CD20-CD46 cells (Fig. 7E). Growth curve experiments and XTT assays were performed together with Dr. Tobias Speck (Fig. 7A,B,D), who also performed the time course BiTE expression ELISA (Fig. 10D). The nCounter Core Facility Heidelberg performed RNA quality testing, hybridization with the CodeSet Panel, and processing using nCounter SPRINT profiler (Fig. 19). Dr. Daniel Santiago assisted with tumor volume measurements in NSG mice (Fig. 20). Manuel Fischer, University Hospital Heidelberg, performed magnetic resonance imaging of T cells I had labeled with iron oxide nanoparticles (Fig. 21). Na Kang and Dr. Claudia R. Ball provided PC05 tumor cells, and Dr. Rūta Veinalde and Lara Jeworowski provided MV-IgG, MV-Nivo, and MV-Pembro viruses (Fig. 22).

List of publications

Heidbuechel JPW, Abate-Daga D, Engeland CE, Enderling H. Mathematical modeling of oncolytic virotherapy. In: Engeland CE (ed.) Oncolytic Viruses: Methods and Protocols. Methods in Molecular Biology, Springer Nature, in press.

Heidbuechel JPW, Engeland CE. Paramyxoviruses for Tumor-targeted Immunomodulation: Design and Evaluation Ex Vivo. J. Vis. Exp. (143), e58651, doi:10.3791/58651 (2019).[†]

Speck T[‡], **Heidbuechel JPW[‡]**, Veinalde R, Jaeger D, von Kalle C, Ball CR, Ungerechts G, Engeland CE. Targeted BiTE expression by an oncolytic vector augments therapeutic efficacy against solid tumors. Clin. Cancer Res. 2018, 24(9), 2128-37.[§]

Santiago DN[‡], **Heidbuechel JPW[‡]**, Kandell WM, Walker R, Djeu J, Engeland CE, Abate-Daga D, Enderling H. Fighting Cancer with Mathematics and Viruses. Viruses 2017, 9(9), 239. (Cover Story)

[†]Main methods of generating and validating recombinant oncolytic measles viruses encoding immunomodulatory transgenes as used in the present thesis have been published in this video article accompanied by a comprehensive protocol.

[‡]Shared first authorship

[§]Main findings of the present thesis have been published in this research paper.

Contributions to scientific conferences

Oral Presentations

ASGCT 21st Annual Meeting in Chicago, IL, USA: "Oncolytic viruses to enhance BiTE and CAR therapy of solid tumors". May 16-19, 2018

International Oncolytic Virus Conference in Oxford, UK: "BiTE delivery by oncolytic measles virus vectors enhances efficacy against solid tumors". April 09-12, 2018[†]

EMBL Cancer Core Europe Cancer Immunotherapy Conference 2017 in Heidelberg, Germany: "BiTE-armed oncolytic measles viruses for cancer immunovirotherapy". February 02-04, 2017

Conference Posters

ESGCT XXV Anniversary Congress in Berlin, Germany: "Oncolytic virotherapy to enhance BiTE and CAR efficacy against solid tumors". October 17-20, 2017

CRI-CIMT-EATI-AACR International Cancer Immunotherapy Conference in Mainz, Germany: "Targeted BiTE expression by an oncolytic vector augments therapeutic efficacy against solid tumors". September 06-09, 2017

International Meeting on Replicating Oncolytic Virus Therapeutics in Vancouver, BC, Canada: "T cell dynamics in oncolytic measles virotherapy". October 01-04, 2016

XXII Annual Meeting of the German Society for Gene Therapy in Heidelberg, Germany: "T cell dynamics in oncolytic measles virotherapy". September 14-16, 2016

[†]Received the Charles Conrad Award for outstanding oral presentation by a junior scientist.

Acknowledgments

Thesis declaration

I hereby declare that I have written the submitted dissertation myself and in this process I have used no other sources or materials than those expressly indicated. I hereby declare that I have not applied to be examined at any other institution, nor have I used the dissertation in this or any other form at any other institution as an examination paper, nor submitted it to any other faculty as a dissertation.

Johannes Heidbüchel

Heidelberg, April 3, 2019